Interaction of Lipid Vesicles with Nanoparticles and Biomolecules: Impacts on Membrane Organization, Stability and Phase Behaviour

Ph.D. Thesis

by

NISHU KANWA

DISCIPLINE OF CHEMISTRY

INDIAN INSTITUTE OF TECHNOLOGY INDORE

SEPTEMBER 2020

Interaction of Lipid Vesicles with Nanoparticles and Biomolecules: Impacts on Membrane Organization, Stability and Phase Behaviour

A THESIS

Submitted in partial fulfillment of the

requirements for the award of the degree

of

DOCTOR OF PHILOSOPHY

by

NISHU KANWA

DISCIPLINE OF CHEMISTRY

INDIAN INSTITUTE OF TECHNOLOGY INDORE

SEPTEMBER 2020

INDIAN INSTITUTE OF TECHNOLOGY INDORE

CANDIDATE'S DECLARATION

I hereby certify that the work which is being presented in the thesis entitled **Interaction of Lipid Vesicles with Nanoparticles and Biomolecules: Impacts on Membrane Organization, Stability and Phase Behaviour** in the partial fulfillment of the requirements for the award of the degree of **DOCTOR OF PHILOSOPHY** and submitted in the **DISCIPLINE OF CHEMISTRY, INDIAN INSTITUTE OF TECHNOLOGY INDORE**, is an authentic record of my own work carried out during the time period from **JULY 2015** to **SEPTEMBER 2020** under the supervision of **DR. ANJAN CHAKRABORTY**, Associate Professor, Discipline of Chemistry, Indian Institute of Technology Indore.

The matter presented in this thesis has not been submitted by me for the award of any other degree of this or any other institute.

10.09.2020

(NISHU KANWA)

This is to certify that the above statement made by the candidate is correct to the best of my/our knowledge.

10.09.2020

(DR. ANJAN CHAKRABORTY)

Ms. NISHU KANWA has successfully given his/her Ph.D. Oral Examination held on 23.02.2021

(Dr. Amit Kumar)	(Prof. Pramit K. Chowdhury)	(Dr. Anjan Chakraborty)
Signature of Chairperson (OEB)	Signature of External Examiner	Signature(s) of Thesis Supervisor(s)
Date: 23.02.2021	Date: 23.02.21	Date: 23.02.2021
(Dr. Preeti Anand Bhobe)	(Dr. Chelvam Venkatesh)	
Signature of PSPC Member #1	Signature of PSPC Member #2	Signature of Convener, DPGC
Date: 23.02.2021	Date: 23.02.2021	Date: 23.02.2021

Signature of Head of Discipline
Date: 23.02.2021

ACKNOWLEDGEMENTS

First and foremost, it is my great pleasure to express my heartfelt gratitude to my PhD thesis supervisor Dr. Anjan Chakraborty for his constant guidance and encouragement throughout the entire course of my PhD program. I sincerely feel honored to be a part of his research group. I am indebted to him for his support, motivation and dedication in developing the thesis. His encouragement and kindness during the unfortunate times when research plans did not work out are gratefully acknowledged.

I am thankful to my PSPC committee members, Dr. Chelvam Venkatesh and Dr. Preeti Anand Bhobe for their valuable suggestions.

I would like to thank IIT Indore and SIC, IIT Indore for providing financial support and instrumentation facility respectively. I would also like to thank all the faculty members of the Discipline of Chemistry, IIT Indore for their guidance and help during the course of the thesis work. I would like to thank Dr. Tridib K. Sarma and his group members for their selfless cooperation and help during DLS experiments. I would also like to thank Dr. Ravinder Kumar, Mr. Kinny Pandey, Mr. Ghanshyam Bhavsar, Mr. Manish Kushwaha and Ms. Vinita Kothari for their technical support without which it would not be possible to continue my work. I would also like to thank Ms. Anjali Bandiwadekar, Mr. Rajesh Kumar, Mr. Lala Ram Ahirwar, Mr. Gati Krushna Nayak, Mr. Ranjit Raghuwanshi, Mr. Pallab Pradhan, Mr. Nitesh Singh Powar, Mrs. Kriti Jain and other library staff for their constant support, whenever required. I would like to acknowledge all the technical and non-technical staff of IIT Indore for their assistance and service.

I extend my heartiest gratitude to my seniors, Dr. Anupam Das and Dr. Chandan Adhikari for their guidance and moral support. I would like to acknowledge my dear group members, Mr. Soumya Kanti De, Ms. Kavana M, Mr. Avijit Maity, Ms. Ananya Patnaik and Mr. Debanjan Bagchi for their selfless co-operation and help to make my work successful. I would like to thank all my co-researchers at IIT Indore.

I also extend my deep gratitude to all my teachers from Miranda House College, Department of Chemistry (Delhi University) and Model School Jhajjar for their years of teaching and guidance.

It has been a wonderful experience to work with many friends during my Ph.D. who helped me in many aspects. I would like to record my thanks to

Neha, Daisy, Preeti, Anupama, Madhurima, Siddarth, Abhiram, Mirajuddin, Bhawna, Shagufi, Reena, Jamuna, Dr. Tamalika Bhattacharya, Dr. Sonam Mandani, Dr. Bhagwati Sharma, Dr. Biju Majumdar, Dr. Roopali Prajapati, Dr. Sagnik Sengupta, Dr. Chinky Binnani, Amrita, Amit, Premansh, Mamta, Nitin, Aishi.

I express my heartiest gratitude to my friend Anshul for always believing in me and keeping my spirits high during the bad times. I extend my gratitude to Ankita, Anurag, Samanvith, Shashank, Tanya, Sachina, Sonam, Ayushi, Roohi, Sukriti, Srishti, Anshu, Dhruv, Himanshu and Abhinav who have been with me in every ups and downs of my professional and personal life.

Most importantly, it would have been almost impossible for me to achieve anything without the support, care and love of my family. I express my respect, love and gratitude to my entire family, especially my grandparents who have made me a capable human. I am eternally grateful to have very supportive siblings, Ritu and Arun, who never missed a chance to turn me into the best version of myself. I am also very grateful to my paternal uncles and aunts for always having my back and believing in my capabilities.

There are many more who have directly or indirectly contributed in making this journey successful. I wish I could thank them all but time and space compel me to stop here.

NISHU KANWA
IIT INDORE

Dedicated to
My Grandparents

ABSTRACT

Artificial lipid membranes mimic the cellular membranes, which are known to have a very complex structure. Lipid membranes can be conveniently designed *in vitro* using lipids which are arranged in a bilayer with a well-known and simpler composition, making them much easier to study. Thus, they serve as significant tools for understanding the physicochemical properties of cellular membranes. The usage of model membranes has been known since the early 1960s and they have been widely investigated to understand the physiological mechanisms and bio-inspired applications. Lipid membranes are prone to fusion which is a fundamental process, but it limits their applications. Thus, in order to modify their structures and properties, they are often treated with external interactive species (nanoparticles, metal ions, biomolecules, polymers etc.). The modification of membrane surfaces by interfacial interactions can lead to the formation of better experimental models and develop new systems for biological applications. In particular, these interaction studies can be potentially used for the design and development of efficient drug delivery systems.

The interactions of lipid membranes with external species can potentially induce changes in the properties and structures of the membranes which are important to analyze. These interactions can influence the fluidity and packing of the lipid membrane. Membrane properties are sensitive towards the presence of ions, small molecules, hydration, temperature and pH of the system. Even minor changes in the membrane structure and properties can have larger impacts on several important biological functions. As a result, the membrane interaction studies which affect the cellular processes account for the underlying mechanisms and the resultant influence at the nano-bio interface. Thus, a better understanding of the interactions is required which can help to bridge the gap between the lipid systems *in vivo* and *in vitro* at the membrane interface.

Because of the immense importance of these systems, the lipid-based interactions and their applications have been of great interest in the recent past. Therefore, we have explored the interactions of different nanoparticles and biomolecules with lipid membrane vesicles (also known as liposomes). The systems studied in the thesis are lipid membrane vesicles, their assemblies with different nanoparticles (including carbon dots) and biomolecules (different amino acids). The possibility of lipid-based system for the controlled release of an anticancer drug, Doxorubicin (DOX) was investigated. For the interaction studies, lipid bilayers of varying chain lengths, surface charges and phase transition temperatures were explored using the properties of a fluorescent membrane probe PRODAN with the help of different spectroscopic as well as imaging techniques.

Objectives: The main objective of this thesis is to explore the interactions of nanoparticles and biomolecules with biomimetic lipid vesicles, which can potentially modify the membrane dynamics and properties and thus help in the development of better drug delivery systems and bio-imaging models. The research work reveals the binding behaviour of different nanoparticles, including carbon dots, and biomolecules with varying properties based on their size, surface ligands, isomeric precursors and hydrophobicity with different lipid vesicles. The thesis addresses the following points:

(a) It is well-known that nanoparticles interact with lipid vesicles and can potentially modify their properties (fluidity, order and hydration). Here, our primary objective is to understand the extent of interaction between nanoparticles of different surface functionalization and lipid vesicles through spectroscopic means. The binding of nanoparticles with lipid vesicles is governed by different forces. Therefore, the experimental results also need to be fitted within the existing theoretical framework. So one of the main objectives is to validate the

results obtained from experimental data in the light of theoretical models to describe the lipid vesicle-nanoparticle interaction.

(b) Bare lipid vesicles suffer from premature drug leakage, which limits their usage. The interaction of nanoparticles (and polymers) can result into formation of hybrid systems with modified properties which could be better for bioinspired applications. Therefore, our objective is to exploit the lipid-nanoparticles system to build up a stable drug delivery system (DDS) which will inhibit its premature release and be suitable for controlled drug delivery. Moreover, modulation of the rate of drug release of anti-cancer drug at the pH of cancer cells is another objective of the work.

(c) While gold nanoparticles can be employed for an effective and successful drug delivery system, the carbon nanoparticles i.e. carbon dots (c-dots), have been successfully employed for cellular imaging. In this context, the selection of c-dots is crucial because wrong selection of c-dots synthesized from different precursors may have adverse effect on the cellular processes. Here, our objective is to investigate the effect of fluorescent c-dots derived from different isomeric (ortho, meta and para) precursors on the model lipid membrane. Our primary focus is to find the suitability of c-dots for the cellular imaging purpose. We also aim to investigate the role of precursors in governing the interaction.

(d) Interactions between membranes and amino acids are crucial considering they affect the membrane protein folding, membrane protein channels and transport of metabolites in the membranes. Since the amino acid residues are present in the body, the understanding of such interactions is important to analyze in order to realize their impact on several cellular processes.The thesis accounts for the interaction of lipid vesicles with amino acids of different charges and hydrophobicity. We aim to understand if interactions influence the fluidity and packing of the lipid membrane and more importantly

whether the interaction depends on the properties of the amino acids. We have carried out a systematic approach in order to focus on specific parameters (charge and hydrophobicity) to study the changes in lipid hydration and ordering. The study aids in understanding the interaction of amino acids in the light of existing theory.

(e) The thesis demonstrates how we can probe the interaction of various interactive entities with lipid vesicles by exploiting the properties of a fluorescent membrane probe by means of different spectroscopic methods. Moreover, the employment of imaging techniques to understand the membrane dynamics visually has been focused upon.

Summary of research work:

1. **Effect of surface ligand and temperature on lipid vesicle−gold nanoparticle interaction: a spectroscopic investigation**

In this section, we explored the interactions of differently functionalized gold nanoparticles (AuNPs) with zwitterionic lipid vesicles of varying phase transition temperatures. AuNPs were functionalized with surface ligands on the basis of varying bulkiness and charge. Anionic ligands i.e. citrate (cit), 3-mercaptopropionic acid (MPA) and glutathione (GSH) and cationic ligand cysteamine was used. We used zwitterionic lipids DMPC (Tm = 24 °C) and DOPC (Tm = −20 °C) for the study. We conducted the experiments at different temperatures, above and below the phase transition temperature of the lipid, i.e. 15 °C and 35 °C. The AuNPs were found to bring in stability to the lipid vesicle but the extent of interaction and thus gelation of the lipid vesicles depended largely on the surface ligands (Scheme 1). The cit-capped AuNPs were found to interact the strongest and effectively raised the phase-transition temperature of the lipid vesicles. On the other hand, more bulky ligands (MPA and GSH) were found to distant the AuNP core from the bilayer surface, exert less van der Waals force and the interactions were comparatively weaker. The anionic nanoparticles interacted stronger than the cationic one. The

interactions were also found to be more strongly pronounced when the vesicles were near the phase-transition temperature of the lipid as compared to the vesicles present in Lα (fluid) or Lβ (gel) phase. The study also demonstrated the surface modification due to these interactions on the lipid vesicles.

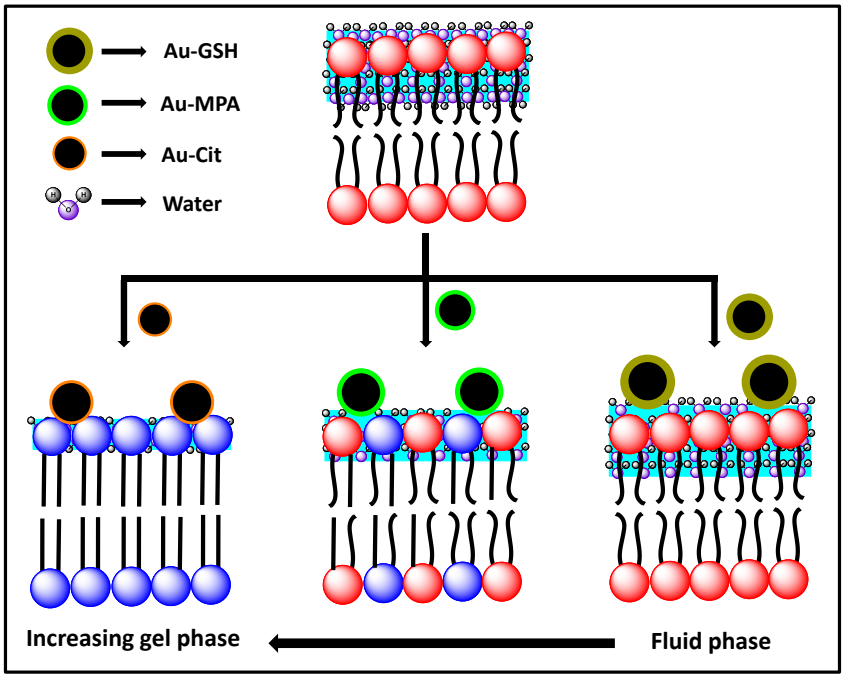

Scheme 1: *Representative image showing the interaction of differently functionalized gold nanoparticles with lipid vesicles. Cit-AuNPs stabilize the bilayer to a higher extent and raise the phase transition temperature of the lipid. MPA and GSH-AuNPs adsorb on the bilayer surface less strongly due to their bulky structures.*

2. Spectroscopic study of the interaction of carboxyl-modified gold nanoparticles with lipid vesicles of different chain lengths and controlled drug release by layer-by-layer technology

In the current section, we reported the interactions of carboxyl-modified gold nanoparticles (AuC) with zwitterionic phospholipid vesicles composed of lipids with different chain lengths and phase transition temperatures. Three zwitterionic lipids namely DPPC, DMPC, and DLPC were used in this experiment. These lipids are widely different in their phase transition temperature. DPPC has a phase transition temperature around 42 °C while DMPC and DLPC have phase

transition temperatures around 23 °C and -2 °C respectively. The nanoparticles were found to bring in stability toward the vesicles by local gelation and the vesicle−AuC assemblies were fairly stable as compared to bare lipid vesicles. The fusion activity of the vesicles could be effectively controlled by decoration of AuC nanoparticles at the interface of phospholipid vesicles (Scheme 2a). The bound AuC was found to detach from the surface of the vesicles under acidic conditions. The detachment rate of AuC from the vesicle−AuC assemblies differed due to variations in the phase transition temperatures and fluidity of the systems.

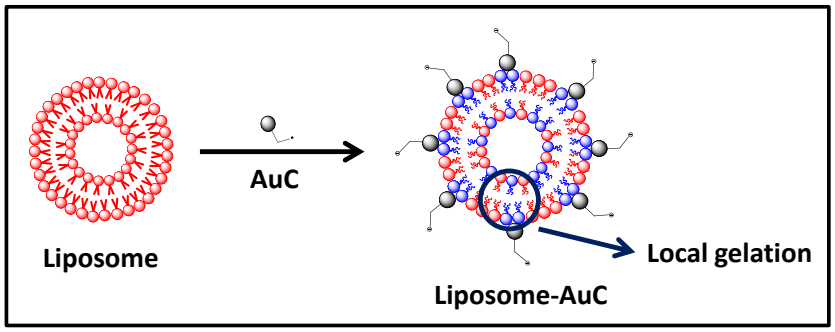

Scheme 2a: *Local gelation of the lipid bilayer induced upon interaction with carboxyl-modified gold nanoparticles.*

The system was used for exploiting the controlled release of an anti cancer drug, Doxorubicin (DOX) under acidic conditions for different zwitterionic lipid vesicles. The drug release rate was optimized by formation of capsule structures by coating the lipid vesicle−AuC assemblies with layers of oppositely charged polymer (P), lipid (L) and again with a polymer following a layer-by-layer approach (Scheme 2b). We used alternating layers of the poymer polydiallyldimethylammonium chloride, and lipid mixture L (DMPC: DMPG) to synthesize the capsules. The lipid-based capsules were found to be highly stable for weeks and inhibited premature release of the drug.

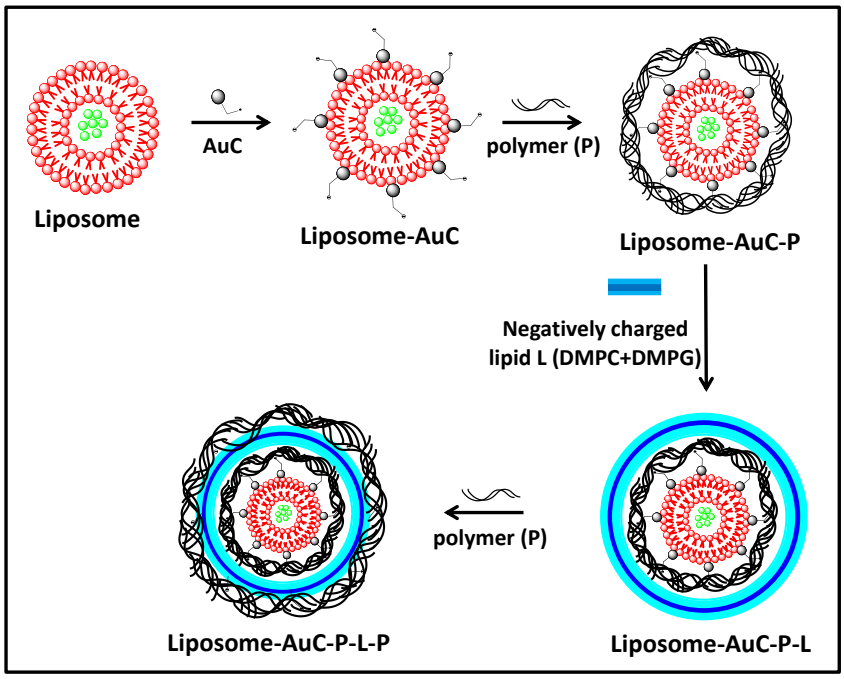

Scheme 2b: *Layer-by-layer deposition of polymer (P) and lipid (L) on liposome-AuC assemblies forming capsule-like structures for controlled release of encapsulated drug molecules.*

3. Discriminatory interaction behaviour of lipid vesicles towards diversely emissive carbon dots synthesized from ortho, meta and para isomeric carbon precursors

In the current section, we reported the interaction of zwitterionic lipid vesicles with photoluminescent carbon dots (C-dots) derived from different isomeric (ortho, meta and para) precursors of phenylenediamine. The C-dots synthesized from different isomers of the same carbon precursor were found to be significantly different from each other in terms of their interaction phenomena with lipid vesicles. We used DMPC and DPPC lipids for this study. The ortho C-dots (oCD) showed strong interaction with the lipid vesicles, while the other analogues meta and para C-dots (mCD and pCD) did not display such interaction. We found that oCD were selectively embedded in the lipid vesicles and vesicles retained their morphology upon interaction with oCD. On the contrary, mCD and pCD being located in the interfacial region induced instability in the lipid vesicles and resulted in aggregation of the vesicles. The discriminatory behaviour of lipid vesicles was explained in terms of the location of the C-dots on the lipid vesicles,

their electrostatic attraction at the vesicle interface, possible cross linking with other vesicles and different hydrophobicities of the isomeric precursors of the C-dots. We found that among all C-dots, only oCD is favorable for bio-imaging purpose. This study provides guidance to understand and predict the binding interactions and attachment processes at the bilayer membranes.

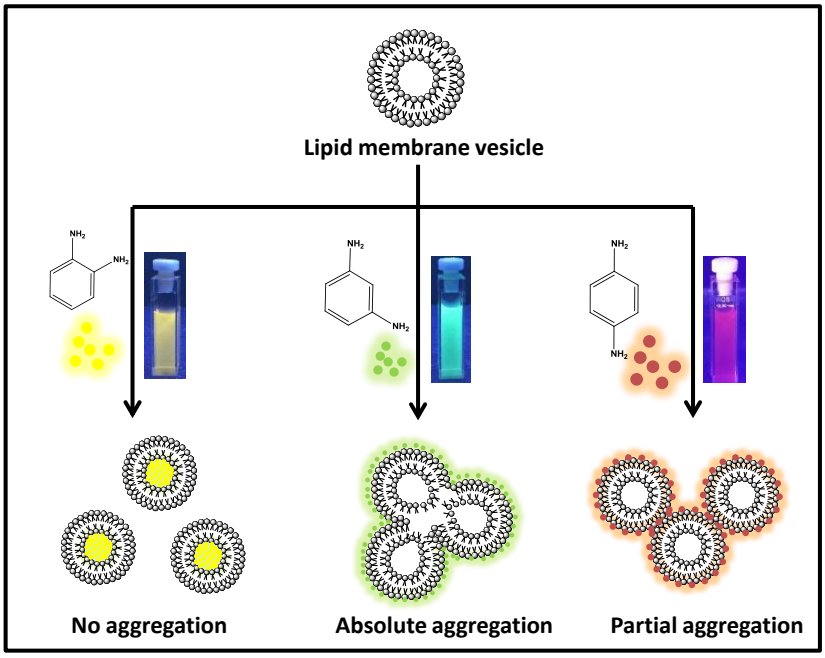

Scheme 3: *Representation of the interaction of C-dots derived from different isomeric carbon precursors. While ortho C-dots (oCD) remain embedded inside the membrane vesicles and do not cause aggregation, meta and para C-dots (mCD and pCD) are located on the membrane interface and cause absolute and partial aggregation respectively.*

4. Interaction of aliphatic amino acids with zwitterionic and charged lipid membranes: hydration and dehydration phenomena

In this section, we investigated the interactions of lipid bilayer membranes of different charges and phase states with aliphatic amino acids of varying charge (aspartic acid, glutamic acid, arginine and lysine) and hydrophobicity (serine, leucine and valine). We used different lipids varying in phase transition temperature (DPPC, DMPC and DOPC) as well as charge (DMPG and DMTAP) for this study. The interaction of lipid bilayer membranes with amino acids were found to depend on the properties of both the amino acid and the membrane itself.

Charge of the amino acid played a major role in the interaction strength with the lipid bilayer membrane. The negatively charged amino acids interacted strongly with the lipid membranes by stabilizing their gel phase and resulted in very large dehydration. On the other hand, positively charged amino acids brought in hydration in the membranes and significantly fluidized the system. We also found that hydrogen bonding played a significant role in governing the interaction of aliphatic amino acids with zwitterionic lipid membranes. The more polar serine bearing a hydroxyl group at the terminal carbon offered a stronger interaction with the lipid membranes as compared to its analogues leucine and valine, which are hydrophobic in nature. In the case of anionic lipid membrane, the interaction strength was found to be similar for all aliphatic amino acids irrespective of their hydrophobicity. The cationic lipid membrane, on the other hand, did not induce any substantial changes in the bilayer membrane.

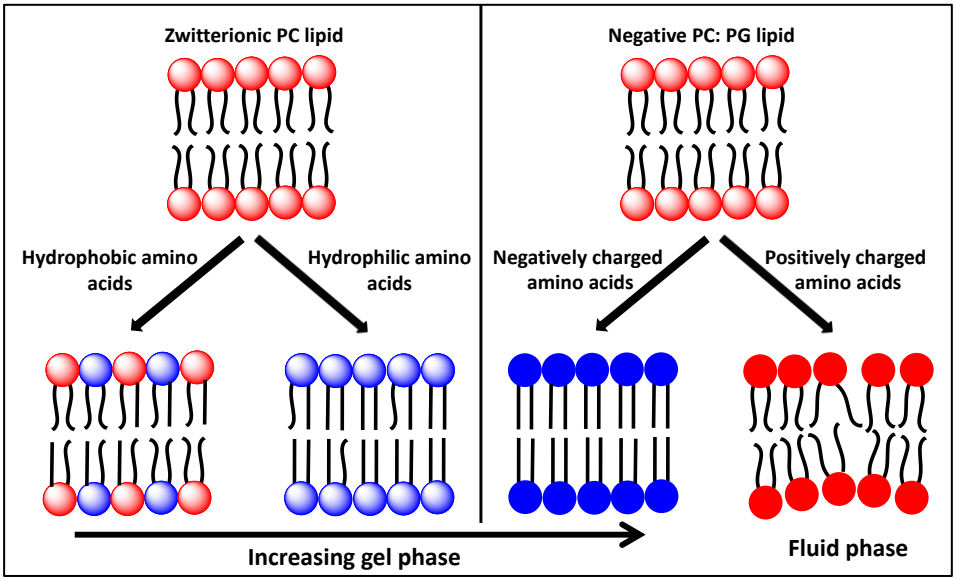

Scheme 4: *Aliphatic amino acids interact differently in order to induce gelation or fluidization in the zwitterionic and charged lipid membranes as a result of hydration or dehydration of the membrane surface. Here shaded red colored lipid membrane represents nearly fluid phase at room temperature, shaded blue represents nearly gel phase; whereas deep blue colored lipid membrane represents highly gel and ordered phase (stiffened acyl chains) and deep red represents completely fluid or disordered phase (loosely packed acyl chains).*

Conclusion: Research work reported in this thesis describes the significance of the binding of various nanoparticles and biomolecules to model lipid membranes and the impact they cast on the overall membrane properties. It was found that variation of charge, phase transition temperature (T_m) of the vesicles and change in properties of nanoparticles and biomolecules influence the pattern of interaction. Even minor changes in the interactive entities (size, charge, surface ligands, precursors, hydrophobicity) and medium (temperature, pH etc.) can largely affect the membrane structure and properties (such as fluidity, order and hydration behavior). As a future prospect, these developments are expected to form better hybrid systems and add new dimensions toward the potential usage of lipid membrane based assemblies for drug delivery, bioimaging and several bio-inspired applications.

LIST OF PUBLICATIONS

1. **Kanwa, N.**, De, S. K., Maity, A., Chakraborty, A. (2020) Interaction of aliphatic amino acids with zwitterionic and charged lipid membranes: hydration and dehydration phenomena. *Phys. Chem. Chem. Phys.* 22, 3234-3244 (DOI: 10.1039/c9cp06188f).

2. **Kanwa, N.**, Patnaik, A., De, S. K., Ahamed, M., Chakraborty, A. (2019) Effect of surface ligand and temperature on lipid vesicle–gold nanoparticle interaction: a spectroscopic investigation. *Langmuir* 35, 1008–1020 (DOI: 10.1021/acs.langmuir.8b03673).

3. **Kanwa, N.**, De, S. K., Adhikari, C., Chakraborty, A. (2017) Spectroscopic study of the interaction of carboxyl-modified gold nanoparticles with liposomes of different chain lengths and controlled drug release by layer-by-layer technology. *J. Phys. Chem. B* 121, 11333-11343 (DOI: 10.1021/acs.jpcb.7b08455).

4. **Kanwa, N.**, M, K., Chakraborty, A. (2020) Discriminatory interaction behaviour of lipid vesicles towards diversely emissive carbon dots synthesized from ortho, meta and para isomeric carbon precursors. *Langmuir* 36, 10628-10637 (DOI: 10.1021/acs.langmuir.0c02207).

5. De, S. K., **Kanwa, N.**, Chakraborty, A. (2019), Influence of trivalent metal ions on lipid vesicles: Gelation and fusion phenomena. *Langmuir* 35, 6429-6440 (DOI: 10.1021/acs.langmuir.9b00682).

6. De, S. K., **Kanwa, N.**, Ahamed, M., Chakraborty, A. (2018), Spectroscopic evidence for hydration and dehydration of lipid bilayers upon interaction with metal ions: a new physical insight. *Phys. Chem. Chem. Phys.* 20, 14796-14807 (DOI: 10.1039/C8CP01774C).

(*Publications 5-6 are not included in the thesis*)

TABLE OF CONTENTS

NOMENCLATURE

α	Alpha
β	Beta
γ	Gamma
τ	Fluorescence Lifetime
a_i	Relative Amplitude
ϕ	Quantum Yield
Å	Angstrom
χ	Chi
λ	Wavelength
μ	Micro
π	Pi
Σ	Summation
nm	Nanometer
ns	Nanosecond
ps	Picosecond
mM	Milli Molar
μM	Micro Molar
η	Viscosity
Ksv	Stern Volmer Quenching Constant

Kp	Partition Coefficient
ε	Molar Extinction coefficient
cm	Centimeter
°	Degree
N_A	Avogadro Number
K	Kelvin
mL	Milliliter
μL	Microliter
a. u.	Arbitrary Unit
λ_{ex}	Excitation Wavelength
λ_{em}	Emission Wavelength
pH	The negative logarithm of hydronium-ion concentration
pK_a	Dissociation constant of an acid in ground state
ζ	Zeta Potential

ACRONYMS

AFM	Atomic force microscopy
ANS	8-Anilinonaphthalene-1-sulfonic acid
Arg	Arginine
Asp	Aspartic Acid
CMC	Critical Micelle Concentration
Cys	Cysteamine
DLPC	1,2-dilauroyl-sn-glycero-3-phosphocholine
DMPC	1,2-dimyristoyl-sn-glycero-3-phosphocholine
DMPG	1,2-dimyristoyl-sn-glycero-3-phospho-(1'-rac-glycerol) sodium salt
DMTAP	1,2-dimyristoyl-3-trimethylammonium-propane chloride salt
DOPC	1,2-dioleoyl-sn-glycero-3-phosphocholine
DOTAP	1,2-dioleoyl-3-trimethylammonium- propane chloride salt
DPPC	1,2-dipalmitoyl-sn-glycero-3-phosphocholine
DLS	Dynamic Light Scattering
FWHM	Full Width Half Maxima
Glu	Glutamic Acid
GSH	Glutathione
IRF	Instrument Response Function
Leu	Leucine
Lys	Lysine

MPA	3-mercaptopropionic acid
O.D.	Optical Density
PDA	Phenylenediamine
POPC	2-Oleoyl-1-palmitoyl-sn- glycero-3-phosphocholine
PRODAN	6-propionyl-2-dimethyl-aminonaphthalene
Ser	Serine
TCSPC	Time Correlated Single Photon Counting
TEM	Transmission Electron Microscope
Val	Valine

LIST OF FIGURES

LIST OF SCHEMES

LIST OF TABLES

Chapter 1

Interactions at the nano-bio interface using model membrane

1.1 Introduction

Lipids are one of the major constituents of cellular membranes. They are actively involved in a set of essential cellular functions [1-5]. They are present in different compositions along with membrane proteins rendering cellular membranes complex and difficult to study [6]. Artificial lipid membranes synthesized in vitro mimic the cell membranes [5, 7-11]. Thus, they are used as model systems for understanding the physicochemical properties of cellular membranes. They can be studied with much ease provided they are synthesized using a limited number of components. However, lipid membranes are prone to fusion [5], which limits their applications. In order to modify and stabilize their structures, they are often treated with external interactive species (nanoparticles, biomolecules, polymers etc.) [12-21]. The modifications of membrane surfaces by interfacial interactions lead to the formation of better experimental models and develop new systems for biological applications [16-17, 22-23]. Membrane properties are sensitive towards the presence of ions, small molecules, hydration, temperature and pH of the system [24]. Even small changes in the membrane structure and properties can have severe impacts on several important biological functions [25]. Thus, these studies help in the better understanding of the interactions at the membrane interface and bridge the gap between the lipid systems in vivo and in vitro. They also account for the underlying mechanisms and the possible effects of membrane interactions at the nano-bio interface which affect the cellular processes. The following section proceeds with a brief description of the biomimetic lipid vesicles and their interaction with nanoparticles and biomolecules.

1.2 Lipid membrane vesicles: General introduction

First discovered in 1965 by Dr. Alec D. Bangham, a British biophysicist, lipid vesicles (or liposomes) have been an area of interest for scientists since then [26]. They were first described as swollen phospholipid systems and were observed to be forming vesicular structures consisting of lipid bilayers. The name "liposome" was acquired from the combination of two Greek words, "lipos" denoting fat and "soma" denoting body.

Lipid membranes are composed of lipids which are generally non-toxic and biocompatible in nature. They typically have a hydrophilic head group and a hydrophobic carbon tail. They form closed structures impulsively upon hydration resulting into spherical lipid bilayer with the hydrophilic head groups oriented towards the outer as well as inner aqueous medium and the hydrophobic chains are centered within the bilayer [27-28]. The lipid membrane is organized based on the hydrophobic interactions between several amphiphilic molecules that constitute the hydrophobic-hydrophilic interface in an aqueous system. This structure is thermodynamically favorable and is stabilized by van der Waals forces, hydrogen bonding and other electrostatic interactions [29-30].

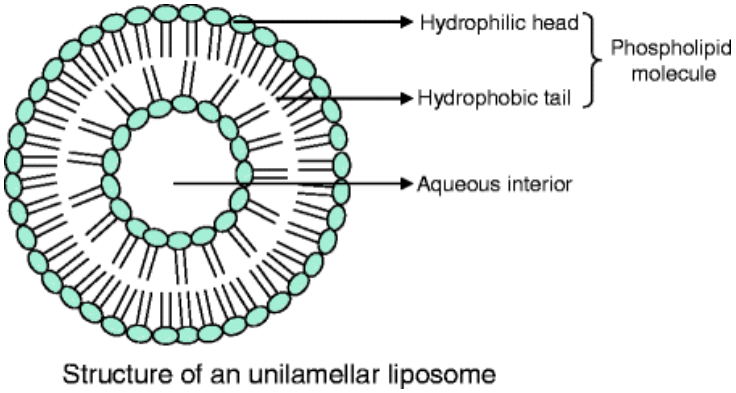

Figure 1.1 *Structure of unilamellar liposome with a hydrophilic head and hydrophobic tail organized into a spherical structure [31].*

In a lipid membrane, lipids can adopt solid and/or fluid phase. These phase states are characterized by a typically different spatial arrangement and entropy of the individual lipids. Solid phase is defined by a closely packed rigid and ordered gel

phase whereas fluid phase comprises of a disordered phase. The phase state in a membrane determines the membrane properties, organization and permeability [1]. The permeability of vesicles increases upon the transition from solid to fluid phase. This process takes place at the phase transition temperature (T_m). It involves the loosening of packed phospholipids resulting into empty spaces between the lipids [32-34].

The phase state majorly depends on the van der Waals interaction between neighboring lipid molecules. This is determined by the chain length of the lipids. Lipids with longer chains exhibit stronger van der Walls forces, resulting into more ordered packing. However, short chain lipids are more fluid at a given temperature [35]. The choice of bilayer components used for synthesis determines the rigidity and fluidity of the bilayer [36]. For example, lipids with shorter hydrophobic chain (eg DOPC) and unsaturated phosphatidylcholine (PC) from natural sources (egg or soyabean PC) give permeable and less stable bilayers, whereas saturated PC with long acyl chains (eg DPPC) form rigid and impermeable structures [37-40].

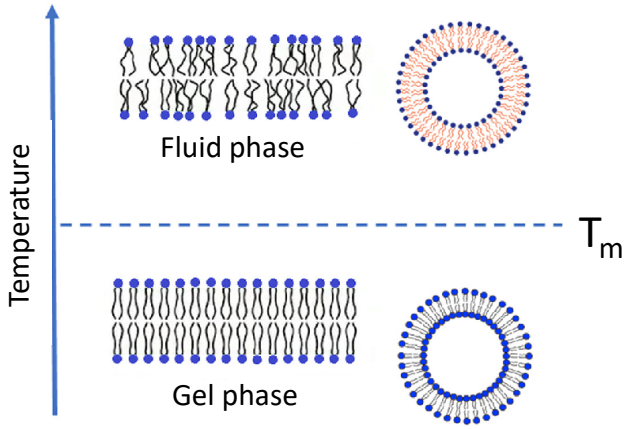

Figure 1.2 *Phase states and membrane fluidity of vesicles. At lower temperatures, $T < T_m$ of phospholipids, bilayer exists in ordered gel phase and at higher temperatures, $T > T_m$, bilayer exists in disordered fluid phase [41].*

Apart from phase state and lipid composition, the properties of lipid vesicles depend on size as well as their method of preparation. Lipid vesicles have a size ranging from very small (25 nm) to large (2.5 μm) vesicles. They consist of one or

more bilayer membranes surrounding the aqueous environment. The amphipathic nature and self assembling characteristics of lipid bilayers influence the hydrophobic layers (or lamellarity) of the bilayers [40, 42-44]. On the basis of their size, lamellarity and methods of preparation, lipid vesicles are broadly divided into two categories [40]:

1) Unilamellar vesicles: They have a single phospholipid bilayer sphere enclosing the aqueous solution. These can be of either small unilamellar vesicles (SUV) or large unilamellar vesicles (LUV) depending on their size [43]. SUVs are generally prepared by the "ethanol injection method". For this, lipid dispersed in ethanol is rapidly injected in aqueous medium kept well above the phase transition temperature of the particular lipid. They are generally of the size ≤ 100 nm. On the other hand, LUVs are large vesicles with single lamellarity but have higher aqueous volume to lipid ratio. They have a larger size than SUV (> 100 nm). Similar vesicles with even larger size (> 500 nm) are termed giant unilamellar vesicles (GUVs).
2) Multilamellar vesicles (MLV): MLVs are formed when several unilamellar vesicles form on one another making concentric phospholipid spheres, each layer separated by a consecutive layer of water [44]. Their vesicle structure resembles the onion structure. These vesicles result into multi-lamellar structures with an average size > 500 nm. They are prepared by "thin film hydration" method, in which the dry lipid film is hydrated by an aqueous medium heated well above the phase transition temperature.

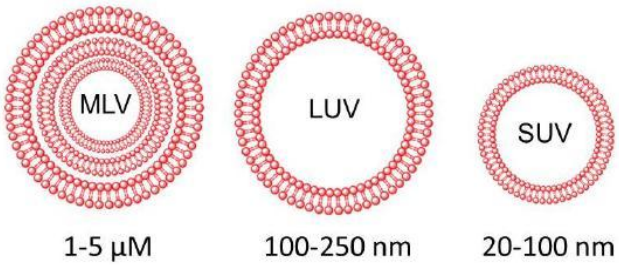

Figure 1.3 *Types of liposomes based on their size and lamellarity [45].*

1.3 Lipid vesicles as model systems: Applications and limitations

1.3.1 Biomimetic behaviour:

Lipid bilayers constitute the cell membranes and play a significant role in maintaining the cellular homeostasis. They providing a physical barrier to prevent the free permeation of water and separate the water-soluble compounds [46-50]. They act as barriers between the cells and the extracellular environment [47, 51]. Artificial lipid membranes serve as model membranes as they efficiently mimic the properties of cellular membranes [5, 52-53].

While cellular membranes have a complex structure and a diverse composition, lipid membranes can be conveniently designed with known lipid composition which makes them much easier to study [53-54]. They can be synthesized in vitro using lipids which are arranged in a bilayer with a well-known and simpler composition. Several model systems have been developed with a wide variety of size, geometry, morphology and chemical composition apart from lipid vesicles, such as supported lipid bilayers, lipid monolayers etc. [4, 6, 8, 55]. Although the complexity of cellular membranes cannot be entirely imitated by lipid vesicles, their chemical composition and properties (such as charge and phase transition temperature) can be easily modulated during their synthesis, which is a great advantage. These systems can be easily tuned as per the experimental and biological requirements.

Lipid vesicles act as simple model systems which help in the understanding of functions and structure of the complex biological systems [56]. The properties of a lipid membrane such as fluidity, continuity and defect and the related processes such as fusion and phase separation can be studied using model systems, which help in the understanding of several important biological phenomena [56-57].

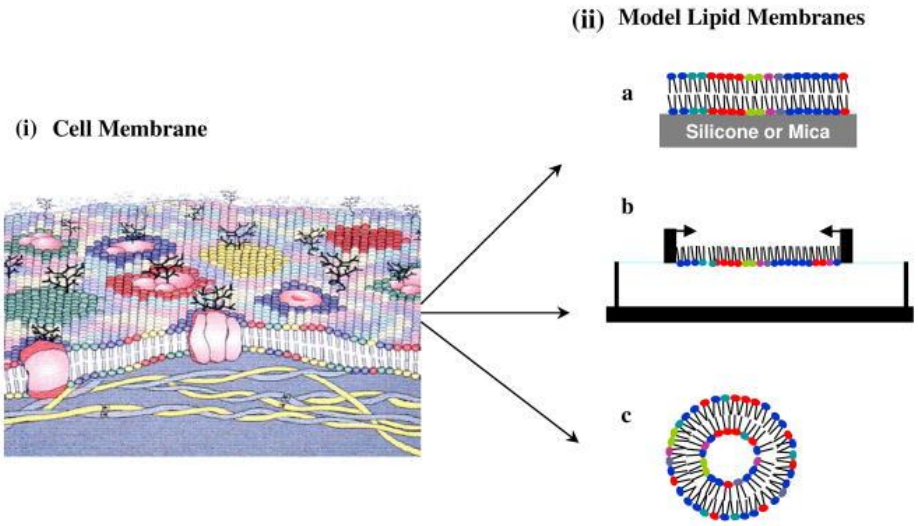

Figure 1.4 *Illustration of cellular membrane and various model systems. (i) Cell membrane depicting membrane lipid asymmetry and (ii) model membrane systems mimic the cell membrane: a) supported lipid bilayer, b) lipid monolayer and c) lipid vesicle [6, 58].*

1.3.2 Applications:

Lipid membranes may be natural or synthetic, but lipids are biocompatible and biodegradable, which makes them apt for biomedical applications [9, 23-31, 37-43, 59-60]. Due to the presence of both hydrophilic as well as hydrophobic environment in the lipid membranes, they can be used as potential drug carriers which can carry a broad spectrum of drugs. They have the unique property to solubilize both hydrophilic and hydrophobic materials in different compartments. While hydrophobic drugs are located inside the bilayer, hydrophilic drugs are located at the interface or entrapped within the aqueous core of the vesicles.

Over the recent years, researchers have resorted to biocompatible carriers, composed of bioinspired materials. Particularly, lipid-based drug carriers have been used for a long time [9, 23, 25, 28, 31, 37-43, 59-60]. They have served as in vivo carrier systems for anti cancer drugs, such as Doxil (also known as Doxorubicin). Lipid vesicles are advantageous compared to conventional systems (such as nanoparticles and microemulsions) because of their efficient biodistribution [59]. However, premature and non-targeted release has been a major challenge for the researchers.

In this regard, interaction between foreign materials (nanoparticles, polymers, biomolecules etc.) and host (lipid vesicles) [12-25] has been used to synthesize improved systems for optimized, controlled and targeted delivery and imaging. Such interactions are designed to cater to precise specifications and requirements, such as controlled surface properties and stimuli-responsive systems [61]. These systems have emerged as better models in contrast with the traditional drug nanocarriers such as bare liposomes, micelles and nanospheres [61]. The most commonly developed structures for drug delivery and imaging using these interactions can be core-shell structure, capsules or particles with nanocompartments [61].

Table 1.1 *Advantages and disadvantages of lipid vesicles used for drug delivery [40]:*

	Advantages	**Disadvantages**
1.	Biocompatible, biodegradable and non-toxic	Less stability
2.	Ability to carry both water and lipid soluble drugs	Low solubility
3.	Flexibility to bind with site-specific ligands to obtain active targeting	Difficult to target tissues due to their large size
4.	Stabilization of entrapped drug from hostile environment of biological membranes	Leakage and/or fusion of encapsulated drug, dyes and molecules
5.	Drugs can be stabilized from oxidation	Phospholipid may undergo oxidation and hydrolysis.
6.	Liposome increased stability via encapsulation of drug	High production cost
7.	Liposomes increased efficacy and therapeutic index of drug	

1.3.3 Limitations (Fusion and stability issues):

The fusion phenomenon in biological membranes is a fundamental process essential for cell survival [62]. It aids cell membranes with the transport of metabolites within and across the membranes. However, it is a major limitation of artificial membranes for their application in the field of drug delivery and

imaging. Fusion of membranes can lead to loss of membrane integrity and its properties [63-65]. The fusion process in artificial lipid membranes can potentially lead to loss of the contents from the vesicle interior, which is highly undesirable [22, 62-65]. Fusion can take place due to a number of reasons such as changes in medium (pH, temperature and pressure), lipid composition, prolonged time period, response to external stimuli (fusion-inducing interactive species) etc. [22, 57, 62]. Membrane fusion results in the generation of bilayer defects, increase in bilayer permeability and surface tension, exchange of lipid contents between originally separate bilayers, change in vesicle size and morphology [62].

Thus, physical and chemical stability of the vesicles is a major concern, particularly because it limits their application as potential drug carriers. Chemical instability can arise due to degradation of phospholipid structures (by hydrolysis or oxidation) and physical instability is defined by non-uniform size distribution and low encapsulation efficiency. These limitations arise due to the inability of lipid vesicles to withstand mechanical stress which leads to leakage. Drug leakage is a common problem which may occur due to the instability of the membrane. Thus, tougher mechanical properties are required to be imparted to lipid vesicles for enhanced stability [66]. In this regard, surface modification is an efficient method to achieve stability both in vivo and in vitro. In order to stabilize the structures, they are treated with several external moieties [12-28]. The interactions of lipid membranes with various biological moieties are likely to induce changes in the properties and structures of the membranes [1-2, 67-68]. For this, nanoparticles and polymer systems have been used in the past [59]. Moreover, peptides (or even amino acids) incorporation makes the lipid vesicles more rigid because of change in packing and order [59]. While the binding of proteins and peptides can sometimes trigger vesicle aggregation, there are molecules which upon binding create steric or electric barriers between the membranes in order to prevent the fusion process [62]. Vesicle aggregation can also be avoided by introducing charge inside the vesicles, either by adding phospholipid or by decorating their surface by charged materials. This eliminates attraction and fusion by causing repulsion between vesicle surfaces [59]. The rigidification of

membrane and hence increase in its stability takes place with an enlarged bilayer separation [62]. The interaction of nanoparticles, amino acids, metal ions and peptides could be significant for altering and bringing about desired changes in the properties of the lipid membranes.

1.3.4 Membrane probes:

One of the most facile methods to study the highly sensitive as well as specific information regarding the membrane interface can be observed via the usage of molecular probes. Several fluorescent probes have been developed and employed to analyze the hydration environment at the membrane interface, in which the probes are sensitive to the local environment [69]. Specifically, the probe molecules preferentially bind to the target molecule and emit strong fluorescence signals representative of the respective microscopic surroundings. In particular, the solvent sensitive probes such as 6-propionyl-2-dimethyl-aminonaphthalene (PRODAN), 6-dodecanoyl-2-dimethylaminonaphthalene (LAURDAN) and 8-anilino-1-naphthalenesulfonic acid (ANS) are extensively used for the characterization and study of membrane properties [70-73]. These molecules have a dipole moment arising from their excitation and relaxation of the surrounding water molecules. Thus, they exhibit fluorescence characteristics depending on the degree of solvent relaxation [74-76]. Several properties of the membranes such as phase behavior, effects of membrane permeability and curvature can be understood by using these probes for studying model membranes.

1.4 Interaction of lipid vesicles with nanoparticles and biomolecules

1.4.1 Interaction with nanoparticles: The interaction of metal nanoparticles with lipid membrane has been studied a lot in the past few years owing to their several biological applications [16-17, 77-79]. Nanoparticles have a typical size of less than 100 nm. They can effectively give rise to significant interactions with lipids both on the surface as well as inside the membrane. This resultant assembly is capable of forming better systems for cancer diagnosis and treatment [80-83].

Among the nanostructured materials, gold nanoparticles (AuNPs) have emerged as particularly interesting candidates due to their stability, low toxicity, surface plasmon resonance effect and distinct catalytic properties [84-90]. Moreover, their unique optoelectronic properties as well as tunable size and morphology have found applications in the field of bio-nanotechnology as biomarkers, biosensors, cancer diagnostic and drug delivery [84-88]. AuNPs have been effectively employed for photothermal cancer therapy [86-88]. However, it is met with several drawbacks at the cellular levels, such as short circulation lifetimes, cellular toxicity and limited accumulation of particles at the required site [89-90].

In lieu of these limitations and to enhance the efficacy in biomedical applications, AuNPs are complexed with lipid vesicles, which help in improving the stability of the system as well as targeting of the cells. This can be done either by incorporating AuNPs into the vesicles or by adsorption on the surface of the lipid bilayer. The nanoparticles display similar dimensions to those of biomolecules. Thus, their complexation with biomaterials results into unique recognition, catalytic and inhibition properties. The surface of lipid vesicles can be modified and improved with these interactions, which results in increased stability, targeting and labeling capabilities. Particularly, lipid-AuNP assemblies provide significant opportunities in terms of nanoscale delivery systems as therapeutic or diagnostic multimodal agents [91-92]. Moreover, they can be used as probes to monitor biological processes through microscopic techniques [93-94].

The interaction of lipid vesicles with nanoparticles depends on the properties of nanoparticles and their localization on/in/around the vesicle [95-96]. Particularly in case of gold nanoparticles, the interaction behaviour depends on the surface functionalization and resultant charge as well as the hydrophobicity of the nanoparticles. Depending on these properties, different kinds of assemblies can be obtained, such as (i) liposomes having surface-bound nanoparticles, (ii) liposomes with bilayer-embedded nanoparticles, (iii) liposomes having core-encapsulated nanoparticles, (iv) lipid assemblies arising from hydrophobic core-encapsulated nanoparticles and (v) lipid bilayer-coated nanoparticles [95].

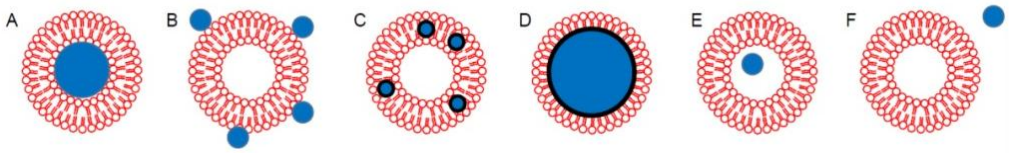

Figure 1.5 *Illustration of different types of binding interactions between liposomes and nanoparticles. (A) supported lipid bilayer, (B) adsorption of nanoparticles on the surface of bilayer, (C) embedded hydrophobic nanoparticles in the bilayer, (D) large hydrophobic nanoparticles wrapped inside a lipid monolayer, and non-interacting nanoparticles entrapped (E) or repelled (F) by the vesicle [96].*

1.4.2 Interaction with carbon dots:

Carbon dots (C-dots) are a subclass of nanoparticles. They are zero-dimensional carbonaceous nanomaterials which have small size (≤ 10 nm) and strong fluorescence characteristics [97-100]. They have a quasi-spherical morphology with a carbon-based core functionalized with surface groups [101]. First discovered in 2004 by Xu and coworkers [102], c-dots have widely found applications in several fields such as biomedicine, sensing, photovoltaic devices and catalysis since then [98-99, 103–120].

C-dots are superior to conventional semiconductor nanomaterials (i.e. quantum dots) because of their low cytotoxicity, environment friendly and biocompatible nature [99, 121]. Moreover, they have good chemical stability, water solubility and are resistant to photobleaching [99, 122]. The fluorescence properties of C-dots are achieved by finely tuning their size and surface groups. Their ease of surface functionalization with a wide range of groups (carboxyl, hydroxyl, amines etc.) allows for a diverse range of properties and applications [99, 122-125]. While the carbon core accounts for its low toxicity, the surface functionalization is responsible for its dispersibility and tunes its photoluminescence. They also exhibit the property to both donate as well as accept electrons, which accounts for its electron transfer property [100, 116,118-119, 126-127]. Thus, in view of the wide range of properties and applications of c-dots, they can serve better than the conventional molecular probes and organic dyes to analyze the membrane properties and can potentially act as biomarkers. While the probes suffer from

several limitations such as inefficient insertion into the systems, disruption of the bilayer, photobleaching etc. [128-132], C-dots can be efficient substitutes having size-dependent optical properties that facilitate new opportunities for imaging and detection. They are known to be photostable and provide a broad excitation and emission spectral range as compared to organic dyes. Thus c-dots could be employed as potential substitutes of the fluorescence dyes. Their photoluminescent properties can be used to visualize the bilayer morphology, fluidity, lipid mobility and molecular diffusion in membranes [127-130].

Depending on the surface functionalization, C-dots can interact differently with the bilayer membrane [127-130, 132-133]. While hydrophobic C-dots insert inside the hydrophobic core of the bilayer, hydrophilic c-dots are located either on the interface or within the aqueous core. These locations are likely to affect the bilayer differently. In this regard, only specific c-dots must be chosen which do not induce undesired effects on the membrane properties by interacting with them. Thus, the right selection of C-dots and their surface functionalization must be done, so as to not affect the membrane properties adversely.

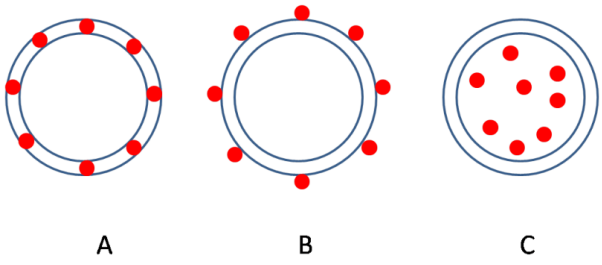

Figure 1.6 *Different interaction models of carbon dots with lipid vesicles. A) hydrophobic quantum dots encapsulated inside the bilayer, B) hydrophilic quantum dots adsorbed on the bilayer surface and C) hydrophilic quantum dots encapsulated inside the bilayer aqueous region [134].*

1.4.3 Interaction with biomolecules:

Cellular membranes are composed of lipid bilayer and several membrane proteins. Membrane proteins play an important role in biological processes and constitute ~30% of the cellular composition [14]. The integral proteins engage in the crucial responsibility for several cellular functions, such as transport and

signaling [14]. The position of these proteins and peptides in the cellular membranes is governed by the composition, orientation and hydrophobicity [6, 20-21, 46, 58, 135, 137]. One type of membrane proteins is membrane spanning proteins (integral or intrinsic), which are embedded inside the lipid bilayer. These proteins also control lipid structure in the membrane. Thus, the lipid environment of membrane regulates and governs the functions of intrinsic membrane proteins [6, 14].

These lipid modifications and the surrounding amino acids are not only involved in the interaction with membranes but that they also modulate membrane lipid structure as well as the formation of lipid domains in membranes [136-137]. In this regard, the electrostatic interactions at the surface of the lipid membranes play a crucial role resulting into binding of proteins and peptides to membranes [138]. The protein structure largely determines the interaction of lipids and amino acids in the membrane core having a hydrophobic environment or at the interface of the membrane.

The charge of the residues is another important factor which helps with the functions of the membrane proteins. It depends on the position of the residues inside or on the surface of the lipid membrane, which may affect the pKa of the amino acids as a result of the surrounding microenvironment [135]. The interaction of amino acids affects the lipid fluidity and stability and thus its behavior. Thus, understanding the partitioning of amino acid side chains into lipid bilayer is important for understanding the thermodynamics of membrane protein structure and stability. It is also important to understand the subsequent effect of side chain length, backbone spacing and their stereochemistry on the interaction strength [139].

The perturbing effects arising from the interaction of biomolecules (amino acids, proteins and peptides) with biological as well as model membranes are important to understand. Therefore, their physical and biochemical aspects must be analyzed at the molecular level. Since these moieties are largely present inside the body, the understanding of such interactions is important to analyze in order to realize

their impact on several cellular processes. These studies help in the advancement and understanding of underlying diseases and malfunctioning of cellular activities and the root cause of it.

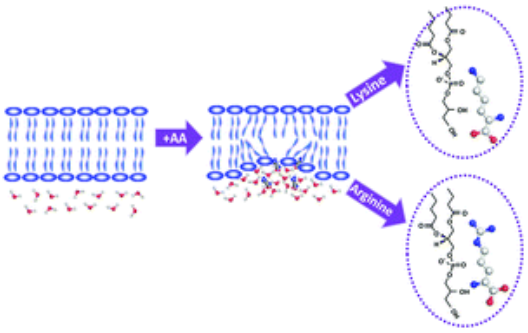

Figure 1.7 *Interaction of amino acids (lysine/arginine) with lipid bilayer (d-DMPG) and their specific binding sites indicating that different amino acids can perturb membrane dynamics differently [140].*

1.5 Motivation and organization of the thesis

Interaction of biomimetic lipid vesicles with external moieties has led to the formation of hybrid nano-bio systems, which have found applications in several biological fields over the past few years. These systems can result into superior models than bare lipid vesicles due to better stability imparted as a result of interactions taking place at their interface. The aim of the research works included in this thesis is to explore the interaction behavior of different nanoparticles, including carbon dots and biomolecules with lipid vesicles based on the different properties of these interactive species. The binding interactions were explored based on different features such as size, surface ligands, hydrophobicity, charge, bulkiness, isomeric precursor etc. The binding behavior was investigated for their potential to stabilize the fusion prone vesicles, resulting into the development of better model systems for drug delivery and bio-imaging. Moreover, in lieu of the complex composition of cell membranes, the interaction behavior of biomolecules was explored using these model membranes. The interactions account for the mechanism of membrane protein interactions with biological membranes. These systems help in understanding the mechanisms involved in cellular processes and

serve to bridge the gap between in vivo and in vitro systems. The following section provides a brief description of the contents and organization of the thesis:

Chapter 2 explores the interactions of lipid vesicles with gold nanoparticles (AuNPs) functionalized with different surface ligands based on their bulkiness and charge. AuNPs were functionalized with anionic ligands citrate, 3-mercaptopropionic acid, glutathione, and cationic ligand cysteamine. AuNPs were observed to bring in stability to the lipid vesicle, but the interaction strength differed with the different surface ligands. AuNPs functionalized with smaller ligands effectively increased the phase-transition temperature of the vesicles and stabilized them. However, the bulkier ligands exerted less van der Waals force, resulting in a weaker interaction. Anionic nanoparticles were found to interact stronger than cationic nanoparticles. The interactions were more strongly pronounced near the phase-transition temperature of the lipid. These surface interactions between bilayer AuNPs were found to effectively stabilize the bilayer. The interactions resulted in biocompatible systems capable of being employed for bioinspired applications, such as imaging, drug delivery, biosensing, etc.

Chapter 3 demonstrates that the interactions of carboxyl-modified gold nanoparticles (AuC) with zwitterionic phospholipid lipid vesicles of different chain lengths (DPPC, DMPC, DLPC) bring in stability toward the vesicles by local gelation. These lipids were chosen because of their widely different phase transition temperatures. The effect of lipid fluidity was explored for the interaction behaviour. The bound AuC were found to detach from the surface of the vesicles under acidic conditions due to protonation of the carboxyl group. The detachment rate of AuC from the vesicle−AuC assemblies varied with fluidity of the lipid vesicles. The system was explored for the controlled release of a prominent anticancer drug Doxorubicin (DOX) under acidic conditions. The drug release rate was optimized by formation of lipid-based capsule structures following layer-by-layer method. This was achieved by coating the vesicle−AuC assemblies with alternating layers of oppositely charged polymer and lipid. The

lipid-based capsule system was highly stable for weeks and inhibited premature release of the drug.

Chapter 4 discusses the employment of c-dots as fluorescent probes to study their interaction with lipid membrane. The interaction of zwitterionic lipid membrane with photoluminescent c-dots derived from different isomeric (ortho, meta and para) precursors of phenylenediamine (PDA) was investigated. The interaction behavior was found to be dependent on the properties of the isomeric precursors of c-dots. The lipid vesicles retained their morphology upon interaction with otho C-dots (oCD), which were found to be selectively embedded inside the lipid vesicles. On the contrary, meta and para C-dots (mCD and pCD) being located in the interfacial region induced aggregation in the vesicles. Thus, only c-dots synthesized from ortho isomer could effectively be used for bioimaging purpose.

Chapter 5 explores the interactions of lipid bilayers of different charges and different phase states with aliphatic amino acids of varying charge (aspartic acid, glutamic acid, arginine and lysine) and hydrophobicity (serine, leucine and valine). The negatively charged amino acids were found to interact strongly and stabilized the lipid membranes, particularly negatively charged membranes. On the other hand, positively charged amino acids were found to bring in hydration in the membranes. The hydrogen bonding played a significant role in governing the interaction of aliphatic amino acids with zwitterionic lipid membranes. The more polar serine bearing a hydroxyl group at the terminal carbon offered a stronger interaction with the lipid bilayer membranes as compared to its hydrophobic analogues leucine and valine. The interactions account for the binding phenomena of membrane proteins with biological membranes.

1.6 References

1. van Meer, G., Voelker, D. R., Feigenson, G. W. (2008), Membrane lipids: where they are and how they behave. *Nat Rev Mol Cell Biol.,* 9, 112–124. (DOI: 10.1038/nrm2330)

2. Casares, D., Escribá, P. V., Rosselló, C. A. (2019), Membrane lipid composition: Effect on membrane and organelle structure, function and compartmentalization and therapeutic avenues. *Int J Mol Sci.,* 20, 2167. (DOI: 10.3390/ijms20092167)

3. Harayama, T., Riezman, H. (2018), Understanding the diversity of membrane lipid composition. *Nat. Rev. Mol. Cell Biol.,* 19, 281-296. (DOI:10.1038/nrm.2017.138)

4. Chan, Y.-H. M., Boxer, S. G. (2007), Model membrane systems and their applications. *Curr Opin Chem Biol.,* 11, 581–587. (DOI: 10.1016/j.cbpa.2007.09.020)

5. Siontorou, C. G., Nikoleli, G.-P., Nikolelis, D. P., Karapetis, S. K. (2017), Artificial lipid membranes: Past, present, and future. *Membranes,* 7, 1-24. (DOI:10.3390/membranes7030038)

6. Escribá, P. V., González-Ros, J. M., Goñi, F. M., Kinnunen, P. K., Vigh, L., Sánchez-Magraner, L., Fernández, A. M., Busquets, X., Horváth, I., & Barceló-Coblijn, G. (2008), Membranes: a meeting point for lipids, proteins and therapies. *J Cell Mol Med.*, 12, 829–875. (DOI: 10.1111/j.1582-4934.2008.00281.x)

7. Heberle, F. A., Pabst, G. (2017), Complex biomembrane mimetics on the sub-nanometer scale. *Biophys. Rev.*, 9, 353–373. (DOI: 10.1007/s12551-017-0275-5)

8. Salehi-Reyhani, A., Ces, O., Elani, Y. (2017), Artificial cell mimics as simplified models for the study of cell biology. *Exp. Biol. Med. (Maywood)*, 242, 1309–1317. (DOI: 10.1177/1535370217711441)

9. Peetla, C., Stine, A., Labhasetwar, V. (2009), Biophysical interactions with model lipid membranes: applications in drug discovery and drug delivery. *Mol Pharm.*, 6, 1264–1276. (DOI: 10.1021/mp9000662)

10. Rodriguez-Emmenegger, C., Xiao, Q., Kostina, N. Y., Sherman, S. E., Rahimi, K., Partridge, B. E., Li, S., Sahoo, D., Perez, A. M. R., Buzzacchera, I., Han, H., Kerzner, M., Malhotra, I., Möller, M., Wilson, C. J., Good, M. C., Goulian, M., Baumgart, T., Klein, M. L., Percec, V. (2019), Encoding biological recognition in a bicomponent cell-membrane mimic. *Proc. Natl. Acad. Sci. U.S.A.*, 116, 5376-5382. (DOI: 10.1073/pnas.1821924116)

11. Berg, J. M., Tymoczko, J. L., Stryer, L. (2002), *Biochemistry*, 5th edition. New York: W H Freeman. Section 12.3, There are three common types of membrane lipids. (Available from: https://www.ncbi.nlm.nih.gov/books/NBK22361/)

12. Hu, W., Haddad, P. R., Hasebe, K., Mori, M., Tanaka, K., Ohno, M., Naoki Kamo, N. (2002), Use of a biomimetic chromatographic stationary phase for study of the interactions occurring between inorganic anions and phosphatidylcholine membranes. *Biophys. J.*, 83, 3351–3356. (DOI: 10.1016/S0006-3495(02)75335-6).

13. Mozsolits, H., Lee, T., Wirth, H., Perlmutter, P., Aguilar, M. (1999), The interaction of bioactive peptides with an immobilized phosphatidylcholine monolayer. *Biophys. J.*, 77, 1428–1444. (DOI: 10.1016/S0006-3495(99)76991-2)

14. Alberts, B., Johnson, A., Lewis, J., Raff, M., Roberts, K., Walter, P. (2002), Membrane proteins *Mol. Biol. Cell*, 4th edition. (Available from: https://www.ncbi.nlm.nih.gov/books/NBK26878/)

15. Fan, R., Gan, L., Liu, M., Zhu, D., Chen, L., Xu, Z., Hao, Z., Chen, L. (2011), An interaction of helicid with liposome biomembrane. *Appl. Surf. Sci.*, 257, 2102–2106. (DOI: 10.1016/j.apsusc.2010.09.057)

16. Luchini, A., Vitiello, G. (2019), Understanding the nano-bio interfaces: Lipid-coatings for inorganic nanoparticles as promising strategy for biomedical applications. *Front. Chem.*, 7, 343. (DOI: 10.3389/fchem.2019.00343)

17. Vargas, K. M., Shon , Y.-S. (2019), Hybrid lipid–nanoparticle complexes for biomedical applications. *J. Mater. Chem. B*, 7, 695-708. (DOI: 10.1039/C8TB03084G)

18. Rascol, E., Devoisselle, J.-M., Chopineau, J. (2016), The relevance of membrane models to understand nanoparticles–cell membrane interactions. *Nanoscale*, 8, 4780-4798. (DOI: 10.1039/C5NR07954C)

19. Schulz, M., Olubummo, A., Binder, W. H. (2012), Beyond the lipid-bilayer: Interaction of polymers and nanoparticles with membranes. *Soft Matter*, 8, 4849-4864. (DOI: 10.1039/C2SM06999G)

20. Zhao, H., Lappalainen, P. (2012), A simple guide to biochemical approaches for analyzing protein–lipid interactions. *Mol Biol Cell.*, 23, 2823–2830. (DOI: 10.1091/mbc.E11-07-0645)

21. Bechinger, B. (2008), A dynamic view of peptides and proteins in membranes. *Cell Mol. Life Sci.*, 65, 3028-39. (DOI: 10.1007/s00018-008-8125-z)

22. Jahn, R., Lang, T., Südhof, T. C. (2003), Membrane fusion. *Cell*, 112, 519-533. (DOI: 10.1016/S0092-8674(03)00112-0)

23. Jang, H.-S., (2017), The diverse range of possible cell membrane interactions with substrates: Drug delivery, interfaces and mobility. *Molecules*, 22, 2197. (DOI: 10.3390/molecules22122197)

24. Niemeyer, C. M., Mirkin, C. A. (2004), Nanobiotechnology: concepts, applications and perspectives. *Wiley-VCH*, Weinheim, Germany. (ISBN: 978-3-527-30658-9)

25. Peetla, C., Stine, A., Labhasetwar, V. (2009), Biophysical interactions with model lipid membranes: applications in drug discovery and drug delivery. *Mol Pharm.*, 6, 1264–1276. (DOI: 10.1021/mp9000662)

26. Bangham A. D., Standish M. M., Watkins J. C. (1965), Diffusion of univalent ions across the lamellae of swollen phospholipids. *J. Mol. Biol.*, 13, 238−252. (DOI: 10.1016/S0022-2836(65)80093-6)

27. Abu Lila A. S., Ishida, T. (2017), Liposomal delivery systems: Design optimization and current applications. *Biol Pharm Bull.,* 40, 1-10. (DOI: 10.1248/bpb.b16-00624)

28. Pattni B. S., Chupin V. V., Torchilin V. P. (2015), New developments in liposomal drug delivery. *Chemical Reviews*, 115, 10938-10966. (DOI: 10.1021/acs.chemrev.5b00046)

29. Israelachvili J. N., Marcelja S., Horn R. G. (1980), Physical principles of membrane organization. *Q. Rev. Biophys*., 13, 121−200. (PMID: 7015403)

30. Lasic D. D. (1998), Novel applications of liposomes. *Trends Biotechnol*., 16, 307−321. (PMID: 9675915)

31. Swaminathan J., Ehrhardt C. (2011), Liposomes for pulmonary drug delivery. *Controlled Pulmonary Drug Delivery*, 313-334. (DOI: 10.1007/978-1-4419-9745-6_14)

32. Chen, W., Duša, F., Witos, J., Ruokonen, S. K., and Wiedmer, S. K. (2018), Determination of the main phase transition temperature of phospholipids by nanoplasmonic sensing. *Sci. rep*., 8, 14815. (DOI: 10.1038/s41598-018-33107-5)

33. Noothalapati, H., Iwasaki, K., Yoshimoto, C., Yoshikiyo, k., Nishikawa, T., Ando, M., Hamaguchi, H., Yamamoto, T. (2017), Imaging phospholipid conformational disorder and packing in giant multilamellar liposome by confocal Raman microspectroscopy. *Spectrochim Acta A Mol Biomol Spectrosc.,* 187, 186-190. (DOI:10.1016/j.saa.2017.06.060)

34. Kinnunen, P. K. J. (1991), On the principles of functional ordering in biological membranes. *Chem. Phys. Lipids.,* 57, 375–399. (DOI: 10.1016/0009-3084(91)90087-R)

35. Rawicz, W., Olbrich, K. C., McIntosh, T., Needham, D., and Evans, E. (2000), Effect of chain length and unsaturation on elasticity of lipid bilayers. *Biophys J.*, 79. 328-39. (DOI: 10.1016/S0006-3495(00)76295-3)

36. Liu, W., Wang, Z., Fu, L., Leblanc, R. M., and Yan, E. C. Y. (2013), Lipid compositions modulate fluidity and stability of bilayers: Characterization by surface pressure and sum frequency generation spectroscopy. *Langmuir*, 29, 15022-15031. (DOI: 10.1021/la4036453)

37. Sahoo, S. K., Labhasetwar, V. (2003), Nanotech approaches to drug delivery and imaging. *Drug Discov Today*. 8, 1112-1120. (DOI: 10.1016/s1359-6446(03)02903-9)

38. Gabizon, A., Goren, D., Cohen, R., Barenholz, Y. (1998), Development of liposomal anthracyclines: from basics to clinical applications. *J Control Release*, 53, 275–279. (DOI: 10.1016/S0168-3659(97)00261-7)

39. Allen, T. M. (1997), Liposomes. Opportunities in drug delivery. *Drugs*, 54, Suppl 4, 8–14. (DOI: 10.2165/00003495-199700544-00004).

40. Akbarzadeh, A., Rezaei-Sadabady, R., Davaran, S., Joo, S. W., Zarghami, N., Hanifehpour, Y., Samiei, M., Kouhi, M., and Nejati-Koshki, K. (2013), Liposome: classification, preparation, and applications. *Nanoscale Res Lett.*, 8, 102. (DOI: 10.1186/1556-276X-8-102)

41. Wang, N., Chen, M., Wang, T. (2019), Liposomes used as a vaccine adjuvant-delivery system: From basics to clinical immunization. *J Control Release*, 303, 130-150. (DOI: 10.1016/j.jconrel.2019.04.025)

42. Zhu, Y., Negmi, A., Moran-Mirabal, J. (2015), Multi-stacked supported lipid bilayer micropatterning through polymer stencil lift-off. *Membranes*, 5, 385–398. (DOI: 10.3390/membranes5030385)

43. Amarnath. S., Sharma, U. S. (1997), Liposomes in drug delivery: progress and limitations. *Int J Pharm*, 154, 123–140. (DOI: 10.1016/S0378-5173(97)00135-X)

44. Nagle, J. F., Tristram-Nagle, S. (2000), Structure of lipid bilayers. *Biochimica et biophysica acta*, 1469, 159–195. (DOI: 10.1016/s0304-4157(00)00016-2)

45. Pandey, H., Rani, R., Agarwal, V. (2016), Liposome and their applications in cancer therapy. *Braz. arch. biol. technol*., 59, 1-10. (DOI: 10.1590/1678-4324-2016150477)

46. Escribá, P. V., González-Ros, J. M., Goñi, F. M., Kinnunen, P. K. J., Vigh, L., Asia, L. S. -M., Fernández, M., Busquets, X., Horváth, I., Barceló-Coblijn, G. (2008), Membranes: a meeting point for lipids, proteins and therapies. *J. Cell Mol. Med.*, 12, 829–875. (DOI: 10.1111/j.1582-4934.2008.00281.x)

47. Cooper, G. M. (2000), The cell: a molecular approach. 2nd edition. Sunderland (MA): Sinauer Associates. *Cell Membranes*. Available from: https://www.ncbi.nlm.nih.gov/books/NBK9928/

48. Enkavi, G., Javanainen, M., Kulig, W., Róg, T., Vattulainen, I. (2019), Multiscale simulations of biological membranes: The challenge to understand biological phenomena in a living substance. *Chem. Rev.*, 119, 9, 5607–5774. (DOI: 10.1021/acs.chemrev.8b00538)

49. Watson, H. (2015), Biological membranes. *Essays Biochem*, 59, 43–69. (DOI: 10.1042/bse0590043)

50. Casares, D., Escribá, P. V., Rosselló, C. A. (2019), Membrane lipid composition: Effect on membrane and organelle structure, function and compartmentalization and therapeutic avenues. *Int J Mol Sci*., 20, 2167. (DOI: 10.3390/ijms20092167)

51. Alberts, B., Johnson, A., Lewis, J., Raff, M., Roberts, K., and Walter, P. (2002), Molecular Biology of the Cell. 4th edition. New York: Garland Science. The Lipid Bilayer. Available from: www.ncbi.nlm.nih.gov/books/ NBK26871.

52. Lin, Q., London, E. (2014), Preparation of artificial plasma membrane mimicking vesicles with lipid asymmetry. *PLoS ONE*, 9, e87903. (DOI: 10.1371/journal.pone.0087903)

53. Muro, E., Atilla-Gokcumen, G. E., Eggert, U. S. (2014), Lipids in cell biology: how can we understand them better? *Mol Biol Cell.*, 25, 1819–1823. (DOI: 10.1091/mbc.E13-09-0516)

54. Fahy, E., Cotter, D., Sud, M., Subramaniam, S. (2011), Lipid classification, structures and tools. *Biochim. Biophys. Acta,*, 1811, 637-647. (DOI: 10.1016/j.bbalip.2011.06.009)

55. Brodland, G. W. (2015), How computational models can help unlock biological systems. *Semin. Cell Dev. Biol.*, 47–48, 62-73. (DOI: 10.1016/j.semcdb.2015.07.001)

56. Schubert, T., Römer, W. (2015), How synthetic membrane systems contribute to the understanding of lipid-driven endocytosis. *Biochim. Biophys. Acta - Molecular Cell Research*, 1853, 2992-3005. (DOI: 10.1016/j.bbamcr.2015.07.014)

57. Oshima, A., and Sumitomo, K. (2017), Vesicle fusion with bilayer lipid membrane controlled by electrostatic interaction. *Biochem Biophys Rep*. 11, 58–63. (DOI: 10.1016/j.bbrep.2017.06.003)

58. Escriba, P. V., Gonzalez-Ros, J. M., Goni, F. M., Kinnunen, P. K., Vigh, L., Sanchez-Magraner, L., Fernandez, A. M., Busquets, X., Horvath, I., Barcelo-Coblijn, G. (2008), Membranes: a meeting point for lipids, proteins and therapies. *J Cell Mol Med*., 12, 829–875. (DOI: 10.1111/j.1582-4934.2008.00281.x)

59. Çağdaş, M., Sezer, A. D., and Bucak, S. (2014), Liposomes as potential drug carrier systems for drug delivery. *Application of Nanotechnology in Drug Delivery*, (DOI: 10.5772/58459)

60. Pinheiro, M., Lúcio, M., Lima, J. L. F. C., Reis, S. (2011), Liposomes as drug delivery systems for the treatment of TB. *Nanomedicine*, 6, 1413-1428. (DOI: 10.2217/nnm.11.122)

61. Rabanel, J. M., Latreille, P. L., Lalloz, A., Hildgen, P., and Banquy, X. (2017), Nanostructured nanoparticles for improved drug delivery. *Nanostructures for Drug Delivery*, 149–182. (DOI:10.1016/b978-0-323-46143-6.00004-x)

62. Cevc, G., Richardsen, H. (1999), Lipid vesicles and membrane fusion. *Adv. Drug Deliv. Rev.*, 38, 207–232. (DOI: 10.1016/S0169-409X(99)00030-7)

63. Chernomordik, L. V., Kozlov, M. M. (2008), Mechanics of membrane fusion, *Nat Struct Mol Biol.*, 15, 675–683. (DOI: 10.1038/nsmb.1455)

64. Wang, H., Zhang, C., Xiao, H. (2019), Mechanism of membrane fusion: protein-protein interaction and beyond. *Int. J. Physiol. Pathophysiol. Pharmacol.*, 11, 250–257. (PMID: 31993099)

65. van Uitert, I., Le Gac, S., van der Berg, A. (2010), The influence of different membrane components on the electrical stability of bilayer lipid membranes. *Biochim. Biophys. Acta*.- Biomembranes, 1798, 21-31. (DOI: 10.1016/j.bbamem.2009.10.003)

66. Petralito, S., Paolicelli, P., Nardoni, M., Trilli, J., Di Muzio, L., Cesa, S., Relucenti, M., Matassa, R., Vitalone, A., Adrover, A., Antonietta Casadei, M. (2020), Gelation of the internal core of liposomes as a strategy for stabilization and modified drug delivery I. Physico-chemistry study. *Int. J. Pharm*., 585, 119467. (DOI: 10.1016/j.ijpharm.2020.119467)

67. Pichler, H., Emmerstorfer-Augustin, A. (2018), Modification of membrane lipid compositions in single-celled organisms – From basics to applications. *Methods*, 147, 50-65. (DOI: 10.1016/j.ymeth.2018.06.009)

68. Nazemidashtarjandi, S., Vahedi, A., and Farnoud, A. M. (2020), Lipid chemical structure modulates the disruptive effects of nanomaterials on membrane models. *Langmuir*, 36, 4923-4932. (DOI: 10.1021/acs.langmuir.0c00295)

69. Lakowicz, J. R. (1999), Principles of fluorescence spectroscopy. Kluvert Academic/Plenum Publishers, New York, NY, USA. (ISBN: 978-0-387-46312-4)

70. Cwiklik, L., Aquino, A. J. A., Vazdar, M., Jurkiewicz, P., Pittner, J., Hof, M., and Lischka, H. (2011), Absorption and fluorescence of PRODAN in phospholipid bilayers: a combined quantum mechanics and classical molecular dynamics study. *J Phys Chem A*, 115, 11428–11437. (DOI: 10.1021/jp205966b)

71. Bagatolli, L. A. (2012), LAURDAN fluorescence properties in membranes: a journey from the fluorometer to the microscope, in *Fluorescent Methods to Study Biological Membranes*, 3–35, Springer, Berlin, Heidelberg.

72. Gasymov, O. K., and Glasgow, B. J. (2007), ANS fluorescence: potential to augment the identification of the external binding sites of proteins. *Biochim. Biophys. Acta.*, 1774, 403–411. (DOI: 10.1016/j.bbapap.2007.01.002)

73. Albani, J.-R. (2008), Fluorescence origin of 6, P-toluidinylnaphthalene-2-sulfonate (TNS) bound to proteins. *J. Fluoresc.*, 19, 399–408. (DOI: 10.1007/s10895-008-0426-y)

74. Bagatolli, L. A., and Gratton, E. (2000), Two photon fluorescence microscopy of coexisting lipid domains in giant unilamellar vesicles of binary phospholipid mixtures. *Biophys J.*, 78, 290–305. (DOI: 10.1016/S0006-3495(00)76592-1)

75. Malacrida, L., Astrada, S., Briva, A., Bollati-Fogol´ın, M., Gratton, E., and Bagatolli, L. A. (2016), Spectral phasor analysis of LAURDAN fluorescence in live A549 lung cells to study the hydration and time evolution of intracellular lamellar bodylike structures. *Biochim. Biophys. Acta.*- Biomembranes, 1858, 2625–2635. (DOI: 10.1016/j.bbamem.2016.07.017)

76. Watanabe, N., Suga, K., and Umakoshi, H. (2019), Functional hydration behavior: Interrelation between hydration and molecular properties at lipid membrane interfaces. *Journal of Chemistry*, 2019, 1-15. (DOI: 10.1155/2019/4867327)

77. Rascol, E., Devoisselle, J.-M., Chopineau, J. (2016), The relevance of membrane models to understand nanoparticles–cell membrane interactions. *Nanoscale*, 8, 4780-4798. (DOI: 10.1039/C5NR07954C)

78. Patra, J. K., Das, G., Fraceto, L. F., Campos, E. V. R., Rodriguez-Torres, M. del P., Acosta-Torres, L. S., Diaz-Torres, L. A., Grillo, R., Swamy, M. K., Sharma, S., Habtemariam, S., Shin, H.-S. (2018), Nano based drug delivery systems: recent developments and future prospects. *J Nanobiotechnol.*, 16, 71. (DOI: 10.1186/s12951-018-0392-8)

79. Mashaghi, S., Jadidi, T., Koenderink, G., Mashaghi, A. (2013), Lipid Nanotechnology. *Int J Mol Sci.*, 14, 4242–4282. (DOI: 10.3390/ijms14024242)

80. García-Pinel, B., Porras-Alcalá, C., Ortega-Rodríguez, A., Sarabia, F., Prados, J., Melguizo, C., López-Romero, J. M. (2019), Lipid-based nanoparticles: application and recent advances in cancer treatment. *Nanomaterials (Basel)*, 9, 638. (DOI: 10.3390/nano9040638)

81. Senapati, S., Mahanta, A. K., Kumar, S., Maiti, P. (2018), Controlled drug delivery vehicles for cancer treatment and their performance. *Sig. Transduct. Target. Ther.*, 3, 7. (DOI: 10.1038/s41392-017-0004-3)

82. Tzakos, A. G., Briasoulis, E., Thalhammer, T., Jäger, W., Apostolopoulos, V. (2013), Novel oncology therapeutics: Targeted drug delivery for cancer. *J. Drug Deliv.*, 2013, 1-9. (DOI: 10.1155/2013/918304)

83. Jaishree, V., Gupta, P. D. (2012), Nanotechnology: A revolution in cancer diagnosis. *Indian J Clin Biochem.*, 27, 214–220. (DOI: 10.1007/s12291-012-0221-z)

84. Farka, Z., Juřík, T., Kovář, D., Trnková, L., Skládal, P. (2017), Nanoparticle-based immunochemical biosensors and assays: Recent advances and challenges. *Chem. Rev.*, 117, 15, 9973–10042. (DOI: 10.1021/acs.chemrev.7b00037)

85. Huang, X., Liu, Y., Yung, B., Xiong, Y., Chen, X. (2017), Nanotechnology-enhanced no-wash biosensors for in vitro diagnostics of cancer. *ACS Nano*, 11, 6, 5238–5292. (DOI: 10.1021/acsnano.7b02618)

86. Vashist, S. K., Venkatesh, A. G., Mitsakakis, K., Czilwik, G., Roth, G., von Stetten, F., Zengerle, R. (2012), Nanotechnology-based biosensors and

diagnostics: Technology push versus industrial/healthcare requirements. *BioNanoSci.* 2, 115–126. (DOI: 10.1007/s12668-012-0047-4)

87. Singh, P., Pandit, S., Mokkapati, V. R. S. S., Garg, A., Ravikumar, V., Mijakovic, I. (2018), Gold nanoparticles in diagnostics and therapeutics for human cancer. *Int J Mol Sci.*, 19, 1979. (DOI: 10.3390/ijms19071979)

88. Cai, W., Gao, T., Hong, H., Sun, J. (2008), Applications of gold nanoparticles in cancer nanotechnology. *Nanotechnol Sci Appl.*, 1, 17–32. (DOI: 10.2147/NSA.S3788)

89. De Jong, W. H., Borm, P. J. (2008), Drug delivery and nanoparticles: Applications and hazards. *Int J Nanomedicine.*, 3, 133–149. (DOI: 10.2147/ijn.s596)

90. Alkilany, A. M., Murphy, C. J. (2010), Toxicity and cellular uptake of gold nanoparticles: what we have learned so far? *J Nanopart Res.*, 12, 2313–2333. (DOI: 10.1007/s11051-010-9911-8)

91. Kim, C. K., Ghosh, P., Rotello, V. M. (2009), Multimodal drug delivery using gold nanoparticles. *Nanoscale*, 1, 61-67. (DOI: 10.1039/B9NR00112C)

92. Al-Jamal, W. T., Kostarelos, K. (2007), Liposome-nanoparticle hybrids for multimodal diagnostic and therapeutic applications. *Nanomedicine (Lond).*, 2, 85-98. (DOI:10.2217/17435889.2.1.85)

93. Thomas, J. A. (2015), Optical imaging probes for biomolecules: an introductory perspective. *Chem. Soc. Rev.*, 44, 4494-4500. (DOI: 10.1039/C5CS00070J)

94. Wang, E. C., Wang, A. Z. (2014), Nanoparticles and their applications in cell and molecular biology. *Integr Biol (Camb).*, 6, 9–26. (DOI: 10.1039/c3ib40165k)

95. Vargas, K. M., Shon, Y.-S. (2019), Hybrid lipid–nanoparticle complexes for biomedical applications. *J. Mater. Chem. B*, 7, 695-708. (DOI: 10.1039/c8tb03084g)

96. Liu, J. (2016), Interfacing zwitterionic liposomes with inorganic nanomaterials: surface forces, membrane integrity and applications. *Langmuir*, 32, 4393–4404. (DOI: 10.1021/acs.langmuir.6b00493)

97. Semeniuk, M., Yi, Z., Poursorkhabi, V., Tjong, J., Jaffer, S., Lu, Z.-H., Sain, M. (2019), Future perspectives and review on organic carbon dots in electronic applications. *ACS Nano*, 13, 6224–6255. (DOI: 10.1021/acsnano.9b00688)

98. Wang, X., Feng, Y., Dong, P., Huang. J. (2019), A mini review on carbon quantum dots: Preparation, properties, and electrocatalytic application. *Front. Chem.*, 7, 671. (DOI: 10.3389/fchem.2019.00671)

99. Xia, C., Zhu, S., Feng, T., Yang, M., Yang, B. (2019), Evolution and synthesis of carbon dots: From carbon dots to carbonized polymer dots. *Adv. Sci.*, 6, 1901316. (DOI: 10.1002/advs.201901316)

100. Yao, B., Huang, H., Liu, Y., Kang, Z. (2019), Carbon dots: A small conundrum. *Trends Chem.*, 1, 235-246. (DOI: 10.1016/j.trechm.2019.02.003)

101. Lim, S. Y., Shen, W., Gao, Z. (2015), Carbon quantum dots and their applications. *Chem. Soc. Rev.*, 44, 362–381. (DOI: 10.1039/c4cs00269e)

102. Xu, X. Y., Ray, R., Gu, Y. L., Ploehn, H. J., Gearheart, L., Raker, K., Scrivens, W. A. (2004), Electrophoretic analysis and purification of fluorescent single-walled carbon nanotube fragments. *J. Am. Chem. Soc.*, 126, 12736–12737. (DOI: 10.1021/ja040082h)

103. Yuan, F., Li, S., Fan, Z., Meng, X., Fan, L., Yang, S. (2016), Shining carbon dots: synthesis and biomedical and optoelectronic applications. *Nano Today*, 11, 565–586. (DOI: 10.1016/j.nantod.2016.08.006)

104. Yuan, T., Meng, T., He, P., Shi, Y., Li, Y., Li, X., Fan, L., Yang, S. (2019), Carbon quantum dots: an emerging material for optoelectronic applications. *J. Mater. Chem. C*, 7, 6820–6835. (DOI: 10.1039/C9TC01730E)

105. Sun, X., Lei, Y. (2017), Fluorescent carbon dots and their sensing applications. *TrAC Trend. Anal. Chem.*, 89, 163–180. (DOI: 10.1016/j.trac.2017.02.001)

106. Sciortino, A., Cannizzo, A., Messina, F. (2018), Carbon nanodots: A review—from the current understanding of the fundamental photophysics to the full control of the optical response. *C*, *4*, 1-35. (DOI: 10.3390/c4040067)

107. Liu, M. L., Chen, B. B., Li, C. M., Huang, C. Z. (2019), Carbon dots: synthesis, formation mechanism, fluorescence origin and sensing applications. *Green Chem.*, *21*, 449-471. (DOI: 10.1039/C8GC02736F)

108. Semeniuk, M., Yi, Z., Poursorkhabi, V., Tjong, J., Jaffer, S., Lu, Z.-H., Sain, M. (2019), Future perspectives and review on organic carbon dots in electronic applications. *ACS Nano*, *13*, 6224-6255. (DOI: 10.1021/acsnano.9b00688)

109. Li, M., Chen, T., Gooding, J. J., Liu, J. (2019), Review of carbon and graphene quantum dots for sensing. *ACS Sens.*, *4*, 1732-1748. (DOI: 10.1021/acssensors.9b00514)

110. Wang, X., Feng, Y., Dong, P., Huang, J. (2019), A mini review on carbon quantum dots: Preparation, properties, and electrocatalytic application. *Front. Chem.*, *7*, 1-9. (DOI: 10.3389/fchem.2019.00671)

111. Song, L., Cui, Y., Zhang, C., Hu, Z., Liu, X. (2016), Microwave-assisted facile synthesis of yellow fluorescent carbon dots from o-phenylenediamine for cell imaging and sensitive detection of Fe^{3+} and H_2O_2. *RSC Adv.*, *6*, 17704-17712. (DOI: 10.1039/C6RA02554D)

112. Jiang, K., Sun, S., Zhang, L., Lu, Y., Wu, A., Cai, C., Lin, H. (2015), Red, green, and blue luminescence by carbon dots: Full-color emission tuning and multicolor cellular imaging. *Angew. Chem. Int. Ed.*, *54*, 5360 –5363. (DOI: 10.1002/anie.201501193)

113. Kudr, J., Richtera, L., Xhaxhiu, K., Hynek, D., Heger, Z., Zitka, O., Adam, V. (2017), Carbon dots based FRET for the detection of DNA damage. *Biosens. Bioelectron., 92,* 133–139. (DOI: 10.1016/j.bios.2017.01.067)

114. Hsu, C. -P., Hejazi, Z., Armagan, E., Zhao, S., Schmid, M., Zhang, H., Guo, H., Weidenbacher, L., Rossi, R. M., Koebel, M. M., Boesel, L. F., Toncelli, C. (2017), Carbon dots and fluorescein: The ideal FRET pair for the fabrication of a precise and fully reversible ammonia sensor. *Sensor Actuat. B-Chem., 253,* 714–722. (DOI: 10.1016/j.snb.2017.07.001)

115. Sidhu, J. S., Singh, A., Garg, N., Singh, N. (2017), Carbon dot based, naphthalimide coupled FRET pair for highly selective ratiometric detection of thioredoxin reductase and cancer screening. *ACS Appl. Mater. Interfaces*, *9*, 25847−25856. (DOI: 10.1021/acsami.7b07046)

116. Dong, W., Wang, R., Gong, X., Dong, C. (2019), An efficient turn-on fluorescence biosensor for the detection of glutathione based on FRET between N, S dual-doped carbon dots and gold nanoparticles. *Anal. Bioanal. Chem., 411*, 6687–6695. (DOI: 10.1007/s00216-019-02042-3)

117. Essner, J. B., Baker, G. A. (2017), The emerging roles of carbon dots in solar photovoltaics: a critical review. *Environ. Sci.: Nano*, *4*, 1216-1263. (DOI: 10.1039/C7EN00179G)

118. Narayanan, R., Deepa, M., Srivastava, A. K. (2013), Förster resonance energy transfer and carbon dots enhance light harvesting in a solid-state quantum dot solar cell. *J. Mater. Chem. A, 1*, 3907-3918. (DOI: 10.1039/C3TA01601C)

119. Miao, S., Liang, K., Kong, B. (2020), Förster resonance energy transfer (FRET) paired carbon dot-based complex nanoprobes: versatile platforms for sensing and imaging applications. *Mater. Chem. Front., 4*, 128-139. (DOI: 10.1039/C9QM00538B)

120. Song, Y., Zhu, S., Yang, B. (2014), Bioimaging based on fluorescent carbon dots. *RSC Adv., 4*, 27184-27200. (DOI: 10.1039/C3RA47994C)

121. Ding, H., Yu, S.-B., Wei, J.-S., Xiong, H.-M. (2016), Full-color light-emitting carbon dots with a surface-state-controlled luminescence mechanism. *ACS Nano*, *10*, 484-491. (DOI: 10.1021/acsnano.5b05406)

122. Yang, S., Sun, J., Li, X., Zhou, W., Wang, Z., He, P., Ding, G., Xie, X., Kang, Z., Jiang, M. (2014), Large-scale fabrication of heavy doped carbon quantum dots with tunable-photoluminescence and sensitive fluorescence detection. *J. Mater. Chem. A*, 2, 8660–8667. (DOI: 10.1039/c4ta00860j)

123. Jiang, K., Zhang, L., Lu, J., Xu, C., Cai, C., Lin, H. (2016), Triple-mode emission of carbon dots: Applications for advanced anti-counterfeiting. *Angew. Chem. Int. Ed.*, 55, 7231-7235. (DOI: 10.1002/anie.201602445)

124. Li, J., Wang, B., Zhang, H., Yu, J. (2019), Carbon dots-in-matrix boosting intriguing luminescence properties and applications. *Small*, 15, 1805504. (DOI: 10.1002/smll.201805504)

125. Kong, B., Zhu, A., Ding, C., Zhao, X., Li, B., Tian, Y. (2012), Carbon dot-based inorganic-organic nanosystem for two-photon imaging and biosensing of pH variation in living cells and tissues. *Adv Mater.*, 24, 5844-5848. (DOI: 10.1002/adma.201202599)

126. Liang, Z., Kang, M., Payne, G. F., Wang, X., Sun, R. (2016), Probing energy and electron transfer mechanisms in fluorescence quenching of biomass carbon quantum dots. *ACS Appl. Mater. Interfaces*, *8*, 17478−17488. (DOI: 10.1021/acsami.6b04826)

127. Pritzl, S. D., Pschunder, F., Ehrat, F., Bhattacharyya, S., Lohmüller, T., Huergo, M. A., Feldmann, J. (2019), Trans-membrane Fluorescence Enhancement by Carbon Dots: Ionic Interactions and Energy Transfer. *Nano Lett.*, *19*, 3886−3891. (DOI: 10.1021/acs.nanolett.9b01071)

128. Klymchenko, A. S., Kreder, R. (2014), Fluorescent probes for lipid rafts: From model membranes to living cells. *Chem. Biol.*, *21*, 97-113. (DOI: 10.1016/j.chembiol.2013.11.009)

129. Maekawa, M., Fairn, G. D. (2014), Molecular probes to visualize the location, organization and dynamics of lipids. *J. Cell Sci.*, *127*, 4801–4812. (DOI: 10.1242/jcs.150524)

130. Faller, R. (2016), Molecular modeling of lipid probes and their influence on the membrane. *Biochim. Biophys. Acta*, *1858*, 2353–2361. (DOI: 10.1016/j.bbamem.2016.02.014)

131. Akhunzada, M. J., D'Autilia, F., Chandramouli, B., Bhattacharjee, N., Catte, A., Rienzo, R. D., Cardarelli, F., Brancato, G. (2019), Interplay between lipid lateral diffusion, dye concentration and membrane permeability unveiled by a combined spectroscopic and computational study of a model lipid bilayer. *Sci. Rep.*, *9*, 1-12. (DOI: 10.1038/s41598-018-37814-x)

132. Nandi, S., Malishev, R., Bhunia, S. K., Kolusheva, S., Jopp, J., Jelinek, R. (2016), Lipid-bilayer dynamics probed by a carbon dot- phospholipid conjugate. *Biophys. J.*, *110*, 2016–2025. (DOI: 10.1016/j.bpj.2016.04.005)

133. Nandi, S., Malishev, R., Kootery, K. P., Mirsky, Y., Kolusheva, S., Jelinek, R. (2014), Membrane analysis with amphiphilic carbon dots. *Chem. Commun.*, *50*, 10299-10302. (DOI: 10.1039/C4CC03504F)

134. Wang, Q., Chao, Y.-M. (2018), Multifunctional quantum dots and liposome complexes in drug delivery. *J Biomed Res.*, 32, 91-106. (DOI: 10.7555/JBR.31.20160146)

135. Panahi, A., Brooks III, C. L. (2015), Membrane environment modulates the pka values of transmembrane helices. *J. Phys. Chem. B*, 119, 4601−4607. (DOI: 10.1021/acs.jpcb.5b00289)

136. Funari, S. S., Prades, J., Escribá, P. V., Barceló, F. (2005), Farnesol and geranylgeraniol modulate the structural properties of phosphatidylethanolamine model membranes. *Mol Membr Biol.*, 22, 303–311. (DOI: 10.1080/09687860500135411)

137. Barceló, F., Prades, J., Encinar, J. A., Funari, S. S., Vögler, O., Gonzalez-Ros, J. M., Escribá, P.V. (2007), Interaction of the C-terminal region of the G{gamma} protein with model membranes. *Biophys J.*, 93, 2530–2541. (DOI: 10.1529/biophysj.106.101196)

138. Schwieger, C., Blume, A. (2007), Interaction of poly (L-lysines) with negatively charged membranes: an FT-IR and DSC study. *Eur Biophys J.*, 36, 437–450. (DOI: 10.1007/s00249-006-0080-8)

139. Schwieger, C., Blume, A. (2009), Interaction of poly (L-arginine) with negatively charged DPPG membranes: Calorimetric and monolayer studies. *Biomacromolecules*, 10, 2152–2161. (DOI: 10.1021/bm9003207)

140. Zhang, J., Yang, W., Tan, J., Ye, S. (2018), In situ examination of a charged amino acid-induced structural change in lipid bilayers by sum frequency generation vibrational spectroscopy. *Phys. Chem. Chem. Phys.*, 20, 5657-5665. (DOI: 10.1039/C7CP07389E)

Chapter 2

Effect of surface ligand and temperature on lipid vesicle−gold nanoparticle interaction

2.1 Introduction

The interaction of nanoparticles, polymers and metal ions with lipid membranes has been a subject of great interest in the recent past [1−8]. These interactions affect the membrane polarity, fluidity, order, phase transition and surrounding water content [1−12]. The introduction of guest molecules such as cholesterol and proteins modifies the membrane properties by bringing in stability and order [7−12]. Similarly, interactions between lipid bilayers and metal nanoparticles are particularly important as they usually result in distinctly biocompatible systems [13−18]. These systems have found applications in various fields like imaging, drug delivery, separation and biosensing [16−20]. The interaction of nanoparticles with lipid bilayers has been used to efficiently provide stability to the membrane [21−26].

Among the variety of these nanoparticles, gold nanoparticles (AuNPs) are of great significance. Their surface chemistry can be easily controlled by various capping agents, majorly with thiol ligands [27−30]. They are also known to exhibit a strong van der Waals interaction giving rise to strong physisorption [31]. The colloidal solution containing gold nanoparticles show inter particle distance-dependent color due to localized Surface Plasmon Resonance (SPR) coupling, which makes them easy to monitor visually [32-33]. Gold nanoparticles are known to have a strong tendency to interact with lipid membranes [34−43].

The bilayer membrane remains more intact and loses its tendency to fuse with one another when coated with nanoparticles with a high charge density, even when the nanoparticles adsorb onto the liposome surface up to 25% surface coverage [23]. This technique to stabilize the otherwise transient liposomes renders them useful

for several applications [44−48]. Considering the biocompatible nature and a vast range of applications of liposome−gold nanoparticle assemblies, their mode of interaction remains an area of interest. In this regard, the literature lacks systematic investigation regarding the interaction behaviour of nanoparticles based on their charge and surface ligands. Moreover, membrane fluidity and lipid headgroup play an important role in the binding phenomena. In this context, fluorescent molecular probes are of immense significance to monitor the changes in the membrane dynamics. Fluorescent probes are particularly sensitive to membrane polarity [49−58].

Therefore, we explored the interaction phenomena of zwitterionic phosphocholine (PC) and inverse phosphocholine (iPC) zwitterionic lipids with anionic and cationic gold nanoparticles functionalized with ligands of varying bulkiness. The binding was explored for varying fluidities of the membrane. The experimental results were explained under the framework of the existing theory. Here we used PC lipids DMPC (Tm = 24 °C), DOPC (Tm = −20 °C) and iPC lipid DOCP (Tm = −20 °C). We exploited the membrane probe PRODAN by using steady-state fluorescence and time-resolved spectroscopic techniques to unravel the interaction. We also conducted dynamic light scattering (DLS) and confocal laser scanning microscopy (CLSM) measurement to investigate the changes in the size and morphology of the membrane.

2.2 Results and Discussion

2.2.1 <u>Characterization of gold nanoparticles</u>: Three types of differently functionalized anionic gold nanoparticles were synthesized using surface ligands: citrate, (3-mercaptopropionic acid) MPA and (glutathione) GSH (Figure 2.1a). Anionic nanoparticles were obtained by the simple ligand exchange of citrate-capped AuNPs with MPA and GSH. Thus, they possess an identical core diameter. AuNPs were characterized by TEM, which reveals a narrow distribution with diameter of 12−14 nm (Figure 2.1b-c). The citrate group bound to AuNPs

can be easily replaced by thiol bearing ligands [27-28, 59-61]. The UV−vis absorption spectra reveal that the nanoparticle monodispersity is maintained after the ligand exchange (Figure 2.1d). Citrate-stabilized gold nanoparticles display a surface plasmon resonance (SPR) band at 521 nm, which is a characteristic of isolated spherical gold nanoparticles [29-30, 62-63]. A similar plasmon band is obtained for MPA-AuNP and GSH-AuNP without any shift in the SPR wavelength. This indicates that the AuNPs remain unaggregated and are highly stable. ζ potential measurements reveal that all of the synthesized nanoparticles are negatively charged (Figure 2.1e). The high surface potential prevents the AuNPs from undergoing any aggregation. Similarly, the cationic AuNPs were functionalized with cysteamine. They also show an SPR at 520 nm and indicate a size of 10−15 nm. ζ potential measurements reveal that the surface is positively charged. All of these nanoparticles obtained are water-soluble. They are stable in aqueous solutions with no aggregation observed for a period of 1 month when stored at 4 °C.

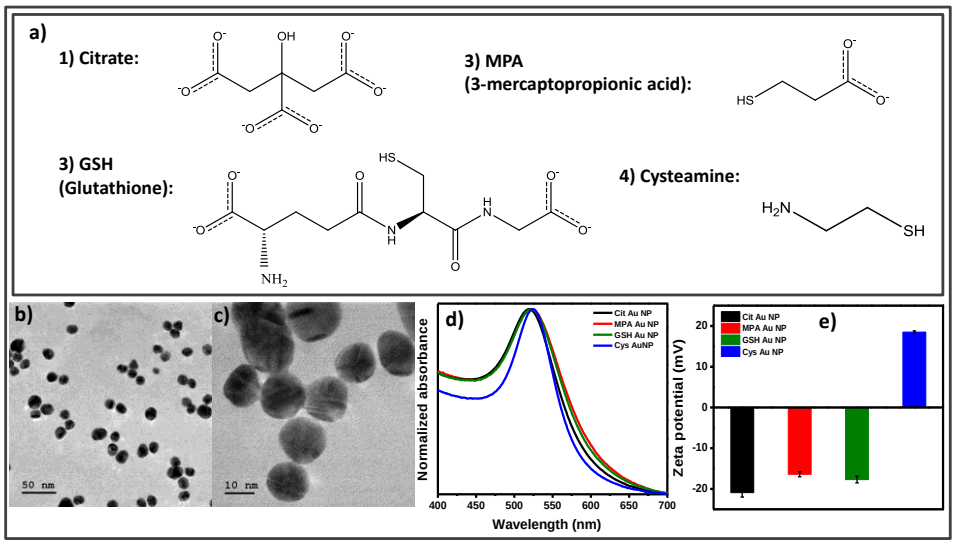

Figure 2.1 *Characterization of functionalized AuNPs. Chemical structures of the surface ligands used to functionalize AuNPs (a); representative TEM images of citrate AuNPs (b, c); UV−vis spectra (d); and ζ potential measurements of functionalized AuNPs (e).*

2.2.2 Interactions of gold nanoparticles with lipid vesicles using PRODAN:

The choice of PRODAN as a spectral probe lies in the fact that the spectral bands

can be distinctly assigned based on the polarity of the medium. PRODAN shows an emission at 527 nm in aqueous medium, which is assigned to charge-transfer (CT) state. There are some reports where this state has been assigned as a twisted intramolecular charge-transfer (TICT) state [64−66]. However, in the presence of less polar medium like lipid bilayer, another emission band arises at around 435−440 nm assigned to locally excited (LE) state. The LE band indicates that PRODAN is partitioned in lipid bilayer [64]. This interesting feature of PRODAN makes the spectral studies simpler to analyze.

Here, we used DMPC (T_m = 24 °C) to study the interaction with differently functionalized gold nanoparticles. It is revealed from Figure 2.2 that the emission spectra of PRODAN shifted to a shorter wavelength upon interaction of the lipid vesicle with all three anionic nanoparticles. The observed blue shift in the emission spectra is due to the dehydration of the lipid bilayer [5, 64]. The lipid undergoes a fluid-to-gel phase (Lα to Lβ) transition due to the adsorption of nanoparticles on the bilayer surface. This transition takes place locally at the point of contact of the nanoparticles. Initially, the head group of the zwitterionic lipid is roughly parallel to the bilayer surface. However upon addition of the nanoparticles, the head group tends to tilt so as to favor the interactions with the negatively charged AuNPs via the positively charged choline group [59]. The phosphorous−nitrogen (P−N) dipole in zwitterionic PC is usually tilted to an angle of about 30° in the Lβ phase from the parallel position (0−3°) in the fluid (Lα) phase [67]. This results in decrease in the in-plane elasticity of the lipid bilayer [68]. Thus, the adsorption of the anionic AuNPs on the zwitterionic lipid bilayer makes it much stiffer. However, the nature of the interaction depends on the surface charge of the nanoparticles. The anionic AuNPs interact only on the surface of the membrane resulting in dehydration rather than penetrating into the bilayer membrane [69].

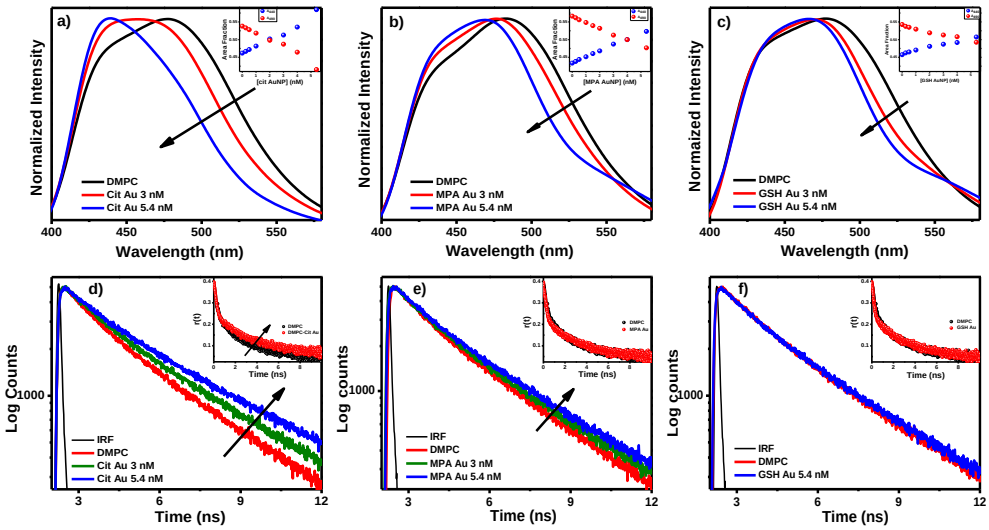

Figure 2.2 *Normalized emission spectra of PRODAN in DMPC solution as a function of AuNP concentration for (a) citrate AuNPs, (b) MPA-AuNPs and (c) GSH-AuNPs at 25 °C, and corresponding area fraction vs concentration of AuNPs plots shown in the insets. Representative time-resolved decay curves of PRODAN in DMPC−AuNPs (d−f) at 440 nm at 25 °C (anisotropy decays for adsorption are shown in the inset).*

Interestingly, a maximum blue shift in the emission spectra was observed for cit-capped AuNPs, followed by MPA-AuNPs and least in GSH-AuNPs. This indicates that the LE state of PRODAN is more pronounced in the case of the lipid vesicle interacting with citrate-capped AuNPs. This also indicates that lipid vesicles are least hydrated upon interaction with cit-AuNPs (inset of Figure 2.2 a−c). The AuNPs undergo physisorption on the surface of the lipid vesicles that exert a strong van der Waals force. The possibility of chemisorption is ruled out in the present case as chemical reaction does not take place between lipid head groups and ligands or nanoparticles [59].

The adsorption efficiency of all of the three anionic AuNPs differs from one another. The citrate-capped AuNPs distinctly affect the bilayer packing by exerting a relatively stronger van der Waals force to bring it to a stronger gel (Lβ) phase. MPA-capped AuNPs can still be efficiently absorbed owing to the small size of the ligand (~0.3 nm). However, the adsorption efficiency is reduced for more bulky GSH group. The bulky surface ligands separate the AuNP core from the bilayer surface, which results in a decrease in the van der Waals force between

the bilayer surface and the AuNP core [59]. The electrostatic interactions in case of the three AuNPs are nearly the same owing to their similar negative ζ potential. However, the bulkiness of the ligands plays a major role in the binding strength [59, 61]. The increasing bulkiness of the ligands causes steric hindrance. This results in increase in AuNP core distance from the bilayer head group. This reduces the interaction between lipid vesicles and incoming nanoparticles. In view of the fact that van der Waals forces are short-ranged interactions, any surface ligand that leads to even a small separation from the AuNP core is efficient enough to affect the adsorption strength.

We further conducted lifetime decays measurements to monitor the influence of the nanoparticles on the gelation of the lipid vesicles (Figure 2.2 d-f, Table 2.1). The observed lifetimes are biexponential, with a shorter component (τ_1) at around 1 ns and the longer component (τ_2) varying from 3 to 5 ns. Interestingly, τ_2 is the longest in the case of lipid vesicle bearing citrate-capped AuNPs, followed by MPA AuNPs and GSH-AuNPs. The longer component τ_2 increases from 3.83 to 5.15 ns upon addition of cit-AuNPs to DMPC bilayer, while the amplitude (a_1 and a_2) remains almost the same. This indicates that the adsorption of cit-AuNPs on the DMPC bilayer surface results in its stabilization [64]. Thus cit-capped AuNPs tend to bring DMPC in the gel (Lβ) phase more effectively. It offers a less hydrated environment to PRODAN due to increased rigidity as compared to AuNPs functionalized with bulkier ligands. This is also validated with anisotropy measurements which reveal that the rotational relaxation in DMPC bilayer becomes significantly slower upon adsorption of cit-AuNPs (Figure 2.2 d inset). However, we did not observe any significant changes in anisotropy decay upon addition of MPA or GSH-AuNPs to the DMPC bilayer (Figure 2.2e-f inset).

Table 2.1 *Lifetime components, normalized amplitudes of lifetime components and average lifetime of DMPC-PRODAN upon addition of AuNPs collected at 440 nm at 25 °C.*[#]

@440 nm, 25 °C						
Sample	**τ_1 (ns)**	**τ_2 (ns)**	**a_1**	**a_2**	**$\langle\tau_{avg}\rangle$ (ns)**	**χ^2**
DMPC	1.09	3.83	0.43	0.57	2.66	1.05

+ Cit-AuNP	1.55	5.15	0.42	0.58	3.63	1.10
+ MPA-AuNP	1.30	4.10	0.41	0.59	2.94	1.08
+ GSH-AuNPs	1.20	3.71	0.40	0.60	2.71	1.10

[#]*Experimental error is within ±10%.*

To discard the possibility of aggregation of the AuNPs on the lipid surface, we conducted UV−visible experiments. The spectra indicate that the adsorption of AuNPs on the vesicles takes place without any abnormal broadening or peak shift with an increase in concentration (Figure 2.3).

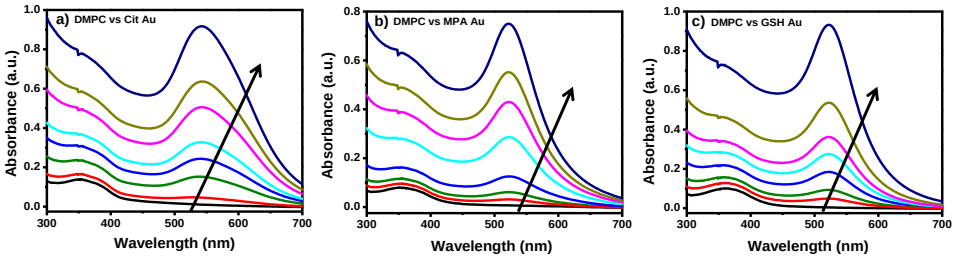

Figure 2.3 *UV-Vis spectra for DMPC-PRODAN upon addition of a) Cit-AuNPs; b) MPA-AuNP; and c) GSH-AuNPs in different concentrations. Upward arrow indicates increasing concentration of AuNPs.*

We performed a control experiment with aqueous PRODAN to further confirm that the subsequent effects are brought by the adsorption of the AuNPs on the bilayer surface rather than by the surface ligands. The results reveal that there appears no peak shift in the emission spectra upon addition of the Cit-AuNPs to aqueous PRODAN and no changes in the lifetime measurements (Figure 2.4).

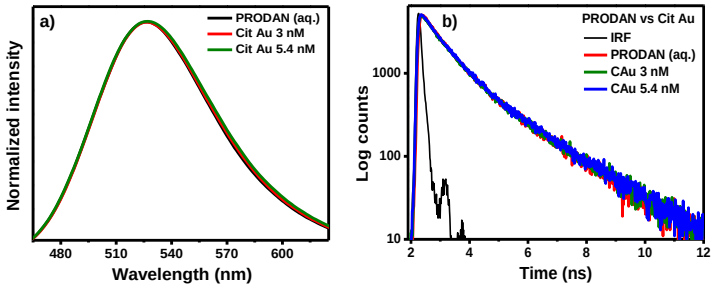

Figure 2.4 *a) Normalized fluorescence emission intensity for PRODAN in aqueous buffer upon addition of Cit-AuNPs; and b) Corresponding lifetime decays for PRODAN with Cit-AuNPs at 520 nm.*

The pronounced effect observed for cit-AuNPs compared to AuNPs functionalized with more bulky surface ligands can be explained by the interaction energy model using the Derjaguin−Landau−Verwey−Overbeek (DLVO) theory, which considers contributions from electrostatic as well as van der Waals forces. Figure 2.5 reveals the total potential as a function of the distance from the bilayer surface for different surface ligands. The maximum energy barrier is observed for AuNPs with the bulkiest surface ligand (GSH). On the other hand, the energy barrier is the least for small cit-AuNPs indicating a stronger interaction with the bilayer surface. We infer that smaller AuNPs distribute most on the surface of the bilayer and they accumulate on the bilayer surface at a higher rate owing to higher number density [70]. This indicates that cit-AuNPs interact most effectively with lipid bilayer rather than AuNPs functionalized with bulkier ligands.

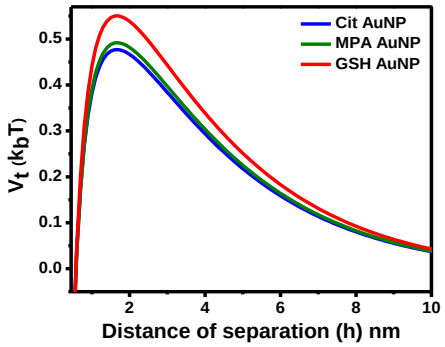

Figure 2.5 *Interaction energy between AuNPs functionalized with citrate, MPA and GSH and lipid vesicles modeled by DLVO theory as a function of distance of separation between the bilayer and AuNPs.*

The interaction energy between the AuNPs and lipid bilayers is evaluated by equation 1:

$$V_t(h) = V_{EDL}(h) + V_{VDW}(h) \qquad (1)$$

where V_t is the total interaction energy as a function of separation distance h (nm). V_t is the sum of electrical double-layer energy (V_{EDL}) and van der Waals interaction energy (V_{VDW}). Since the size of the vesicles is very large compared to the nanoparticles, their interaction can be modeled by considering the surface as

planar at the site of interaction. The electrical double-layer (V_{EDL}) potential can be calculated from equation 2:

$$V_{EDL}(h) = 64\pi\varepsilon_o\varepsilon_r a_p{}^2\left(\frac{k_B T}{ze}\right)^2 \tau_{lip}\tau_{AuNP}\exp(-kh) \qquad (2)$$

where a_p denotes the nanoparticle radius and τ_{lip} and τ_{AuNP} denote the dimensionless surface potential for lipid vesicles and AuNPs, respectively. Further, the van der Waals interaction energy (V_{VDW}) can be calculated from equation 3:

$$V_{VDW}(h) = -\frac{A_{GWL}a_p}{6h\left(1+\frac{14h}{\lambda}\right)} \qquad (3)$$

where A_{GWL} indicates the Hamaker constant for the lipid bilayer-to-AuNP interaction in water. The parameters used for the calculation of equations 2 and 3 are summarized in Table 2.2.

Table 2.2 *Summary of parameters used for the calculation of interaction energy (electrostatic and Van der Waal's forces) using DLVO theory from equations 2 and 3:*

Dielectric permittivity in vacuum ε_0	8.85×10^{-12} (F/m)
Relative dielectric permittivity of solution ε	78.5
Particle radius a_p	$6.5 \times 10^{-9} - 7.02 \times 10^{-9}$ (m)
Boltzmann constant k_B	1.3805×10^{-23} (J/K)
Temperature T	298.15 (K)
Electron charge e	1.602×10^{-19} C
Counterion valence z	1
Inverse Debye length k	2.13×10^{8} (1/m)
Dimensionless surface potential for lipid bilayer $\Gamma_{lip} = \tanh(ze\psi_{lip}/4k_BT)$; Ψ_{lip} is the zeta potential of the lipid bilayer	−0.04
Dimensionless surface potential for Au NP $\Gamma_{AuNP} = \tanh(ze\psi_{AuNP}/4k_BT)$; Ψ_{AuNP} is the zeta potential of Au NPs	−0.15 - −0.20
Hamaker constant for lipid bilayer to Au NP interaction in water A_{GWL}	2.77×10^{-21} (J)
Characteristic wavelength λ	100 (nm)

The binding behaviour of the differently functionalized nanoparticles is summarized in Scheme 2.1.

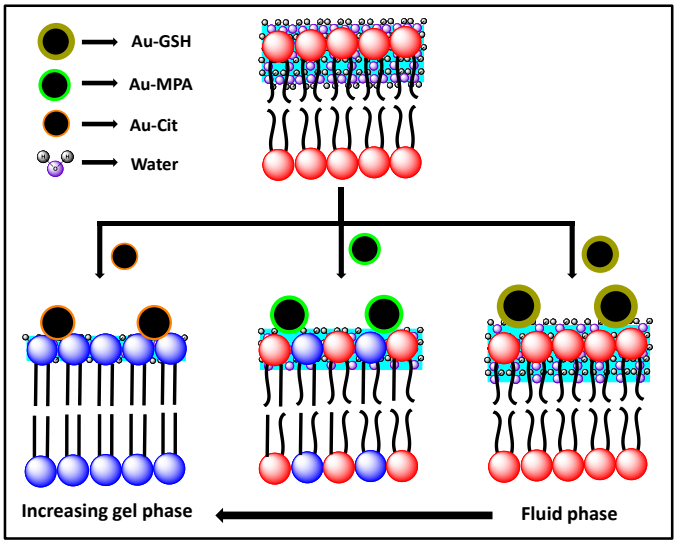

Scheme 2.1 *Interaction of differently functionalized gold nanoparticles with lipid vesicles. Cit-AuNPs stabilize the bilayer to a higher extent and raise the phase-transition temperature of the lipid. MPA and GSH-AuNPs adsorb on the bilayer surface less strongly due to their bulky structures.*

Further, to observe the effect of temperature on the binding behaviour, we exploited the sensitivity of PRODAN using temperature-dependent emission intensity. We observed that the fluorescence intensity of PRODAN corresponding to the LE state (435 nm) decreases and that of the TICT state (490 nm) increases with a rise in temperature, indicating that the bilayer membranes change their phase from a highly ordered gel (Lβ) phase to fluidic (Lα) phase (Figure 2.6 a-b). The changes in the emission spectra of PRODAN were analyzed by plotting area fraction against temperature. The decrease in fluorescence area at blue end is sigmoidal with a maximum change at the phase-transition temperature of the bilayer (Figure 2.6 c). This is more clearly notable in the derivative plot of fluorescence emission intensity (dA/dT) with varying temperature (Figure 2.6 d). The phase-transition temperature of the DMPC bilayer is observed at 23 °C. However, the addition of cit-AuNPs to the lipid vesicle results in an increase in the phase transition from 23 to 25 °C. This indicates stabilization of the vesicles. The adsorption of cit-AuNPs stiffens the phosphatidylcholine (PC) lipid bilayer

and restructures the bound lipid molecules into a raftlike phase [71-72]. The electrostatic forces between the nanoparticles and the bilayer head group make the otherwise loosely packed lipid molecules to tightly pack around the AuNP binding sites. This results in the stitching of the bilayer making it more stable. On the other hand, the phase-transition temperature of the DMPC bilayer did not show any effective changes upon addition of MPA- and GSH AuNPs.

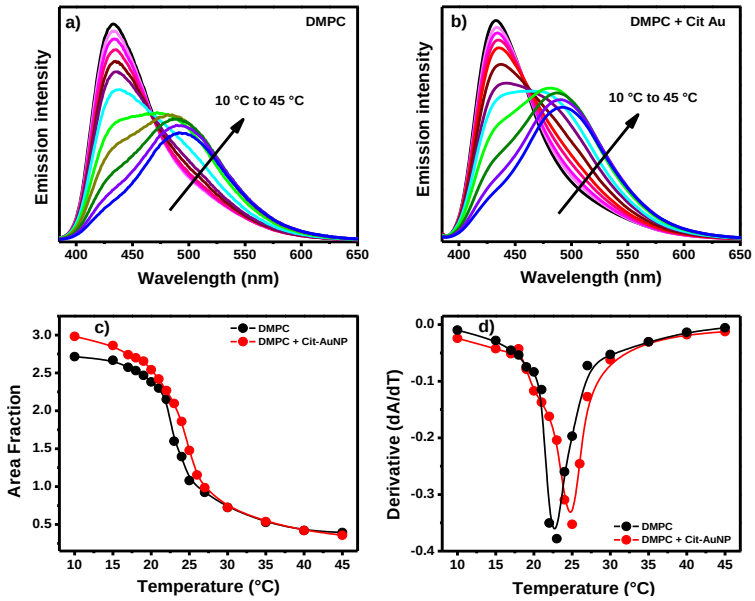

Figure 2.6 *Temperature-induced variations in the steady-state fluorescence spectra of PRODAN in DMPC vesicles. Fluorescence Emission intensity with change in temperature (a) without AuNP addition, after adsorption of citrate-AuNPs (b), area fraction (A435nm/A490nm) vs temperature plot (c) and first derivative of area (dA/dT) vs temperature plot (d).*

We performed the experiment at 15 °C to know the fate of the nanoparticle interaction with the lipid vesicles present in gel phase. From Figure 2.7 a−c, we observe that no peak shift in the emission spectra appears while the peak corresponding to ~490 nm (CT state) decreases upon addition of all of the three anionic AuNPs. The lifetime decay at 440 nm increases moderately for all of the three AuNPs (Figure 2.7 d−f, Table 2.3). Therefore, at lower temperatures, the differently functionalized AuNPs are adsorbed to nearly a similar extent on the surface of the lipid vesicle. Since DMPC is already in gel (Lβ) phase at 15 °C, it is more rigid at this temperature. As a result, there is a moderate effect in terms of instantaneous adsorption and gelation for all of the AuNPs.

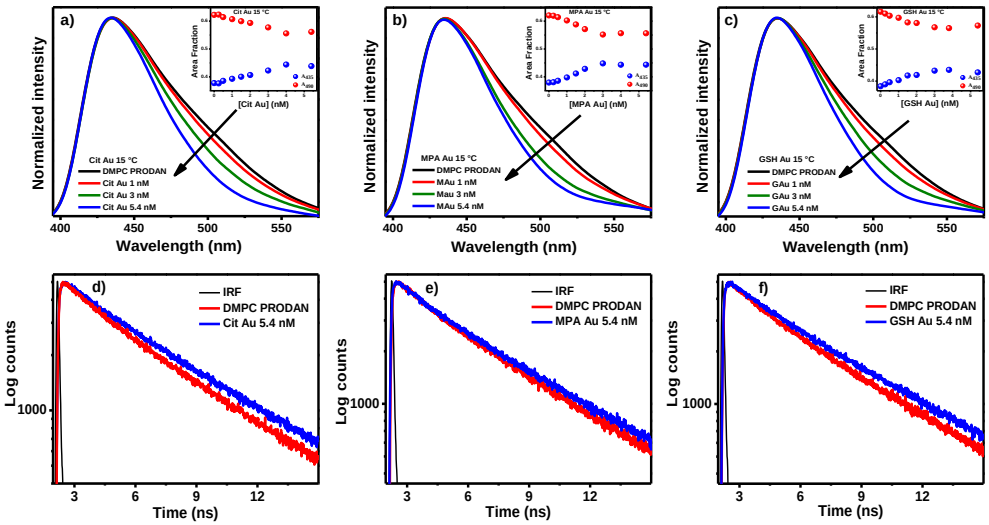

Figure 2.7 *Normalized emission spectra for the addition of AuNPs to DMPC−PRODAN solution for (a) citrate AuNPs, (b) MPA-AuNPs, and (c) GSH-AuNPs at 15 °C (the inset shows the respective area fraction plots) and corresponding time-resolved decay curves at 440 nm (d−f).*

Table 2.3 *Lifetime components, normalized amplitudes of lifetime components and average lifetime of DMPC-PRODAN upon addition of AuNPs collected at 440 nm at temperature 15 °C and 35 °C.*[#]

@440 nm, 15 °C						
Sample	**τ_1 (ns)**	**τ_2 (ns)**	**a_1**	**a_2**	**$<\tau_{avg}>$ (ns)**	**χ^2**
DMPC	2.16	6.47	0.30	0.70	5.17	1.01
+ Cit-AuNP	2.48	6.92	0.24	0.76	5.85	1.04
+ MPA-AuNP	2.22	6.70	0.29	0.71	5.38	1.06
+ GSH-AuNP	2.30	6.88	0.24	0.76	5.78	0.99
@440 nm, 35 °C						
DMPC	0.98	2.99	0.50	0.50	1.98	1.16
+ Cit-AuNP	0.98	3.01	0.47	0.53	2.05	1.13
+ MPA-AuNP	0.96	3.00	0.50	0.50	1.98	1.24
+ GSH-AuNP	1.00	3.08	0.44	0.56	2.16	1.06

Further, we performed the experiment far above the phase transition of the lipid, i.e., at 35 °C, when the bilayer is present in fluid (Lα) phase. We observe that a small blue shift takes place upon addition of AuNPs on the bilayer surface,

indicating gelation, and the intensity corresponding to LE state increases (Figure 2.8 a−c). However, there is apparently no change in the lifetime decay at 440 nm (inset of Figure 2.8 d−f). This can be explained in the light of the fact that since DMPC remains in fluid phase at 35 °C, it is not capable of holding more nanoparticles compared to DMPC in gel (Lβ) or nearly fluid (Lα) phase. The higher increment in lifetime decay at lower temperature stems from the fact that DMPC being in gel (Lβ) phase or nearly fluid (Lα) phase occupies less area per lipid molecule, allowing it to capture more number of nanoparticles. Since the experimental temperature is far above the phase transition temperature of DMPC, it remains in Lα state and any change, howsoever small, that occurs upon the addition of AuNPs cannot change the phase state of the lipid vesicle. It is therefore not possible to detect the small change that appears in the steady state by lifetime measurements at 440 nm. Thus, maximum gelation is observed in the case of DMPC bilayers at 25 °C, not below or above the phase-transition temperatures. We explain this observation by the fact that near the phase transition temperature of the lipid (T = 25 °C), DMPC remains in a nearly Lα phase. Thus, even a little increase in the phase-transition temperature drastically alters DMPC from a nearly fluid (Lα) phase to a more compact gel (Lβ) phase.

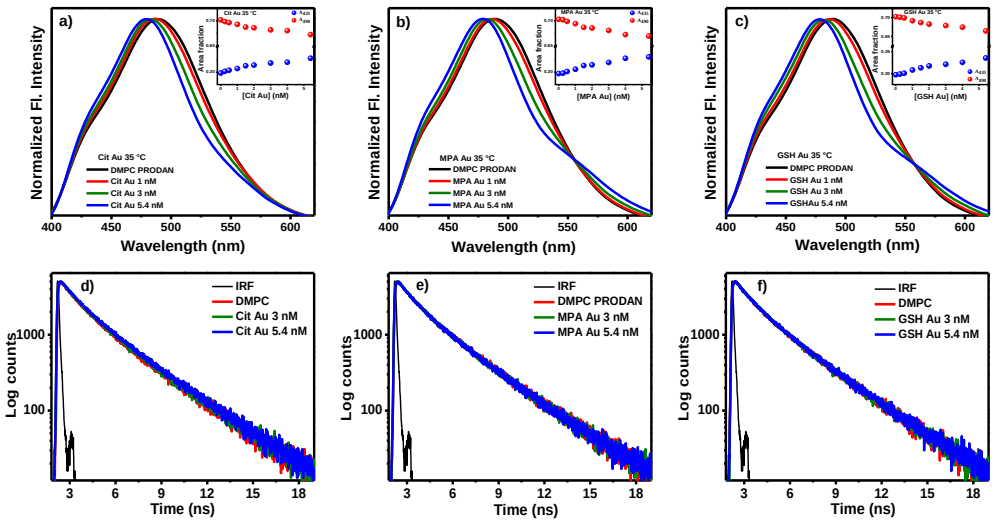

Figure 2.8 *Normalized emission spectra for the addition of AuNPs in different concentrations (0−5.4 nM) to DMPC−PRODAN solution for (a) citrate AuNPs, (b) MPA-AuNPs, and (c) GSH-AuNPs at 35 °C (the inset shows the respective area fraction plots) and corresponding time-resolved decay curves at 440 nm (d−f).*

We further performed the experiment with vesicles synthesized from DOPC (T_m = −20 °C) at an experimental temperature 25 °C. We observe that there appears a blue shift in the emission spectra to nearly a similar extent, also clearly depicted by the area fraction plots (Figure 2.9). The lifetime decay, however, did not reveal any significant changes at 440 nm (Table 2.4). The results are in agreement with those obtained for DMPC liposomes at 35 °C. Thus, we can infer from these data that when the bilayer is present in the LC phase, the peak shift (or gelation) is not that much pronounced as near the phase transition temperature of the lipid. This holds true in our experiment for zwitterionic PC lipids with varying phase transition temperatures.

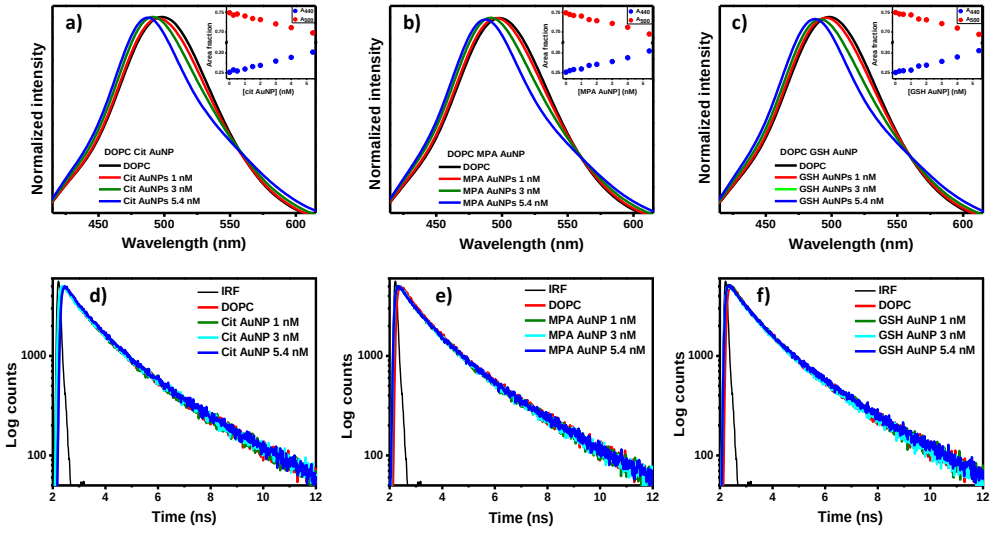

Figure 2.9 *Normalized emission spectra for the addition of AuNPs in different concentrations (0−5.4 nM) to DOPC−PRODAN solution for (a) citrate AuNPs, (b) MPA-AuNPs, and (c) GSH-AuNPs (the inset shows area fraction plots). The corresponding time-resolved decay curves of PRODAN in DOPC−AuNPs solutions at 440 nm (d−f) at 25 °C.*

Table 2.4 *Lifetime components, normalized amplitudes of lifetime components and average lifetime of PRODAN (in DOPC and DOCP) upon addition of AuNPs collected at 440 nm.*[#]

@440 nm, 25 °C						
Sample	**τ_1 (ns)**	**τ_2 (ns)**	**a_1**	**a_2**	**$\langle\tau_{avg}\rangle$ (ns)**	**χ^2**
DOPC	0.95	2.80	0.70	0.30	1.50	1.22

+ Cit-AuNPs	0.97	2.87	0.70	0.30	1.53	1.22
+ MPA-AuNPs	0.97	2.87	0.70	0.30	1.53	1.08
+ GSH-AuNPs	0.98	2.94	0.71	0.29	1.55	1.09
@440 nm, 25 °C						
DOCP	0.91	2.58	0.65	0.35	1.50	1.25
+ Cit-AuNPs	0.91	2.69	0.64	0.36	1.56	1.33
+ MPA-AuNPs	0.86	2.66	0.62	0.38	1.54	1.34
+ GSH-AuNPs	0.87	2.56	0.64	0.36	1.48	1.27

In order to study the effect of headgroup, apart from phosphocholine lipid vesicles (DMPC and DOPC), we further studied their effect on lipid vesicle with inverse phosphocholine (iPC) lipid DOCP at 25 °C. We observed that (Figure 2.10) there appears a blue shift after the addition of anionic AuNPs to the DOCP vesicles. This is also evident from the area fraction plots (Figure 2.10 a−c inset). Moreover, the lifetime decay increases marginally for the addition of AuNPs to DOCP, indicating that the iPC lipid vesicles are also stabilized to a small extent upon interaction with AuNPs. Thus, it is notable that the observation holds true even for iPC lipids that the gelation of the bilayer takes places to a small extent when the bilayer is present below the phase-transition temperature of the lipid.

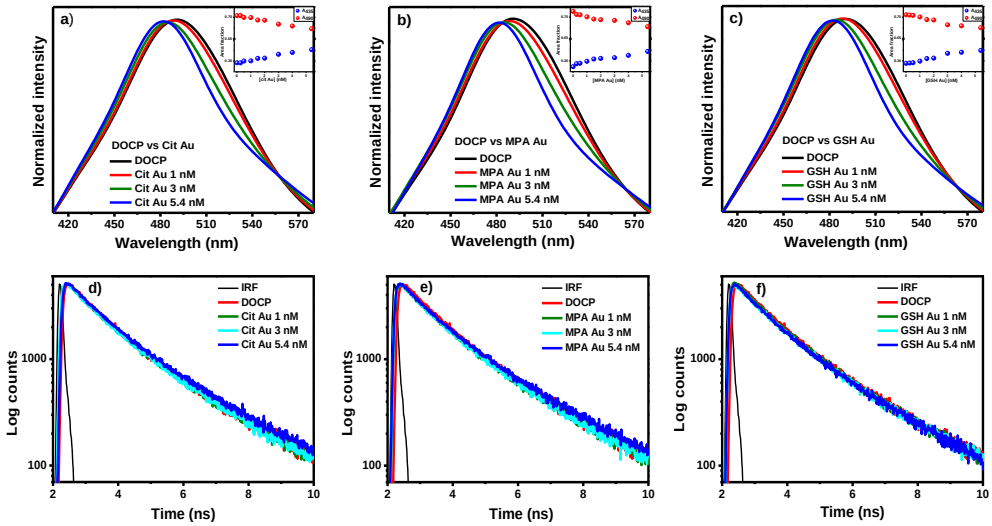

Figure 2.10 *Normalized emission spectra for the addition of AuNPs in different concentrations (0−5.4 nM) to iPC DOCP−PRODAN solution for (a) citrate AuNPs, (b) MPA-AuNPs, and (c) GSH-AuNPs (the inset shows area fraction plots). The corresponding time-resolved decay curves of PRODAN in DOCP−AuNPs solutions at 440 nm (d−f) at 25 °C.*

In order to study the effect of charge on nanoparticles, we explored the effects caused by cationic AuNPs (cys-AuNP) on lipid vesicle. We observed that even for cationic AuNP, there is a blue spectral shift, indicating gelation of the bilayer. However, it is interesting to note that the gelation effect is minimum for cationic AuNPs, indicating that the binding is much weaker on the bilayer surface. The results are also supported by a slight increase in lifetime decay at 440 nm (Figure 2.11). It is known that lipid bilayers interact with both positively and negatively charged AuNPs without structurally affecting the vesicles [73]. But since the phospholipid zwitterionic head group terminates with positive charge, lipids beneath an adsorbed nanoparticle bind more weakly when the nanoparticle charge is cationic [4].

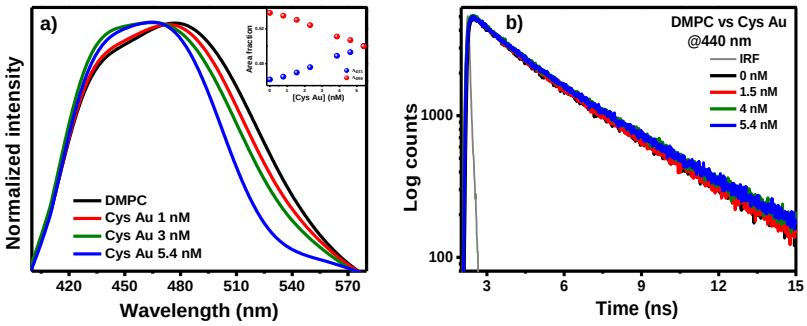

Figure 2.11 *(a) Normalized emission spectra for the addition of Cys- AuNPs in different concentrations to DMPC−PRODAN solution and area fraction plot at blue end (435 nm) and red end (490 nm) (shown in inset) and (b) corresponding time-resolved decay curves of PRODAN in DMPC−CysAuNPs solutions at 440 nm at 25 °C.*

Thus, the lipid vesicle is brought to gelation and stabilized to a different extent at different temperatures. This holds true for both anionic and cationic AuNPs in our experiments for zwitterionic phosphocholine lipids and inverse phosphocholine lipids. There is a scope for gelation, howsoever small, at all of the experimental temperatures but the maximum extent of gelation is brought at a temperature just above the phase transition of the lipid.

2.2.3 <u>Effect on morphology and size</u>: We performed confocal laser scanning microscopy (CLSM) imaging for the DMPC lipid vesicles and that of the vesicles upon interaction with AuNPs. As shown in Figure 2.12, we observe that the

surface of the bilayer is unmodified initially. However, upon addition of AuNPs, the surface of the vesicles undergoes membrane alterations. This also leads to transient leakage of the dye [71]. AuNPs adsorbed on the bilayer surface results in the membrane pore formation, which arises as a result of altered lipid packing. The pores are ruptures resulting from the lateral pressure induced by multiple AuNP adsorptions, rather than from the insertion of AuNPs. A hole is transiently formed before AuNP entry and closed after AuNP translocation [72]. This effect is clearly evident from the CLSM images.

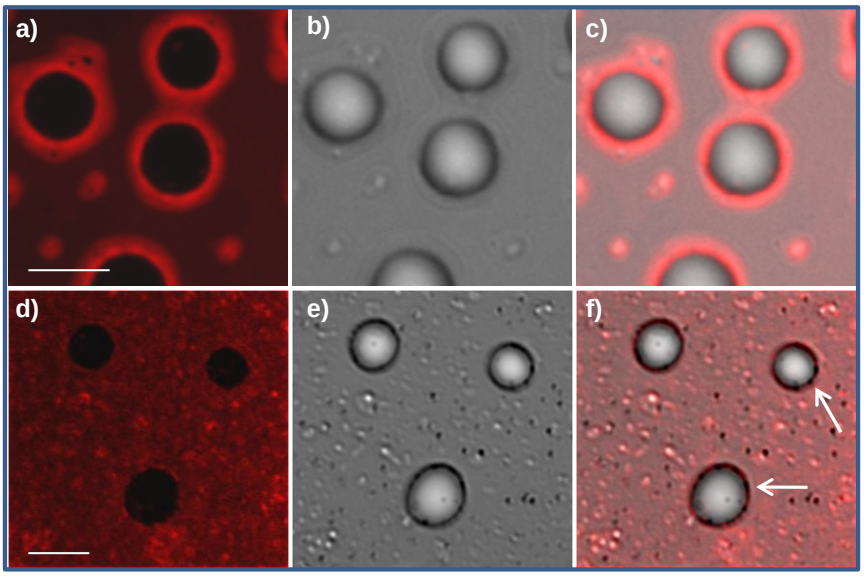

Figure 2.12 *AuNP−DMPC bilayer interaction from confocal laser scanning microscopy (CLSM). Confocal, bright-field, and merged images for blank DMPC bilayers (a−c) and for DMPC−AuNP systems (d−f). The arrows in the DMPC−AuNP indicate the surface alterations caused due to AuNP adsorption on the surface of the bilayer. The bars in the images indicate 2 μm size.*

For further understanding, we analyzed the hydrodynamic size distribution curves of the vesicles and the vesicle−AuNP assemblies. For DMPC vesicles, the average diameter was found to be 135.6 nm (polydispersity index (PDI) = 0.249), whereas upon addition of AuNPs, the size decreased to 66.2 nm (PDI = 0.271 nm) for cit-AuNPs, 64.8 nm (PDI = 0.391) for MPA-AuNPs, and 60.2 nm (PDI = 0.438) for GSH-AuNPs (Figure 2.13). This decrement in size upon AuNP addition can be explained in the light of the formation of more stiff, rigid, and discrete structures upon addition of AuNPs compared to otherwise transient

structures of lipid vesicles. The interaction of such nanoparticles with liposome surface tends to restructure the membrane into structurally stiffened nanoscale domains [71].

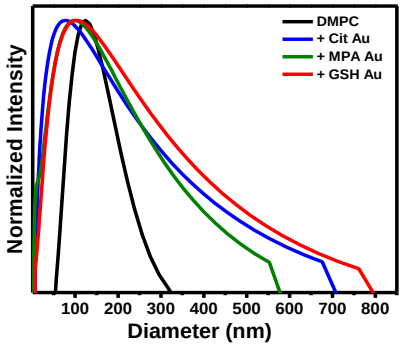

Figure 2.13 *DLS size distribution curve for DMPC upon interaction with citrate AuNPs, MPA AuNPs and GSH AuNPs.*

2.3 Conclusion

We studied the interaction of lipid vesicles (PC and iPC lipids) with anionic and cationic AuNPs and drew the following conclusions:

(a) Lipid vesicles interact with the AuNPs to a maximum extent at a temperature near the phase transition temperature of the lipid and the gelation effect is not that effectively pronounced when the vesicles are present in fluid (Lα) or gel (Lβ) phase. This holds true for both PC lipids and iPC lipids.

(b) The extent of gelation of the lipid vesicles varies with the bulkiness of the surface ligands, and the vesicles experience a minimum gelation when the ligand is bulky. While cit-capped AuNPs interact the strongest and effectively raise the phase-transition temperature of the lipid vesicles, more bulky groups MPA and GSH distant AuNP core from the bilayer surface so that the interactions are comparatively weaker.

(c) Both anionic and cationic AuNPs tend to bring gelation and stability to the lipid vesicles. However, cationic AuNPs bind weakly compared to their anionic counterparts on the vesicle surface.

These surface interactions between bilayer AuNPs are found to effectively stabilize the bilayer, resulting in biocompatible systems and can be used for a variety of bioinspired applications, such as imaging, drug delivery, biosensing, etc.

2.4 References

1. Thamphiwatana, S., Fu, V., Zhu, J., Lu, D., Gao, W., Zhang, L. (2013), Nanoparticle-Stabilized Liposomes for pH-Responsive Gastric Drug Delivery. *Langmuir*, 29, 12228−12233. (DOI: 10.1021/la402695c)

2. Adhikari, C., Das, A., Chakraborty, A. (2015), Controlled Release of a Sparingly Water-Soluble Anticancer Drug through pH-Responsive Functionalized Gold-Nanoparticle-Decorated Liposomes. *ChemPhysChem*, 16, 866−871. (DOI: 10.1002/cphc.201402748)

3. Pornpattananangkul, D., Olson, S., Aryal, S., Sartor, M., Huang, C.-M., Vecchio, K., Zhang, L. (2010), Stimuli-Responsive Liposome Fusion Mediated by Gold Nanoparticles. *ACS Nano*, 4, 1935−1942. (DOI: 10.1021/nn9018587)

4. Yu, Y., Anthony, S. M., Zhang, L., Bae, S. C., Granick, S. (2007), Cationic Nanoparticles Stabilize Zwitterionic Liposomes Better than Anionic Ones. *J. Phys. Chem. C*, 111, 8233−8236. (DOI: 10.1021/jp072680z)

5. De, S. K., Kanwa, N., Ahamed, M., Chakraborty, A. (2018), Spectroscopic Evidence for Hydration and Dehydration of Lipid Bilayers upon Interaction with Metal Ions: A New Physical Insight. *Phys. Chem. Chem. Phys.*, 20, 14796−14807. (DOI: 10.1039/C8CP01774C)

6. Binder, H., Zschörnig, O. (2002), The Effect of Metal Cations on the Phase Behavior and Hydration Characteristics of Phospholipid Membranes. *Chem. Phys. Lipids*, 115, 39−61. (DOI: 10.1016/S0009-3084(02)00005-1)

7. Hong, H., Tamm, L. K. (2004), Elastic Coupling of Integral Membrane Protein Stability to Lipid Bilayer Forces. *Proc. Natl. Acad. Sci. U.S.A.*, 101, 4065−4070. (DOI: 10.1073/pnas.0400358101)

8. Vafaei, S., Tabaei, S. R., Cho, N.-J. (2017), Optimizing the Performance of Supported Lipid Bilayers as Cell Culture Platforms Based on Extracellular Matrix Functionalization. *ACS Omega*, 2, 2395−2404. (DOI: 10.1021/acsomega.7b00158)

9. Sankaram, M. B., Thompson, T. E. (1991), Cholesterol-Induced Fluid-Phase Immiscibility in Membranes. *Proc. Natl. Acad. Sci. U.S.A.*, 88, 8686−8690. (DOI: 10.1073/pnas.88.19.8686)

10. de Almeida, R. F. M., Fedorov, A., Prieto, M. (2003), Sphingomyelin/ Phosphatidylcholine/Cholesterol Phase Diagram: Boundaries and Composition of Lipid Rafts. *Biophys. J.*, 85, 2406−2416. (DOI: 10.1016/S0006-3495(03)74664-5)

11. Raffy, S., Teissié, J. (1999), Control of Lipid Membrane Stability by Cholesterol Content. *Biophys. J.*, 76, 2072−2080. (DOI: 10.1016/S0006-3495(99)77363-7)

12. Róg, T., Pasenkiewicz-Gierula, M., Vattulainen, L., Karttunen, M. (2009), Ordering Effects of Cholesterol and its Analogues. *Biochim. Biophys. Acta, Biomembr.*, 1788, 97−121. (DOI: 10.1016/j.bbamem.2008.08.022)

13. Al-Jamal, W. T., Kostarelos, K. (2007), Liposome-Nanoparticle Hybrids for Multimodal Diagnostic and Therapeutic Applications. *Nanomedicine*, 2, 85−98. (DOI: 10.2217/17435889.2.1.85)

14. Preiss, M. R., Bothun, G. D. (2011), Stimuli-Responsive Liposome Nanoparticle Assemblies. *Expert Opin. Drug Delivery*, 8, 1025−1040. (DOI: 10.1517/17425247.2011.584868)

15. Paasonen, L., Sipila, T., Subrizi, A., Laurinmaki, P., Butcher, S. J., Rappolt, M., Yaghmur, A., Urtti, A., Yliperttula, M. (2010), Gold-Embedded Photosensitive Liposomes for Drug Delivery: Triggering Mechanism and Intracellular Release. *J. Controlled Release*, 147, 136−143. (DOI: 10.1016/j.jconrel.2010.07.095)

16. Liu, J., Jiang, X., Ashley, C., Brinker, C. J. (2009), Electrostatically Mediated Liposome Fusion and Lipid Exchange with a Nanoparticle Supported Bilayer for Control of Surface Charge, Drug Containment, and Delivery. *J. Am. Chem. Soc.*, 131, 7567−7569. (DOI: 10.1021/ja902039y)

17. Roiter, Y., Ornatska, M., Rammohan, A. R., Balakrishnan, J., Heine, D. R., Minko, S. (2008), Interaction of Nanoparticles with Lipid Membrane. *Nano Lett.*, 8, 941−944. (DOI: 10.1021/nl080080l)

18. Abraham, S., Narine, S. S. (2011), A Facile Synthesis of Lipid Stabilized Gold Nanoparticles: A Step towards Biodegradable Biosensors. *J. Nanosci. Nanotechnol.*, 11, 7027−7032. (DOI: 10.1166/jnn.2011.4878)

19. Huang, H.-C., Chang, P.-Y., Chang, K., Chen, C.-Y., Lin, C.-W., Chen, J.-H., Mou, C.-Y., Chang, Z.-F., Chang, F.-H. (2009), Formulation of Novel Lipid-Coated Magnetic Nanoparticles as the Probe for In Vivo Imaging. *J. Biomed. Sci.*, 16, 86. (DOI: 10.1186/1423-0127-16-86)

20. Castellana, E. T., Gamez, R. C., Russell, D. H. (2011), Label-Free Biosensing with Lipid-Functionalized Gold Nanorods. *J. Am. Chem. Soc.*, 133, 4182−4185. (DOI: 10.1021/ja109936h)

21. Wang, B., Zhang, L., Bae, S. C., Granick, S. (2008), Nanoparticle-Induced Surface Reconstruction of Phospholipid Membranes. *Proc. Natl. Acad. Sci. U.S.A.*, 105, 18171−18175. (DOI: 10.1073/pnas.0807296105)

22. Wang, F., Liu, J. (2015), A Stable Lipid/TiO2 Interface with Headgroup Inversed Phosphocholine and a Comparison with SiO2. *J. Am. Chem. Soc.*, 137, 11736−11742. (DOI: 10.1021/jacs.5b06642)

23. Zhang, L., Granick, S. (2006), How to Stabilize Phospholipid Liposome (Using Nanoparticles). *Nano Lett.*, 6, 694−698. (DOI: 10.1021/nl052455y)

24. Tan, S., Li, X., Guo, Y., Zhang, Z. (2013), Lipid-Enveloped Hybrid Nanoparticles for Drug Delivery. *Nanoscale*, 5, 860−872. (DOI: 10.1039/c2nr32880a)

25. Liu, J. (2016), Interfacing Zwitterionic Liposomes with Inorganic Nanomaterials: Surface Forces, Membrane Integrity, and Applications. *Langmuir*, 32, 4393−4404. (DOI: 10.1021/acs.langmuir.6b00493)

26. Liu, X., Li, X., Xu, W., Zhang, X., Huang, Z., Wang, F., Liu, J. (2018), Sub-Angstrom Gold Nanoparticle/Liposome Interfaces Controlled by Halides. *Langmuir*, 34, 6628−6635. (DOI: 10.1021/acs.langmuir.8b01138)

27. Gao, J., Huang, X., Liu, H., Zan, F., Ren, J. (2012), Colloidal Stability of Gold Nanoparticles Modified with Thiol Compounds: Bioconjugation and Application in Cancer Cell Imaging. *Langmuir*, 28, 4464−4471. (DOI: 10.1021/la204289k)

28. Zhao, J., Wu, Y., Tao, H., Chen, H., Yang, W., Qiu, S. (2017), Colorimetric Detection of Streptomycin in Milk Based on Peroxidase-Mimicking Catalytic Activity of Gold Nanoparticles. *RSC Adv.*, 7, 38471−38478. (DOI: 10.1039/C7RA06434A)

29. Piella, J., Bastús, N. G., Puntes, V. (2016), Size-Controlled Synthesis of Sub-10-nanometer Citrate-Stabilized Gold Nanoparticles and Related Optical Properties. *Chem. Mater.*, 28, 1066−1075. (DOI: 10.1021/acs.chemmater.5b04406)

30. Magura, J., Zeleňáková, A., Zeleňák, V., Kaňuchová, M. (2014), Thiol-Modified Gold Nanoparticles Deposited on Silica Support Using Dip Coating. *Appl. Surf. Sci.*, 315, 392−399. (DOI: 10.1016/j.apsusc.2014.07.173)

31. Rance, G. A., Marsh, D. H., Bourne, S. J., Reade, T. J., Khlobystov, A. N. (2010), van der Waals Interactions between Nanotubes and Nanoparticles for

Controlled Assembly of Composite Nanostructures. *ACS Nano*, 4, 4920−4928. (DOI: 10.1021/nn101287u)

32. Mustafa, D. E., Yang, T., Xuan, Z., Chen, S., Tu, H., Zhang, A. (2010), Surface Plasmon Coupling Effect of Gold Nanoparticles with Different Shape and Size on Conventional Surface Plasmon Resonance Signal. *Plasmonics*, 5, 221−231. (DOI: 10.1007/s11468-010-9141-z)

33. Wang, X., Gogol, P., Cambril, E., Palpant, B. (2012), Near- and Far-Field Effects on the Plasmon Coupling in Gold Nanoparticle Arrays. *J. Phys. Chem. C*, 116, 24741−24747. (doi: 10.1021/jp306292r)

34. Wang, F., Curry, D. E., Liu, J. (2015), Driving Adsorbed Gold Nanoparticle Assembly by Merging Lipid Gel/Fluid Interfaces. *Langmuir*, 31, 13271−13274. (DOI: 10.1021/acs.langmuir.5b03606)

35. Preiss, M. R., Hart, A., Kitchens, C., Bothun, G. D. (2017), Hydrophobic Nanoparticles Modify the Thermal Release Behavior of Liposomes. *J. Phys. Chem. B*, 121, 5040−5047. (DOI: 10.1021/acs.jpcb.7b01702)

36. Moghadam, B. Y., Hou, W.-C., Corredor, C., Westerhoff, P., Posner, J. D. (2012), The Role of Nanoparticle Surface Functionality in the Disruption of Model Cell Membranes. *Langmuir*, 28, 16318−16326. (DOI: 10.1021/la302654s)

37. Salassi, S., Simonelli, F., Bochicchio, D., Ferrando, R., Rossi, G. Au Nanoparticles in Lipid Bilayers: A Comparison between Atomistic and Coarse-Grained Models. J. Phys. Chem. C 2017, 121, 10927−10935. (DOI: 10.1021/acs.jpcc.6b12148)

38. Toledo-Fuentes, X., Lis, D., Cecchet, F. (2016), Structural Changes to Lipid Bilayers and Their Surrounding Water upon Interaction with Functionalized Gold Nanoparticles. *J. Phys. Chem. C*, 120, 21399−21409. (DOI: 10.1021/acs.jpcc.6b05460)

39. Sakaguchi, N., Kimura, Y., Hirano-Iwata, A., Ogino, T. (2017), Fabrication of Au-Nanoparticle-Embedded Lipid Bilayer Membranes Supported on Solid Substrates. *J. Phys. Chem. B*, 121, 4474−4481. (DOI: 10.1021/acs.jpcb.7b00500)

40. Guo, Y., Terazzi, E., Seemann, R., Fleury, J. B., Baulin, V. A. (2016), Direct Proof of Spontaneous Translocation of Lipid-Covered Hydrophobic Nanoparticles through a Phospholipid Bilayer. *Sci. Adv.*, 2, No. e1600261. (DOI: 10.1126/sciadv.1600261)

41. Dichello, G. A., Fukuda, T., Maekawa, T., Whitby, R. L. D., Mikhalovsky, S. V., Alavijeh, M., Pannala, A. S., Sarker, D. K. (2017), Preparation of Liposomes Containing Small Gold Nanoparticles using Electrostatic Interactions. *Eur. J. Pharm. Sci.*, 105, 55−63. (DOI: 10.1016/j.ejps.2017.05.001)

42. Hamilton, D. J., Coffman, M. D., Knight, J. D., Reed, S. M. (2017), Lipid-Coated Gold Nanoparticles and FRET Allow Sensitive Monitoring of Liposome Clustering Mediated by the Synaptotagmin-7 C2A Domain. *Langmuir*, 33, 9222−9230. (DOI: 10.1021/acs.langmuir.7b01397)

43. Rossi, G., Monticelli, L. (2016), Gold Nanoparticles in Model Biological Membranes: A Computational Perspective. *Biochim. Biophys. Acta, Biomembr.*, 1858, 2380−2389. (DOI: 10.1016/j.bbamem.2016.04.001)

44. Pastoriza-Santos, I., Kinnear, C., Pérez-Juste, J., Mulvaney, P., Liz-Marzán, L. M. (2018), Plasmonic polymer nanocomposites. *Nat. Rev. Mater.*, 3, 375−391. (DOI: 10.1038/s41578-018-0050-7)

45. Zhang, S., Geryak, R., Geldmeier, J., Kim, S., Tsukruk, V. V. (2017), Synthesis, Assembly, and Applications of Hybrid Nanostructures for Biosensing. *Chem. Rev.*, 117, 12942−13038. (DOI: 10.1021/acs.chemrev.7b00088)

46. Ferhan, A. R., Kim, D.-H. (2016), Nanoparticle polymer composites on solid substrates for plasmonic sensing applications. *Nano Today*, 11, 415−434. (DOI: 10.1016/j.nantod.2016.07.001)

47. Baffou, G., Quidant, R. (2014), Nanoplasmonics for chemistry. *Chem. Soc. Rev.*, 43, 3898−3907. (DOI: 10.1039/c3cs60364d)

48. Sepúlveda, B., Angelomé, P. C., Lechuga, L. M., Liz-Marzán, L. M. (2009), LSPR-based nanobiosensors. *Nano Today*, 4, 244−251. (DOI: 10.1016/j.nantod.2009.04.001)

49. Mohapatra, M., Mishra, A. K. (2013), Photophysical Behavior of 8-Anilino-1-Naphthalenesulfonate in Vesicles of Pulmonary Surfactant Dipalmitoylphosphatidylcholine (DPPC) and Its Sensitivity toward the Bile Salt−Vesicle Interaction. *Langmuir*, 29, 11396−11404. (DOI: 10.1021/la402355j)

50. Parasassi, T., Krasnowska, E. K., Bagatolli, L., Gratton, E. (1998), Laurdan and Prodan as Polarity-Sensitive Fluorescent Membrane Probes. *J. Fluoresc.*, 8, 365−373. (DOI: 10.1023/A:1020528716621)

51. Krasnowska, E. K., Gratton, E., Parasassi, T. (1998), Prodan as a Membrane Surface Fluorescence Probe: Partitioning between Water and Phospholipid Phases. *Biophys. J.*, 74, 1984−1993. (DOI: 10.1016/S0006-3495(98)77905-6)

52. Wilson-Ashworth, H. A., Bahm, Q., Erickson, J., Shinkle, A., Vu, M. P., Woodbury, D., Bell, J. D. (2006), Differential Detection of Phospholipid Fluidity, Order, and Spacing by Fluorescence Spectroscopy of Bis-pyrene, Prodan, Nystatin, and Merocyanine 540. *Biophys. J.*, 91, 4091−4101. (DOI: 10.1529/biophysj.106.090860)

53. Novaira, M., Biasutti, M. A., Silber, J. J., Correa, N. M. (2007), New Insights on the Photophysical Behavior of PRODAN in Anionic and Cationic Reverse Micelles: From which State or States does it Emit? *J. Phys. Chem. B,* 111, 748−759. (DOI: 10.1021/jp065528q)

54. Gutowicz, J., Krawczyk, A. (1986), Effect of 1-Anilinonaphthalene-8-Sulphonate on Phase Transition Temperature of Dipalmitoylphosphatidylcholine Liposomes. *Chem. Phys. Lipids*, 39, 357−364. (DOI: 10.1016/0009-3084(86)90117-9)

55. Lesslauer, W., Cain, J. E., Blasie, J. K. (1972), X-ray Diffraction Studies of Lecithin Bimolecular Leaflets with Incorporated Fluorescent Probes. *Proc. Natl. Acad. Sci. U.S.A.*, 69, 1499−1503. (DOI: 10.1073/pnas.69.6.1499)

56. Lesslauer, W., Cain, J., Blasie, J. K. (1971), On the Location of 1-Anilino-8-Naphthalene-Sulfonate in Lipid Model Systems: An X-Ray Diffraction Study. *Biochim. Biophys. Acta, Biomembr.*, 241, 547−566. (DOI: 10.1016/0005-2736(71)90054-X)

57. Gulik-Krzywicki, T., Shechter, E., Iwatsubo, M., Ranck, J. L., Luzzati, V. (1970), Correlations between Structure and Spectroscopic Properties in Membrane Model Systems Trytophan and I-Anilino-8-Naphtalene Sulfonate Fluorescence in Protein-Lipid-Water Phases. *Biochim. Biophys. Acta, Biomembr.*, 219, 1−10. (DOI: 10.1016/0005-2736(70)90055-6)

58. Kosower, E. M., Kanety, H. (1983), Intramolecular Donor-Acceptor Systems. 10. Multiple Fluorescences from 8-(Phenylamino) 1-Naphthalenesulfonates. *J. Am. Chem. Soc.*, 105, 6236−6243. (DOI: 10.1021/ja00358a008)

59. Wang, F., Liu, J. (2015), Self-Healable and Reversible Liposome Leakage by Citrate-Capped Gold Nanoparticles: Probing the Initial Adsorption/Desorption Induced Lipid Phase Transition. *Nanoscale*, 7, 15599−15604. (DOI: 10.1039/C5NR04805B)

60. Zhao, J., Wu, Y., Tao, H., Chen, H., Yang, W., Qiu, S. (2017), Colorimetric Detection of Streptomycin in Milk Based on Peroxidase-Mimicking Catalytic Activity of Gold Nanoparticles. *RSC Adv.*, 7, 38471−38478. (DOI: 10.1039/C7RA06434A)

61. Gao, J., Zhang, O., Ren, J., Wu, C., Zhao, Y. (2016), Aromaticity/Bulkiness of Surface Ligands to Promote the Interaction of Anionic Amphiphilic Gold Nanoparticles with Lipid Bilayers. *Langmuir*, 32, 1601−1610. (DOI: 10.1021/acs.langmuir.6b00035)

62. Sen, T., Patra, A. (2009), Formation of Self-Assembled Au Nanoparticles and the Study of Their Optical Properties by Steady-State and Time-Resolved Spectroscopies. *J. Phys. Chem. C*, 113, 13125−13132. (DOI: 10.1021/jp9024188)

63. Bastus, N. G., Comenge, J., Puntes, V. (2011), Kinetically Controlled Seeded Growth Synthesis of Citrate-Stabilized Gold Nanoparticles of up to 200 nm: Size Focusing versus Ostwald Ripening. *Langmuir*, 27, 11098−11105. (DOI: 10.1021/la201938u)

64. Kanwa, N., De, S. K., Adhikari, C., Chakraborty, A. (2017), Spectroscopic Study of the Interaction of Carboxyl-Modified Gold Nanoparticles with Liposomes of Different Chain Lengths and Controlled Drug Release by Layer-by-Layer Technology. *J. Phys. Chem. B*, 121, 11333−11343. (DOI: 10.1021/acs.jpcb.7b08455)

65. Novaira, M., Biasutti, M. A., Silber, J. J., Correa, N. M. (2007), New Insights on the Photophysical Behavior of PRODAN in Anionic and Cationic Reverse Micelles: From Which State or States Does It Emit? *J. Phys. Chem. B*, 111, 748−759. (DOI: 10.1021/jp065528q)

66. Thakur, R., Das, A., Chakraborty, A. (2014), Interaction of Human Serum Albumin with Liposomes of Saturated and Unsaturated Lipids with Different Phase Transition Temperatures: A Spectroscopic Investigation by Membrane Probe PRODAN. *RSC Adv.*, 4, 14335−14347. (DOI: 10.1039/C4RA01214C)

67. Zhang, L., Spurlin, T. A., Gewirth, A. A., Granick, S. (2006), Electrostatic Stitching in Gel-Phase Supported Phospholipid Bilayers. *J. Phys. Chem. B*, 110, 33−35. (DOI: 10.1021/jp055995s)

68. Torrano, A. A., Pereira, Â. S., Oliveira, O. N., Jr., Barros-Timmons, A. (2013), Probing the Interaction of Oppositely Charged Gold Nanoparticles with DPPG and DPPC Langmuir Monolayers as Cell Membrane Models. *Colloids Surf., B*, 108, 120−126. (DOI: 10.1016/j.colsurfb.2013.02.014)

69. Tatur, S., Maccarini, M., Barker, R., Nelson, A., Fragneto, G. (2013), Effect of Functionalized Gold Nanoparticles on Floating Lipid Bilayers. *Langmuir*, 29, 6606−6614. (DOI: 10.1021/la401074y)

70. Hou, W.-C., Moghadam, B. Y., Corredor, C., Westerhoff, P., Posner, J. D. (2012), Distribution of Functionalized Gold Nanoparticles between Water and Lipid Bilayers as Model Cell Membranes. *Environ. Sci. Technol.*, 46, 1869−1876. (DOI: 10.1021/es203661k)

71. Montis, C., Maiolo, D., Alessandri, I., Bergese, P., Berti, D. (2014), Interaction of Nanoparticles with Lipid Membranes: A Multiscale Perspective. *Nanoscale*, 6, 6452−6457. (DOI: 10.1039/C4NR00838C)

72. Bhat, A., Edwards, L. W., Fu, X., Badman, D. L., Huo, S., Jin, A. J., Lu, Q. (2016), Effects of Gold Nanoparticles on Lipid Packing and Membrane Pore Formation. *Appl. Phys. Lett.*, 109, No. 263106. (DOI: 10.1063/1.4972868)

73. Troiano, J. M., Olenick, L. L., Kuech, T. R., Melby, E. S., Hu, D., Lohse, S. E., Mensch, A. C., Dogangun, M., Vartanian, A. M., Torelli, M. D., Ehimiaghe, E., Walter, S. R., Fu, L., Anderton, C. R., Zhu, Z., Wang, H., Orr, G., Murphy, C. J., Hamers, R. J., Pedersen, J. A., Geiger, F. M. (2015), Direct Probes of 4 nm Diameter Gold Nanoparticles Interacting with Supported Lipid Bilayers. *J. Phys. Chem. C*, 119, 534−546. (DOI: 10.1021/jp512107z)

Chapter 3

Interaction of carboxyl-modified gold nanoparticles with liposomes of different chain lengths and controlled drug release by layer-by-layer technology

3.1 Introduction

It takes almost 15 years to bring a drug to the market from synthesis with a cost of more than $500 million [1]. Most of these drugs suffer from high side effects, poor adsorption, poor solubility, high drug dosing, minimum efficiency and uncontrolled and nonspecific delivery with high cytotoxicity, which limit their uses [2-3]. The concern should be more in case of chemotherapeutic drugs because most of the anticancer drugs are highly toxic to healthy cells and damage the same along with the cancer cells [4-5]. This results in severe side effects for the patients. Among all drug delivery systems (DDSs), lipid-based DDSs have found pronounced application during the past few years because of their low cytotoxicity, biocompatibility and biodegradability [6−8]. Thus, systems such as Doxil, DaunoXome, Mycet etc. are already approved by the Food and Drug Administration (FDA) and available in the market [9−11].

Despite several advantages, the use of liposomes is limited due to their tendency of fusion rendering to drug leakage [12−18]. To overcome this problem, several strategies have been adopted in the past few years [19−21]. One approach to stabilize liposomes is to coat their surface with polymers such as poly(ethylene glycol) (PEG) and zwitterionic polymers [22−29]. Another successful approach to stabilize the liposomes is to use nanomaterials to form lipid−nanoparticle assemblies [18, 30−33]. Physical interactions between lipid bilayers and metal nanoparticles play an important role because these interactions increase the biocompatibility of the systems [34−48]. These systems have found applications

in drug delivery, imaging, biosensing and separation [49−52]. The decoration of lipid bilayers with nanoparticles increases the stability of the liposomes and prevents premature fusion [18, 30−33, 52−54].

Lipids with different chain lengths have different phase transition temperatures. Moreover, the dynamics inside of liposomes is different from that of the bulk one due to different surface properties [55−57]. Thus, different lipids can have different binding interactions with nanoparticles [30−54, 58]. The interactions between liposomes and nanoparticles alter surface properties such as polarity, charge, fluidity etc. and affect the packing of the liposomes [59]. Surface modification can be used in biomedical application and DDSs [57, 60−66].

Therefore, we studied interactions between carboxyl-modified gold nanoparticles (AuC) and liposomes of different phase transition temperatures using steady-state and time-resolved spectroscopy using a membrane probe PRODAN. To unravel the underlying mechanism, we used three lipids, namely, dipalmitoylphosphatidylcholine (DPPC), 1,2-dimyristoyl-sn-glycero-3-phosphocholine (DMPC), and 1,2-dilauroyl-sn-glycero-3-phosphocholine (DLPC). We exploited the liposome-nanoparticle assembly for controlled release of a prominent anticancer drug Doxorubicin (DOX) under acidic conditions. We correlated the drug release rate with the extent of liposome−nanoparticle interaction.

Further, a more compact lipid-based capsule system was prepared using layer-by-layer (LBL) method. Alternatively charged layers of polymer and lipid were used to coat the liposome-nanoparticle assembly (Scheme 3.1). This system was explored to further control the rate of drug release. The resulting capsules were stable against further growth and remained unaggregated in solution. The capsules formed were also capable of creating a barrier to prevent premature release of the drug [67−70].

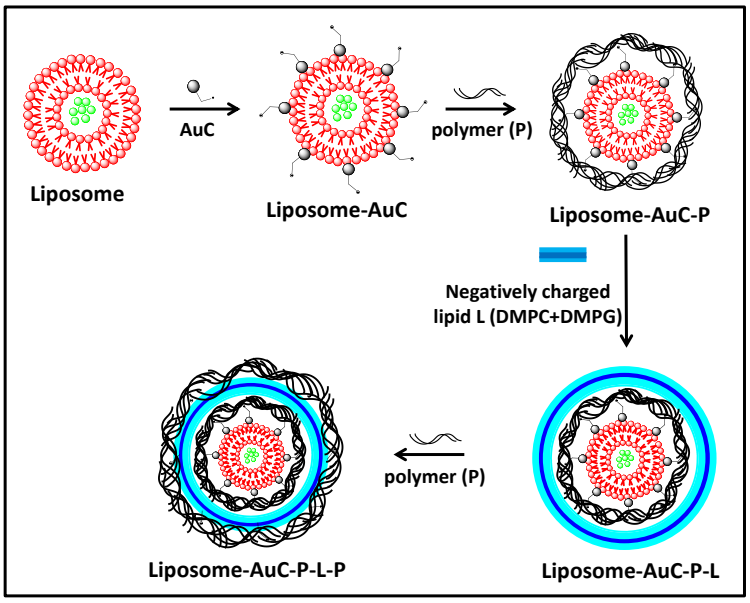

Scheme 3.1 *Layer-by-layer (LBL) deposition of polymer (P) and lipid (L) on liposome−AuC assembly.*

3.2 Results and Discussion

3.2.1 <u>Behaviour of PRODAN in presence of different lipids</u>: PRODAN exhibits emission at 540 nm in aqueous buffer medium, assigned to a charge transfer (CT) state. There are some reports where this state has been assigned as a twisted intramolecular charge transfer (TICT) state [71-72]. The TICT state arises due to rotation of the C−N bond in PRODAN, thus aligning the two methyl groups attached to the N atom in a plane perpendicular to the plane of the naphthalene rings. In the presence of liposomes, another emission band evolves at around 450−460 nm and is attributed to a local excited state (LE state). The appearance of a LE state indicates that PRODAN is partitioned in the lipid bilayer. PRODAN is loosely anchored to the bilayer. The normalized emission spectra of PRODAN in different lipids (DPPC, DMPC and DLPC) are shown in Figure 3.1.

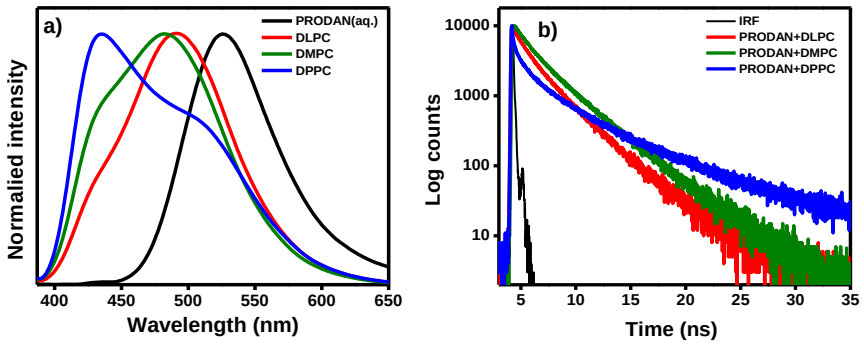

Figure 3.1 *Normalized emission spectra of PRODAN in DPPC, DMPC and DLPC liposomes, showing a blue shift in PRODAN−liposome systems as compared to PRODAN in aqueous buffer solution. (b) Representative time-resolved decay of PRODAN in different liposomes at 440 nm.*

It is revealed from Figure 3.1 that the emission spectra of PRODAN shifted to shorter wavelength in all liposomes while a maximum blue shift took place in DPPC liposomes and a minimum took place in DLPC liposomes. This indicates that PRODAN experiences the most non polar environment in DPPC liposomes. DPPC liposomes are more rigid, thus rotation around the C−N bond leading to a TICT state in PRODAN is most hindered. As a result, the LE state of PRODAN is more prominent in the presence of DPPC. The higher blue shift also indicates that DPPC is least hydrated at room temperature as compared to DMPC and DLPC liposomes. On the other hand, for comparatively softer liposomes like DLPC and DMPC, it is difficult to isolate the emission spectra of PRODAN corresponding to water and the membrane phase due to superposition of these two states in DLPC medium. The estimated partition coefficients of PRODAN are 1.0×10^5, 5.8×10^5, and 10×10^5 for DPPC, DMPC and DLPC, respectively [72]. The comparatively higher partition coefficient in DLPC liposomes is due to the fact that DLPC remains in a completely liquid crystalline (LC) phase at room temperate. Therefore, higher fluidity in DLPC liposomes allows more PRODAN molecules to be incorporated in the bilayer. The total emission intensity of PRODAN increases for DPPC with an increase in temperature due higher fluidity [73]. The lifetime data reveal that PRODAN has a lifetime of around 0.95 ns at 540 nm. However, at 440 nm the observed lifetimes are nonexponential, with a shorter component (τ_1) at around 1 ns and a longer component (τ_2) varying from 3 to 5 ns (Table 3.1). The nonexponential fitting of decay measurements clearly

indicates partition of PRODAN in a lipid bilayer. Notably, we observe that τ_2 is the longest in the case of DPPC liposomes and the shortest in DLPC liposomes. The fact indicates that DPPC in the gel phase offers a more rigid environment to PRODAN as compared to other liposomes. DLPC liposomes being the softest in nature among the three lipids reveal a much lower value of τ_2 as compared to other liposomes. The decays at 500 nm are biexponential for DPPC and DMPC liposomes, while the decay is single exponential for DLPC liposomes. The emissions in DPPC liposomes from the aqueous phase and gel phase are quite distinct. Thus, the component at around 0.80 ns at 500 nm could be due to PRODAN molecules in the aqueous phase. The longer component comes from the PRODAN molecules anchored with the lipid bilayer. As already mentioned, the emission in DLPC is an overlap from both the aqueous phase and bilayer phase; thus, the decay at 500 nm is single-exponential [74]. The decay at longer wavelength proceeded with a rise in component in DLPC liposomes due to dipolar relaxation of the solvent. However, the solvent is tightly bound to DPPC liposomes such that solvent relaxation does not occur in DPPC liposomes.

3.2.2 <u>Interaction of liposomes and nanoparticles</u>: Zwitterionic liposomes offer strong affinity toward negatively charged AuC owing to electrostatic interaction between charged choline groups of liposomes and COO^- groups of AuC [30−32]. We monitored the emission properties of PRODAN confined in the surface of liposomes in the presence of AuC. Upon addition of AuC to PRODAN-loaded liposomes, we observe that at very low concentration of AuC, i.e., when C_{AuC}/ C_L (where C_{AuC} and C_L are the concentrations of gold nanoparticles and liposome, respectively) is very low (∼0.2) the intensity of PRODAN increases for all of the liposomes followed by a slight red shift. This observation could be due to the fact that at low concentration of AuC the fluidity of liposomes increases due to carrying water through the −COOH group. The other explanation is the leakage of the encapsulated probe from DMPC and DLPC liposomes immediately after addition of AuC. It is known that without pore formation its content does release at the phase transition temperature or when there is a fluid to gel transition. The transition takes place locally. However, at relatively higher C_{AuC}/C_L ratios, the

intensity decreases followed by a distinct blue shift (Figure 3.2).

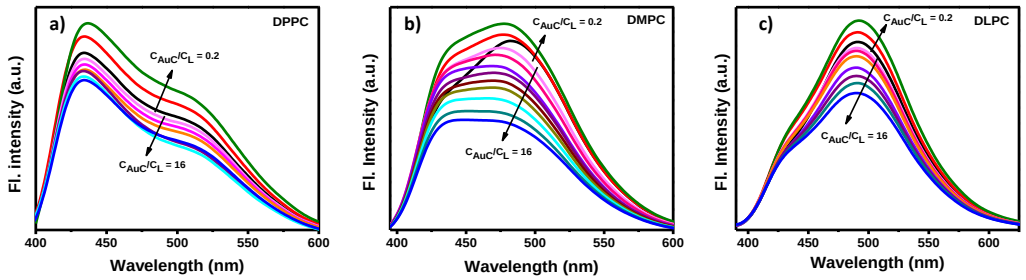

Figure 3.2 *Emission spectra of PRODAN for Liposome-AuC at different concentrations of AuC for a) DPPC, b) DMPC, and c) DLPC. Spectra indicates initial red shift followed by a slight increase in the intensity for lower concentrations of AuC, and blue shift for liposomes followed by decrease in intensity with an increase in the concentration of AuC. Upward arrow denotes an increase in the intensity and downward arrow depicts decrease in the intensity.*

The normalized spectra as revealed by Figure 3.3 clearly indicate that the LE state of PRODAN is being stabilized while the population corresponding to the TICT state decreases. The fact clearly indicates that the liposomes undergo gel formation owing to adsorption of nanoparticles on the surface. The initial binding pattern of nanoparticles with liposomes is exothermic, and at higher concentration, the binding-induced shrinkage takes place and this process is endothermic. Interestingly, it is revealed from Figure 2.3 that the maximum gelation is observed in the case of DMPC liposomes as compared to DPPC and DLPC liposomes. We explain this observation by the fact that the experimental condition (T = 25 °C) was very close to the phase transition temperature (23 °C) of DMPC liposomes. DMPC remains in a nearly LC phase; thus, a little increase in the phase transition temperature drastically alters DMPC from a nearly fluid phase to a gel phase. In the case of DPPC liposomes, the transition temperature increases to 44 from 41 °C in the presence of citrate-capped gold nanoparticles [75]. On the other hand, MPA capped AuNPs did not change the transition temperature of DPPC. Therefore, a small fraction of the lipid directly in contact with nanoparticles might have a much higher transition temperature. We further confirmed the gelation by plotting the intensity fraction (intensity at blue and red emission) at 440 (blue) and 500 nm (red) against the C_{AuC}/C_L ratio. Their normalized difference gives the net polarization given by the following equation:

$$P = \frac{I_B - I_R}{I_B + I_R} \qquad (1)$$

where I_B and I_R are the emitted intensities at these wavelengths at blue and red emission, respectively.

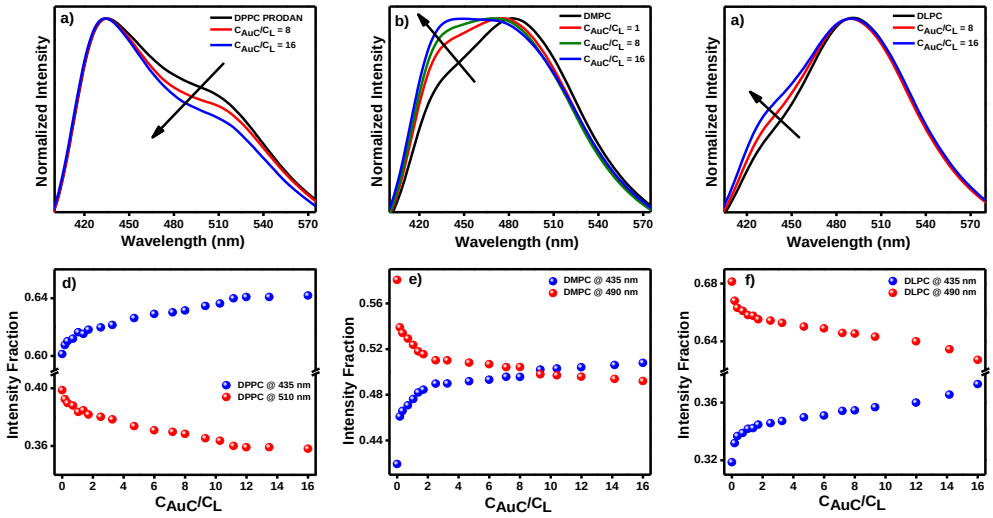

Figure 3.3 *Normalized emission spectra for addition of AuC in different concentrations to a lipid−PRODAN solution for (a) DPPC, (b) DMPC and (c) DLPC liposomes and (d-f) respective intensity fraction versus C_{AuC}/C_L plot for DMPC liposomes at 435 (blue emission) and 490 nm (red emission).*

It is revealed that the intensity fraction for the blue emission increases while that of red emission decreases (Figure 3.3 d). This indicates that in the presence of nanoparticles, liposomes undergo gel formation from the LC phase. Further, we conducted lifetime measurements of PRODAN in different liposomes (Figure 3.4, Table 3.1). It is observed that in DLPC liposomes the decays at longer wavelength (500 nm) remain intact upon addition of AuC. However, in the case of DPPC liposomes, there is a marginal increment in the longer component and its amplitude. As this wavelength corresponds to PRODAN molecules in the aqueous phase, it is not that much affected by AuC particles in DMPC and DLPC liposomes. The marginal increment in the lifetime in the case of DPPC liposomes at 500 nm could be due to the local gelation effect caused by the addition of AuC. The local phase of liposomes can be switched by binding of charged nanoparticles because they alter the tilt angle of phosphatidylcholine head groups terminated by P−−N^+ [33]. The negatively charged nanoparticles preferentially bind with the N^+

terminus and raise the average angle, thus recruiting the lipid tail to increase the density. However, in the case of DPPC, DMPC, and DLPC, this factor is perhaps dominated by increased fluidity.

In the case of decay at 440 nm, Table 3.1 reveals that for DPPC liposomes the longer component increases from 4.90 to 5.60 ns along with the amplitude from 35 to 42%. The increase in the longer component along with the amplitude indicates that DPPC is stabilized by AuC. However, a marginal increment is observed in τ_2 (from 3.90 (45%) to 4.40 ns (52%)) along its amplitude a_2 in DMPC liposomes. The observation indicates that both liposomes gain stability upon addition of AuC. The higher increment in lifetime in DPPC liposomes stems from the fact that DPPC being in the gel phase has occupied less area per lipid molecule as compared to DMPC and DLPC lipid bilayer, allowing DPPC to capture more nanoparticles. On the other hand, DMPC and DLPC being in a nearly LC phase and a complete LC phase are not capable of holding more nanoparticles as compared to DPPC. Therefore, the lifetime changes marginally.

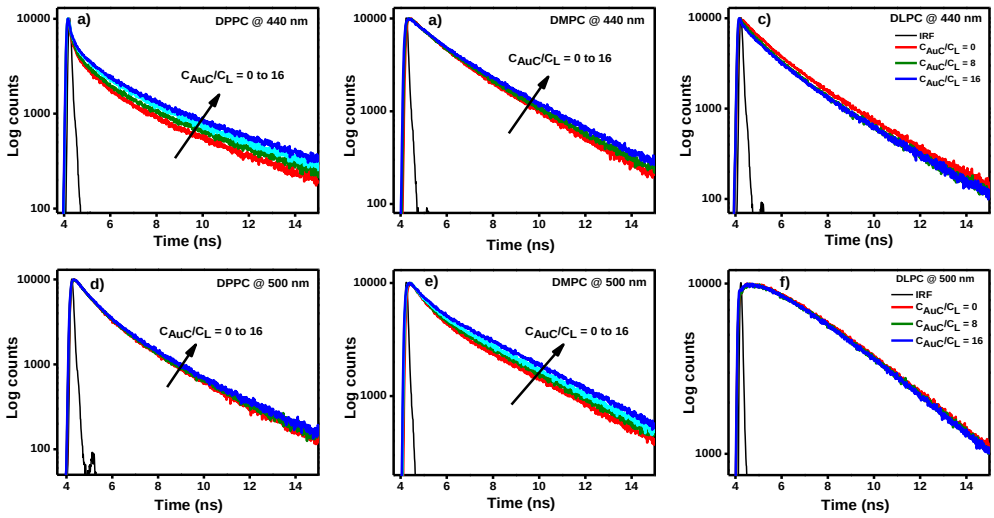

Figure 3.4 *Time-resolved decay curves of PRODAN in liposome−AuC solutions at different concentrations of AuC for (a) DPPC, (b) DMPC and (c) DLPC at 440 nm, and respective decay curves at 500 nm (d-f). The upward arrow indicates an increase in lifetime with an increase in concentration of AuC.*

Table 3.1 (a) *Lifetime components and normalized amplitudes of lifetime components of PRODAN at fixed concentration of AuC (C_{AuC}/C_L = 16) collected at 440 nm.*

Liposomes	a_1	a_2	τ_1 **(ns)**	τ_2 **(ns)**	χ^2
DPPC	0.65	0.35	1.10	4.90	1.20
DMPC	0.55	0.45	1.10	3.90	1.10
DLPC	0.50	0.50	0.97	3.00	1.21
DPPC +AuC	0.58	0.42	1.15	5.60	1.15
DMPC +AuC	0.48	0.52	1.00	4.40	1.10
DLPC + AuC	0.47	0.53	1.00	3.45	1.20

Table 3.1 (b) *Lifetime components and normalized amplitudes of lifetime components of PRODAN at fixed concentration of AuC (C_{AuC}/C_L = 16) collected at 500 nm.*

Liposomes	a_1	a_2	τ_1 **(ns)**	τ_2 **(ns)**	χ^2
DPPC	0.64	0.36	0.85	3.00	1.23
DMPC	0.20	0.80	0.700	3.90	1.20
DLPC	1.00	-	3.80	-	1.22
DPPC +AuC	0.23	0.77	0.65	3.70	1.10
DMPC +AuC	1.00	-	4.70	-	1.25
DLPC +AuC	1.00	-	3.80	-	1.20

From Figures 3.3 and 3.4, one point is clear that AuC delivers strong interaction to all liposomes irrespective of their phase transition temperature. We further confirmed the interaction of AuC with lipid bilayer using DLS and zeta potential measurement, e.g., the size of the liposome−AuC assembly increases from 121.38 ± 15.46 to 150.48 ± 8.94 nm for DPPC liposomes. After addition of AuC, the zwitterionic liposomes become highly negative, the final zeta potential being around −31.31 mV for DPPC liposomes.

3.2.3 <u>Drug release from liposome−nanoparticle assembly</u>: We explored the possibility of controlled release of drug molecules at acidic pH from liposome−AuC assembly. We used a prominent anticancer drug DOX, which is well encapsulated in liposomes. In the present case, we have incorporated 100 μM DOX in liposomes, the lipid concentration being 1 mM. We first checked the stability of the system. It is found that under physiological pH, no drug release is observed. We then checked the possibility of leakage at pH ≈ 6. Remarkably, drug

release does not take place at pH ≈ 6 for a substantial time. Interestingly, we found that at pH ≈ 5 the drug release starts and continues for more than 20 h (Figure 3.5). We estimated the rate constants by fitting the release profile to a single-exponential rate equation using first-order kinetics:

$$f = a(1-\exp(-kt)) \qquad (2)$$

where k measured the rate constant of release and a is the pre-exponential factor which measured the extent of the release of contents.

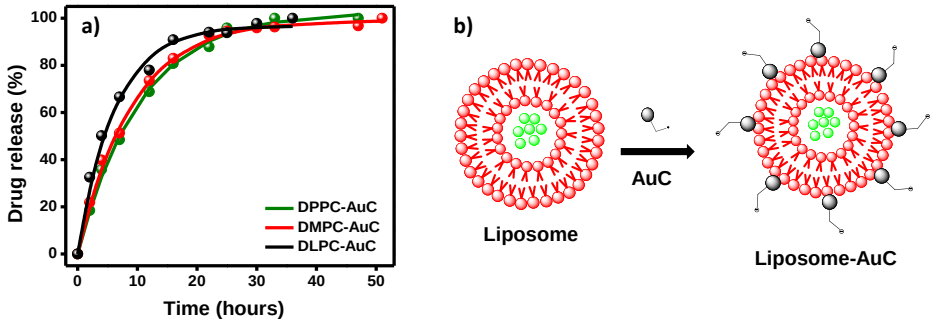

Figure 3.5 *(a) Drug release profile for liposome−AuC assemblies for different lipids at pH ≈ 5. The fitting was done following equation 2. (b) The scheme depicts the pictorial representation of the prepared liposome−AuC assemblies.*

The fitting yields rate constants were calculated to be 0.09, 0.12, and 0.20 h^{-1} for DPPC−AuC, DMPC−AuC and DLPC−AuC systems. Here two observations are important; one is that we do not see any drug release taking place in the pH range of 7.40− 6.0 but the drug release takes place at pH ≈ 5.0. The second and most striking observation is that the rate of drug release takes place in the order of DPPC ≈ DMPC < DLPC liposomes. We explain the first observation in light of the detachment of AuC from the liposomes under acidic pH and the subsequent fusion of liposomes, leading to drug release [31]. The pKa of the carboxyl group is around 5.0. As the pH of the medium is reduced to a value below the pKa of carboxylic acid, the negatively charged AuC obtain protons and become neutral AuCH. The detachment from the liposome takes place due to the elimination of electrostatic interaction. This leads to fusion of the liposomes and results in the release of drug molecules, as revealed by DLS measurement in which the size increases to 419.7 nm (PDI= 0.276 nm) in acidic pH from 160.4 nm (PDI= 0.112)

at pH 7.4 (Figure 3.6).

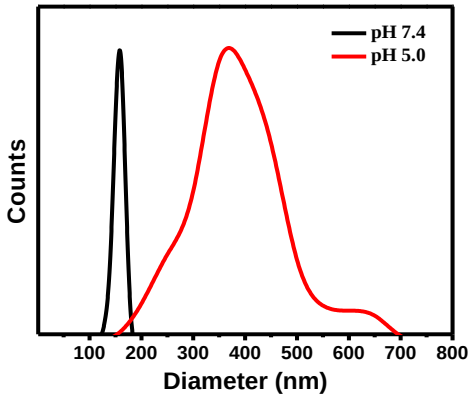

Figure 3.6 *Hydrodynamic size distribution histogram from DLS measurement for DPPC-AuC assembly at physiological and acidic pH.*

The second observation that reveals that drug release takes place in the order DPPC ≈ DMPC < DLPC liposomes led to the conclusion that the nanoparticle-decorated liposomes are more resistant toward pH change as compared to bare liposomes. Further, a lipid with a higher phase transition temperature (DPPC) is more resistant toward pH than a lipid with a lower phase transition temperature (DLPC). The rate constant is slower by a factor of almost 2 in the case of DPPC as compared to that of DLPC liposomes. To account for the observation, the interaction between different liposomes and nanoparticles must be considered. We already mentioned that the nanoparticles are adsorbed on the surface and stabilize liposomes. DPPC being in the gel phase has a larger number of head groups exposed toward water and thus can hold more AuC. For DPPC in the gel phase, the area per lipid head group is around 47 $Å^2$, while DMPC in the LC phase has a lipid area of around 64 $Å^2$ [76−78]. Therefore, more head groups of DPPC are exposed to water, which captures a larger number of AuC and stabilizes the liposomes to a much larger extent by making them more rigid. This makes it effective to avoid premature drug release. Moreover, DPPC is least hydrated among all three liposomes owing to their gel phase. Therefore, the electrostatic interaction is not screened by interfacial water molecules in the case of DPPC offering stronger affinity toward negatively charged AuC. The interfacial region of DPPC is less polar than DMPC and DLPC liposomes [76]. This facilitates electrostatic interaction between AuC and DPPC liposomes. In the case of DMPC

liposomes, addition of AuC perhaps causes phase transition at room temperature from the fluid to gel phase. This transition brings extra stability in the case of DMPC liposomes. Thus, we do not observe any significant differences in the release rate constant for DPPC−AuC and DMPC−AuC assemblies. The other fact that may be crucial in this case is that the gel state fluctuation in the head group region of DPPC is much smaller as compared to that of DMPC and DLPC liposomes. Therefore, the nanoparticles are held tightly in the surface of DPPC liposomes and thus lead to slower detachment. As the detachment leads to fusion of the liposomes among all of the liposomes, the diffusion coefficient of gold nanoparticles should be least in DPPC owing to its SG phase. Therefore, the drug release rate is slowest in DPPC liposomes, while it is fastest for DLPC liposomes.

3.3.4 <u>Capsule formation, characterization and drug release</u>: Although liposome−AuC assemblies are fairly stable but a burst release is observed which could be attributed to fusion of the liposomes at acidic pH. In order to further control the drug release, we coated the liposome−AuC assembly with an oppositely charged polymer, namely, polydiallyldimethylammonium chloride, followed by coating with a mixture of lipids L (DMPC:DMPG) and further with polymer to form capsule-like structures. The formation of each layer of polymer and lipid is confirmed by the subsequent changes in DLS and zeta potential measurements (Figure 3.7).

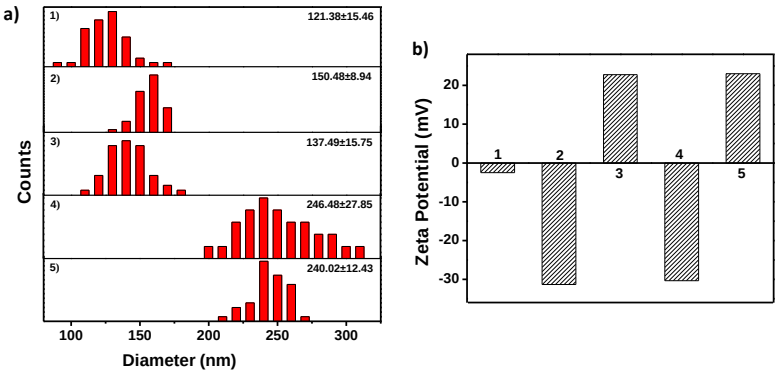

Figure 3.7 *(a) Hydrodynamic size distribution histogram from DLS measurement and (b) zeta potential values for (1) bare liposomes (DPPC), (2) liposome−AuC assembly, (3) liposome−AuC−P, (4) liposome−AuC−P−L, and (5) liposome−AuC−P−L−P capsules.*

The coating of the liposome−AuC assembly by polymer decreases the size from 150.48 ± 8.94 to 137.49 ± 15.75 nm, and the zeta potential increases from −31.31 to +22.77 mV for DPPC liposome. These observations indicate that the liposome−AuC assembly is wrapped with the polymer. Further coating of the capsule with negatively charged liposomes L [DMPC:DMPG (8:2)] increases the size to 246.48 ± 27.85 nm, the zeta potential being −30.35 mV, followed by polymer potential being +23.38 mV. The decrease in the diameter of the capsule upon coating with polymer is probably due to more compact layer packing occurring with an increase in the number of layers. Such behaviour is assumed to occur at the outset of coating (for the initial layers), which is generally characterized by an inconsiderable increase in the shell thickness [79]. DLS measurements and the zeta potential give results following a similar pattern for DMPC and DLPC (Table 3.2).

Table 3.2 *Hydrodynamic diameter as obtained by DLS measurement and zeta potential values for DMPC and DLPC liposomes and subsequent layered capsules.*

Lipid	**System**	**Average size, d (nm)**	**Zeta potential (mV)**
DMPC	DMPC	166.2	-4.17
	DMPC-AuC	181.9	-42.09
	DMPC-AuC-P	179.6	+17.33
	DMPC-AuC-P-L	282.1	-34.42
	DMPC-AuC-P-L-P	278.6	+18.32
DLPC	DLPC	158.5	-1.20
	DLPC-AuC	182.6	-40.31
	DLPC-AuC-P	181.3	+21.89
	DLPC-AuC-P-L	305.3	-18.31
	DLPC-AuC-P-L-P	301.3	+28.31

We characterized the morphology of the obtained capsule structures with SEM imaging (Figure 3.8), which reveals that the capsules have a uniform size of around 150 nm. The SEM images reveal that a layer is formed upon addition of polymer on the liposome−AuC assembly.

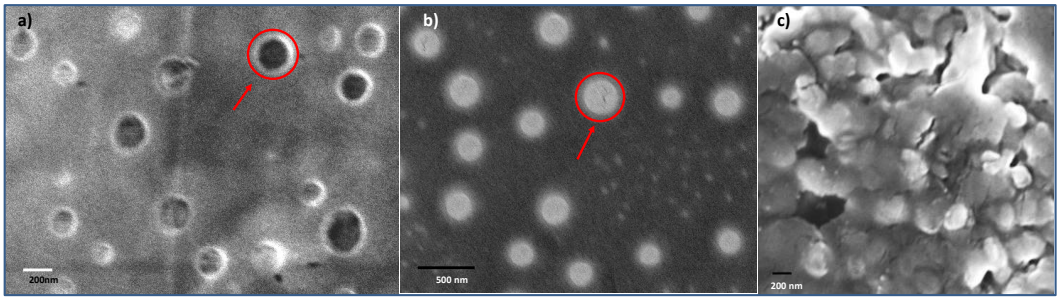

Figure 3.8 *FE-SEM images for the (a) liposome−AuC−P system, b) liposome−AuC−P−L−P system, both intact even after 1 week, and (c) bare liposome (fused after 2 days from synthesis). The arrows depict the formation of a layer over the liposome−AuC assembly.*

Further confocal and bright field images confirm their ability to carry drug or dye molecules inside them (Figure 3.9). These systems are fairly stable as the morphology and other characterization parameters do not change for a prolonged time.

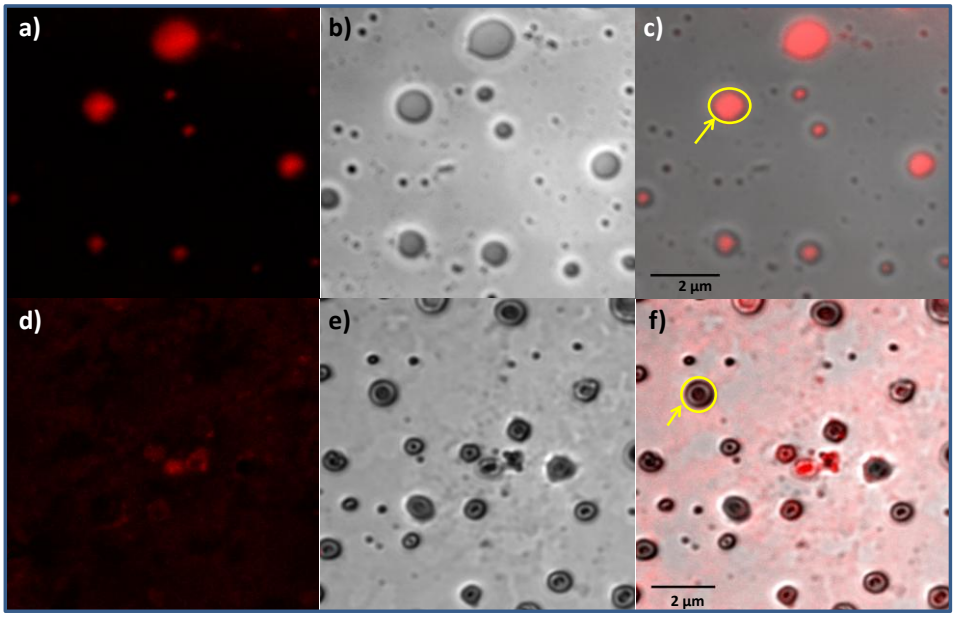

Figure 3.9 *Uptake studies for capsule systems using CLSM. (a−c) Liposome−AuC−P system; (d−f) liposome−AuC−P−L−P system as obtained under confocal, bright field, and merged images. All images taken after 1 week from synthesis.*

The drug release profile reveals that burst release is very successfully prevented in the capsule structures unlike liposome−AuC assemblies (Figure 3.10). The drug release becomes significantly slower, and the fitting results for DPPC, DMPC,

and DLPC are summarized in Table 3.3. Therefore, it is evident that the lipid-based capsules may significantly improve the drug release profile. We found that the degree of drug release significantly decreases and drug release can be continued for a longer time.

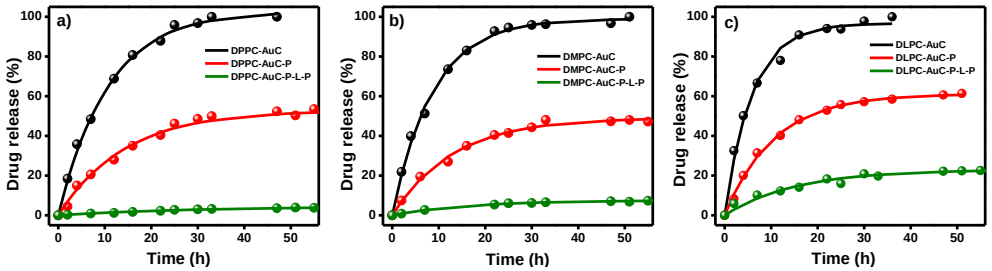

Figure 3.10 *Drug release profile for liposome−AuC assemblies followed by coating with polymer and lipids (l) in an LBL fashion for (a) DPPC, (b) DMPC, and (c) DLPC liposomes. The fitting was done following equation 2.*

Table 3.3 *Rate constants of release profile from different lipid-based systems at pH~5.*

Lipid	System	Rate constant (h^{-1})
1) DPPC	DPPC-AuC	0.09
	DPPC-AuC-P	0.065
	DPPC-AuC-P-L	0.04
	DPPC-AuC-P-L-P	0.032
2) DMPC	DMPC-AuC	0.12
	DMPC-AuC-P	0.08
	DMPC-AuC-P-L	0.061
	DMPC-AuC-P-L-P	0.061
3) DLPC	DLPC-AuC	0.20
	DLPC-AuC-P	0.11
	DLPC-AuC-P-L	0.067
	DLPC-AuC-P-L-P	0.068

3.3 Conclusion

In conclusion, we found that carboxyl-modified gold nanoparticles (AuC) interact strongly with liposomes depending on their fluidities. AuC cause gelation upon contact with the lipid bilayer. This makes the liposome−nanoparticle assembly fairly stable as compared to bare liposomes. The fusion activity of liposomes can be effectively controlled by decoration of AuC nanoparticles on the outer surface of phospholipid liposomes. We found that the detachment rate of AuC from the liposome−AuC assemblies differs due to variations in the phase transition temperatures of different liposomes and the fluidity of the systems. DPPC (gel phase) is more effective at providing a stronger interaction with AuC as compared to that of liposomes that remain in the LC phase (DMPC and DLPC). This is because more head groups in DPPC are exposed to water and thus can hold more nanoparticles. We further controlled drug release via lipid-based capsule structures by coating the liposome−AuC assemblies with alternating layers of oppositely charged with polymer and lipid following an LBL approach. These capsules were found to be more compact and stable. The premature release of drug was controlled to a large extent by the formation of capsules.

3.4 References

1. Bolten, B. M., DeGregorio, T. (2002), Trends in development cycles. *Nat. Rev. Drug Discovery*, 1, 335–336. (DOI: 10.1038/nrd805)
2. Fliri, A. F., Loging, W. T., Thadeio, P. F., Volkmann, R. A. (2005), Analysis of drug-induced effect patterns to link structure and side effects of medicines. *Nat. Chem. Biol.*, 1, 389–397. (DOI: 10.1038/nchembio747)
3. Perez-Nueno, V. I., Souchet, M., Karaboga, A. S., Ritchie, D. W. (2015), GESSE: Predicting drug side effects from drug-target relationships. *J. Chem. Inf. Model.*, 55, 1804–1823. (DOI: 10.1021/acs.jcim.5b00120)
4. Wang, W., Cheng, D., Gong, F., Miao, X., Shuai, X. (2012), Design of multifunctional micelle for tumor-targeted intracellular drug release and

fluorescent imaging. *Adv. Mater.*, 24, 115–120. (DOI: 10.1002/adma.201104066)

5. Du, J.-Z., Sun, T.-M., Song, W.-J., Wu, J., Wang, J. (2010), A tumor-acidity-activated charge-conversional nanogel as an intelligent vehicle for promoted tumoral-cell uptake and drug delivery. *Angew. Chem., Int. Ed.*, 49, 3621–3626. (DOI: 10.1002/anie.200907210)
6. Allen, T. M., Cullis, P. R. (2013), Liposomal drug delivery systems: From concept to clinical applications. *Adv. Drug Delivery Rev.*, 65, 36–48. (DOI: 10.1016/j.addr.2012.09.037)
7. Viitala, L., Pajari, S., Lajunen, T., Kontturi, L.-S., Laaksonen, T., Kuosmanen, P., Viitala, T., Urtti, A., Murtomaki, L. (2016), Photothermally triggered lipid bilayer phase transition and drug release from gold nanorod and indocyanine green encapsulated liposomes. *Langmuir*, 32, 4554–4563. (DOI: 10.1021/acs.langmuir.6b00716)
8. Askes, S. H. C., Leeuwenburgh, V. C., Pomp, W., Arjmandi-Tash, H., Tanase, S., Schmidt, T., Bonnet, S. (2017), Water-dispersible silica-coated upconverting liposomes: can a thin silica layer protect TTA-UC against oxygen quenching? *ACS Biomater. Sci. Eng.*, 3, 322–334. (DOI: 10.1021/acsbiomaterials.6b00678)
9. Barenholz, Y. (2012), Doxil®–the first FDA-approved nano-drug: lessons learned. *J. Controlled Release*, 160, 117–134. (DOI: 10.1016/j.jconrel.2012.03.020)
10. Fassas, A., Anagnostopoulos, A. (2005), The use of liposomal daunorubicin (DaunoXome) in acute myeloid leukemia. *Leuk. Lymphoma.*, 46, 795–802. (DOI: 10.1080/10428190500052438)
11. Gardikis, K., Tsimplouli, C., Dimas, K., Micha-Screttas, M., Demetzos, C. (2010), New chimeric advanced drug delivery nano systems (chi-aDDnSs) as doxorubicin carriers. *Int. J. Pharm.*, 402, 231–237. (DOI: 10.1016/j.ijpharm.2010.10.007)

12. Liu, M., Gan, L., Chen, L., Xu, Z., Zhu, D., Hao, Z., Chen, L. (2012), Supramolecular core-shell nanosilica@liposome nanocapsules for drug delivery. *Langmuir*, 28, 10725–10732. (DOI: 10.1021/la3021645)
13. Kisak, E. T., Coldren, B., Evans, C. A., Boyer, C., Zasadzinski, J. A. (2004), The vesosome– a multicompartment drug delivery vehicle. *Curr. Med. Chem.*, 11, 199–219. (DOI: 10.2174/0929867043456197)
14. Lee, S.-M., Chen, H., Dettmer, C. M., O'Halloran, T. V., Nguyen, S. T. (2007), Polymer-caged lipsomes: a pH-responsive delivery system with high stability. *J. Am. Chem. Soc.*, 129, 15096–15097. (DOI: 10.1021/ja070748i)
15. Haluska, C. K., Riske, K. A., Marchi-Artzner, V., Lehn, J.-M., Lipowsky, R., Dimova, R. (2006), Time scales of membrane fusion revealed by direct imaging of vesicle fusion with high temporal resolution. *Proc. Natl. Acad. Sci. U. S. A.*, 103, 15841–15846. (DOI: 10.1073/pnas.0602766103)
16. Lei, G., MacDonald, R. C. (2003), Lipid bilayer vesicle fusion: intermediates captured by high-speed microfluorescence spectroscopy. *Biophys. J.*, 85, 1585–1599. (DOI: 10.1016/S0006-3495(03)74590-1)
17. Marrink, S., Mark, A. E. (2003), The mechanism of vesicle fusion as revealed by molecular dynamics simulations. *J. Am. Chem. Soc.*, 125, 11144–11145. (DOI: 10.1021/ja036138+)
18. Zhang, L., Granick, S. (2006), How to stabilize phospholipid liposome (using nanoparticles). *Nano Lett.*, 6, 694–698. (DOI: 10.1021/nl052455y)
19. Torchilin, V. P. (2005), Recent advances with liposomes as pharmaceutical carriers. *Nat. Rev. Drug Discovery*, 4, 145–160. (DOI: 10.1038/nrd1632)
20. Deshpande, P. P., Biswas, S., Torchilin, V. P. (2013), Current trends in the use of liposomes for tumor targeting. *Nanomedicine*, 8, 1509–1528. (DOI: 10.2217/nnm.13.118)
21. Levchenko, T. S., Hartner, W. C., Torchilin, V. P. (2012), Liposomes for cardiovascular targeting. *Ther. Delivery*, 3, 501–514. (DOI: 10.4155/tde.12.18)
22. Knop, K., Hoogenboom, R., Fischer, D., Schubert, U. S. (2010), Poly(ethylene glycol) in drug delivery: pros and cons as well as potential

alternatives. *Angew. Chem., Int. Ed.*, 49, 6288–6308. (DOI: 10.1002/anie.200902672)

23. Stepniewski, M., Pasenkiewicz-Gierula, M., Rog, T., Danne, R., Orlowski, A., Karttunen, M., Urtti, A., Yliperttula, M., Vuorimaa, E., Bunker, A. (2011), Study of PEGylated lipid layers as a model for PEGylated liposome surfaces: molecular dynamics simulation and langmuir monolayer studies. *Langmuir*, 27, 7788–7798. (DOI: 10.1021/la200003n)
24. Yan, W., Huang, L. (2007), Recent advances in liposome-based nanoparticles for antigen delivery. *Polym. Rev.*, 47, 329–344. (DOI: 10.1080/15583720701455020)
25. Cao, Z. Q., Zhang, L., Jiang, S. Y. (2012), Superhydrophilic zwitterionic polymers stabilize liposomes. *Langmuir*, 28, 11625–11632. (DOI: 10.1021/la302433a)
26. Jiang, S. Y., Cao, Z. Q. (2010), Ultralow-fouling, functionalizable, and hydrolyzable zwitterionic materials and their derivatives for biological applications. *Adv. Mater.*, 22, 920–932. (DOI: 10.1002/adma.200901407)
27. Davis, M. E., Chen, Z., Shin, D. M. (2008), Nanoparticle therapeutics: an emerging treatment modality for cancer. *Nat. Rev. Drug Discovery*, 7, 771–782. (DOI: 10.1038/nrd2614)
28. Woodle, M. C. (1998), Controlling liposome blood clearance by surface grafted polymers. *Adv. Drug Delivery Rev.*, 32, 139–152. (DOI: 10.1016/S0169-409X(97)00136-1)
29. Rameez, S., Palmer, A. F. (2011), Simple method for preparing poly(ethylene glycol)-surface conjugated liposome-encapsulated hemoglobins: physicochemical properties, long-term storage stability, and their reactions with O_2, CO, and NO. *Langmuir*, 27, 8829–8840. (DOI: 10.1021/la201246m)
30. Thamphiwatana, S., Fu, V., Zhu, J., Lu, D., Gao, W., Zhang, L. (2013), Nanoparticle-stabilized liposomes for pH-responsive gastric drug delivery. *Langmuir*, 29, 12228–12233. (DOI: 10.1021/la402695c)

31. Pornpattananangkul, D., Olson, S., Aryal, S., Sartor, M., Huang, C.–M., Vecchio, K., Zhang, L. (2010), Stimuli-responsive liposome fusion mediated by gold nanoparticles. *ACS Nano*, 4, 1935–1942. (DOI: 10.1021/nn9018587)
32. Adhikari, C., Das, A., Chakraborty, A. (2015), Controlled release of a sparingly water-soluble anticancer drug through pH-responsive functionalized gold-nanoparticle-decorated liposomes. *ChemPhysChem*, 16, 866–871. (DOI: 10.1002/cphc.201402748)
33. Wang, B., Zhang, L., Bae, S. C., Granick, S. (2008), Nanoparticle-induced surface reconstruction of phospholipid membranes. *Proc. Natl. Acad. Sci. U. S. A.*, 105, 18171–18175. (DOI: 10.1073/pnas.0807296105)
34. Preiss, M. R., Bothun, G. D. (2011), Stimuli-responsive liposome nanoparticle assemblies. *Expert Opin. Drug Delivery*, 8, 1025–1040. (DOI: 10.1517/17425247.2011.584868)
35. Ginzburg, V. V., Balijepalli, S. (2007), Modeling the thermodynamics of the interaction of nanoparticles with cell membranes. *Nano Lett.*, 7, 3716–3722. (DOI: 10.1021/nl072053l)
36. Liu, J. W. (2016), Interfacing zwitterionic liposomes with inorganic nanomaterials: surface forces, membrane integrity, and applications. *Langmuir*, 32, 4393–4404. (DOI: 10.1021/acs.langmuir.6b00493)
37. SubWi, H., Lee, K., Kyu Pak, H. (2008), Interfacial energy consideration in the organization of a quantumdot−lipid mixed system. *J. Phys.: Condens. Matter*, 20, 494211. (DOI: 10.1088/0953-8984/20/49/494211)
38. Al-Jamal, W. T., Kostarelos, K. (2007), Liposome-nanoparticle hybrids for multimodal diagnostic and therapeutic applications. *Nanomedicine*, 2, 85–98. (DOI: 10.2217/17435889.2.1.85)
39. Paasonen, L., Sipila, T., Subrizi, A., Laurinmaki, P., Butcher, S. J., Rappolt, M., Yaghmur, A., Urtti, A., Yliperttula, M. (2010), Gold-embedded photosensitive liposomes for drug delivery: triggering mechanism and intracellular release. *J. Controlled Release*, 147, 136–143. (DOI: 10.1016/j.jconrel.2010.07.095)

40. Von White, G., 2nd, Chen, Y., Roder-Hanna, J., Bothun, G. D., Kitchens, C. L. (2012), Structural and thermal analysis of lipid vesicles encapsulating hydrophobic gold nanoparticles. *ACS Nano*, 6, 4678–4685. (DOI: 10.1021/nn2042016)

41. Preiss, M. R., Hart, A., Kitchens, C., Bothun, G. D. (2017), Hydrophobic nanoparticles modify the thermal release behavior of liposome. *J. Phys. Chem. B*, 121, 5040–5047. (DOI: 10.1021/acs.jpcb.7b01702)

42. Bothun, G. D. (2008), Hydrophobic silver nanoparticles trapped in lipid bilayers: size distribution, bilayer phase behavior, and optical properties. *J. Nanobiotechnol.*, 6, 13. (DOI: 10.1186/1477-3155-6-13)

43. Bothun, G. D., Rabideau, A. E., Stoner, M. A. (2009), Hepatoma cell uptake of cationic multifluorescent quantum dot liposomes. *J. Phys. Chem. B*, 113, 7725–7728. (DOI: 10.1021/jp9017458)

44. Jang, H., Pell, L. E., Korgel, B. A., English, D. S. (2003), Photoluminescence quenching of silicon nanoparticles in phospholipid vesicle bilayers. *J. Photochem. Photobiol., A*, 158, 111–117. (DOI: 10.1016/S1010-6030(03)00024-8)

45. Rasch, M. R., Rossinyol, E., Hueso, J. L., Goodfellow, B. W., Arbiol, J., Korgel, B. A. (2010), Hydrophobic gold nanoparticle self-assembly with phosphatidylcholine lipid: membrane-loaded and janus vesicles. *Nano Lett.*, 10, 3733–3739. (DOI: 10.1021/nl102387n)

46. Amstad, E., Kohlbrecher, J., Müller, E., Schweizer, T., Textor, M., Reimhult, E. (2011), Triggered release from liposomes through magnetic actuation of iron oxide nanoparticle containing membranes. *Nano Lett.*, 11, 1664–1670. (DOI: 10.1021/nl2001499)

47. Verma, A., Stellacci, F. (2010), Effect of surface properties on nanoparticle–cell interactions. *Small*, 6, 12–21. (DOI: 10.1002/smll.200901158)

48. Sau, T. K., Urban, A. S., Dondapati, S. K., Fedoruk, M., Horton, M. R., Rogach, A. L., Stefani, F. D., Radler, J. O., Feldmann, J. (2009), Controlling loading and optical properties of gold nanoparticles on liposome membranes. *Colloids Surf. A*, 342, 92–96. (DOI: 10.1016/j.colsurfa.2009.04.014)

49. Gao, W., Hu, C.-M. J., Fang, R. H., Zhang, L. (2013), Liposome-like nanostructures for drug delivery. *J. Mater. Chem. B*, 1, 6569–6585. (DOI: 10.1039/c3tb21238f)

50. Sailor, M. J., Park, J.-H. (2012), Hybrid nanoparticles for detection and treatment of cancer. *Adv. Mater.*, 24, 3779–3802. (DOI: 10.1002/adma.201200653)

51. Liu, J., Jiang, X., Ashley, C., Brinker, C. J. (2009), Electrostatically mediated liposome fusion and lipid exchange with a nanoparticle-supported bilayer for control of surface charge, drug containment, and delivery. *J. Am. Chem. Soc.*, 131, 7567–7569. (DOI: 10.1021/ja902039y)

52. Tan, S., Li, X., Guo, Y., Zhang, Z. (2013), Lipid-enveloped hybrid nanoparticles for drug delivery. *Nanoscale*, 5, 860–872. (DOI: 10.1039/c2nr32880a)

53. Wang, F., Liu, J. (2015), A stable lipid/TiO2 interface with headgroup-inversed phosphocholine and a comparison with SiO_2 . *J. Am. Chem. Soc.*, 137, 11736–11742. (DOI: 10.1021/jacs.5b06642)

54. Wang, F., Liu, J. (2014), Liposome supported metal oxide nanoparticles: interaction mechanism, light controlled content release, and intracellular delivery. *Small*, 10, 3927–3931. (DOI: 10.1002/smll.201400850)

55. Bhattacharyya, K. (2008), Nature of biological water: a femtosecond study. *Chem. Commun.*, 25, 2848–2857. (DOI: 10.1039/b800278a)

56. Bhattacharyya, K. (2003), Solvation dynamics and proton transfer in supramolecular assemblies. *Acc. Chem. Res.*, 36, 95–101. (DOI: 10.1021/ar020067m)

57. Immordino, M. L., Dosio, F., Cattel, L. (2006), Stealth liposomes: review of the basic science, rationale, and clinical applications, existing and potential. *Int. J. Nanomedicine*, 1, 297–315. (PMID: 17717971)

58. Tsukada, C., Tsuji, T., Matsuo, K., Nomoto, T., Kutluk, G., Sawada, M., Ogawa, S., Yoshida, T., Yagi, S. (2015), Spectroscopic and morphological studies on interaction between gold nanoparticle and liposome constructed

with phosphatidylcholine. *IOP Conf. Ser.: Mater. Sci. Eng.*, 76, 012001. (DOI: 10.1088/1757-899X/76/1/012001)

59. Mhashal, A. R., Roy, S. (2014), Effect of gold nanoparticle on structure and fluidity of lipid membrane. *PLoS One*, 9, e114152. (DOI: 10.1371/journal.pone.0114152)
60. Pattni, B. S., Chupin, V. V., Torchilin, V. P. (2015), New developments in liposomal drug delivery. *Chem. Rev.*, 115, 10938–10966. (DOI: 10.1021/acs.chemrev.5b00046)
61. Fahmy, T. M., Fong, P. M., Goyal, A., Saltzman,W. M. (2005), Targeted for drug delivery. *Mater. Today*, 8, 18–26. (DOI: 10.1016/S1369-7021(05)71033-6)
62. Rengan, A. R., Bukhari, A. B., Pradhan, A., Malhotra, R., Banerjee, R., Srivastava, R., De, A. (2015), In vivo analysis of biodegradable liposome gold nanoparticles as efficient agents for photothermal therapy of cancer. *Nano Lett.*, 15, 842–848. (DOI: 10.1021/nl5045378)
63. An, X., Zhan, F., Zhu, Y. (2013), Smart photothermal-triggered bilayer phase transition in AuNPs- liposomes to release drug. *Langmuir*, 29, 1061–1068. (DOI: 10.1021/la304692h)
64. Pilbat, A.-M., Szegletes, Z., Kota, Z., Ball, V., Schaaf, P., Voegel, J.-C., Szalontai, B. (2007), Phospholipid bilayers as biomembrane-like barriers in layer-by-layer polyelectrolyte films. *Langmuir*, 23, 8236–8242. (DOI: 10.1021/la700839p)
65. Decher, G. (1997), Fuzzy nanoassemblies: toward layered polymeric multicomposites. *Science*, 277, 1232–1237. (DOI: 10.1126/science.277.5330.1232)
66. Delajon, C., Gutberlet, T., Steitz, R., Möhwald, H., Krastev, R. (2005), Formation of polyelectrolyte multilayer architectures with embedded DMPC studied in situ by neutron reflectometry. *Langmuir*, 21, 8509–8514. (DOI: 10.1021/la050407n)
67. Kashcooli, Y., Park, K., Bose, A., Greenfield, M., Bothun, G. D. (2016), Patchy layersomes formed by layer-by-layer coating of liposomes with strong

biopolyelectrolytes. *Biomacromolecules*, 17, 3838–3844. (DOI: 10.1021/acs.biomac.6b01467)

68. Fujimoto, K., Toyoda, T., Fukui, Y. (2007), Preparation of bionanocapsules by the layer-by-layer deposition of polypeptides onto a liposome. *Macromolecules*, 40, 5122–5128. (DOI: 10.1021/ma070477w)
69. Shin, S. H. R., Lee, H.-Y., Bishop, K. J. M. (2015), Amphiphilic nanoparticles control the growth and stability of lipid bilayers with open edges. *Angew. Chem., Int. Ed.*, 54, 10816–10820. (DOI: 10.1002/anie.201504362)
70. De Temmerman, M.-L., Rejman, J., Lucas, B., Vandenbroucke, R. E., Libert, C.; Demeester, J., De Smedt, S. C. (2012), Modulation of dendritic cells by lipid grafted polyelectrolyte microcapsules. *Adv. Funct. Mater.*, 22, 4236–4243. (DOI: 10.1002/adfm.201103151)
71. Novaira, M., Biasutti, M. A., Silber, J. J., Correa, N. M. (2007), New insights on the photophysical behavior of PRODAN in anionic and cationic reverse micelles: from which state or states does it emit? *J. Phys. Chem. B*, 111, 748–759. (DOI: 10.1021/jp065528q)
72. Thakur, R., Das, A., Chakraborty, A. (2014), Interaction of human serum albumin with liposomes of saturated and unsaturated lipids with different phase transition temperatures: a spectroscopic investigation by membrane probe PRODAN. *RSC Adv.*, 4, 14335–14347. (DOI: 10.1039/C4RA01214C)
73. Parasassi, T., Krasnowska, E. K., Bagatolli, L., Gratton, E. (1998), Laurdan and prodan as polarity-sensitive fluorescent membrane probes. *J. Fluoresc.*, 8, 365–373. (DOI: 10.1023/A:1020528716621)
74. Krasnowska, E. K., Gratton, E., Parasassi, T. (1998), Prodan as a membrane surface fluorescence probe: partitioning between water and phospholipid phases. *Biophys. J.*, 74, 1984–1993. (DOI: 10.1016/S0006-3495(98)77905-6)
75. Wang, F., Liu, J. (2015), Self-healable and reversible liposome leakage by citrate-capped gold nanoparticles: probing the initial adsorption/desorption induced lipid phase transition. *Nanoscale*, 7, 15599–15604. (DOI: 10.1039/C5NR04805B)

76. Das, A., Adhikari, C., Chakraborty, A. (2016), Lipoplex-mediated deintercalation of doxorubicin from calf thymus DNA−doxorubicin complex. *Langmuir*, 32, 8889–8899. (DOI: 10.1021/acs.langmuir.6b01860)

77. Nagle, J. F., Tristram-Nagle, S. (2000), Structure of lipid bilayers. *Biochim. Biophys. Acta, Rev. Biomembr.*, 1469, 159–195. (DOI: 10.1016/S0304-4157(00)00016-2)

78. Kučerka, N., Liu, Y., Chu, N., Petrache, H. I., Tristram-Nagle, S., Nagle, J. F. (2005), Structure of fully hydrated fluid phase DMPC and DLPC lipid bilayers using X-ray scattering from oriented multilamellar arrays and from unilamellar vesicles. *Biophys. J.*, 88, 2626–2637. (DOI: 10.1529/biophysj.104.056606)

79. Zakharova, L. Y., Ibragimova, A. R., Vasilieva, E. A., Mirgorodskaya, A. B., Yackevich, E. I., Nizameev, I. R., Kadirov, M. K., Zuev, Y. F., Konovalov, A. I. (2012), Polyelectrolyte capsules with tunable shell behavior fabricated by the simple layer-by-layer technique for the control of the release and reactivity of small guests. *J. Phys. Chem. C*, 116, 18865–18872. (DOI: 10.1021/jp305660c)

Chapter 4

Discriminatory interaction behavior of lipid vesicles toward diversely emissive carbon dots synthesized from ortho, meta and para isomeric carbon precursors

4.1 Introduction

The use of conventional membrane probes and organic dyes for the interpretation of membrane properties offer several limitations such as inefficient insertion, bilayer disruption and photobleaching [1-5]. Although metal nanoclusters have been used as potential substitutes [6-7], they are often met with limitations if excessive metal content is used. The employment of photoluminescent C-dots is an efficient way to facilitate the study of membrane properties. They can be used for imaging of cellular and model membranes due to their unique structural and photophysical properties [5, 8-14]. They are photostable, biocompatible and possess low toxicity unlike inorganic quantum dots [5, 8-18]. They are synthesized from natural carbon precursors following top-down and bottom-up approaches [19-22]. They offer beneficial optical properties while overcoming the limitations of fluorescent dyes, which makes them suitable candidates for bioimaging of model as well as cellular membranes [5, 8, 23-27].

The interaction of lipid membranes with C-dots has been studied previously by exploiting several techniques such as FRET and bioimaging [5, 8, 25-26]. However, in most of the literature studies, C-dots used so far were synthesized from only one isomer of any precursor. The literature lacks the information in regard of the interaction of lipid membrane with C-dots synthesized from different isomers of a particular carbon precursor. In this context, the selection of

carbon dots is crucial because the wrong selection of carbon dots may have an adverse effect on the cellular processes.

The o-, m-, or p- substitution of the isomeric groups at the surface of the C-dots can greatly influence the surface properties of the derived C-dots [28]. Therefore, the difference in the surface and optical properties of these C-dots could lead to difference in the interaction phenomena with the lipid bilayer. The interaction between C-dots and lipid vesicles depends on the type of C-dot, their functional groups and the lipid vesicle properties. The attachment of C-dots to vesicle structures is largely driven by the interaction between functional groups on the C-dot surface and headgroup of lipid molecules. This interaction may alter the photoluminescent characteristics of C-dots as well as can potentially induce changes in vesicle morphology.

Therefore, to address this hypothesis, we used C-dots synthesized from phenylenediamine (PDA) isomers (ortho, meta, and para) following a hydrothermal method [29]. The selection of C-dots for this study is based on their biological relevance and their property as efficient fluorescent probes. We studied their interaction with the zwitterionic lipid vesicles (DMPC and DPPC) by monitoring the intrinsic fluorescence of C-dots through steady state and time-resolved spectroscopic techniques. To gain insight regarding the location of the C-dots, we conducted FRET between C-dots and a membrane probe PRODAN which is located on the interfacial region [30-37]. The effect on morphology and size of the lipid vesicles were analyzed using confocal laser scanning microscopy (CLSM), scanning electron microscopy (SEM) and dynamic light scattering (DLS) measurements. We interpreted our results in the light of existing theory and structural differences of the different isomeric precursors.

4.2 Results and Discussion

4.2.1 <u>Characterization of C-dots</u>: The synthesized C-dots from different isomeric PDA precursors show yellow, brown, and wine-red colored solutions (Figure 4.1) when dispersed in water under visible light and emit yellow, green, and red colors, respectively, under single-wavelength UV irradiation (λ = 365 nm). The absorption and emission spectra of the C-dots reveal a very large Stokes shift in water (Figure 4.1 a–c). The time-resolved fluorescence decays (Figure 4.1 a–c inset) for all the C-dots are nonexponential, and the average lifetimes for oCD, mCD and pCD were found to be 1.63 ns, 5.28 ns, and 0.07 ns, respectively (Table 4.1). Moreover, the anisotropy measurements reveal that the rotational relaxation is slowest for pCD and fastest for mCD (Figure 4.1 e). The long residual tail in the case of pCD indicates that it is larger in size than its analogue C-dots.

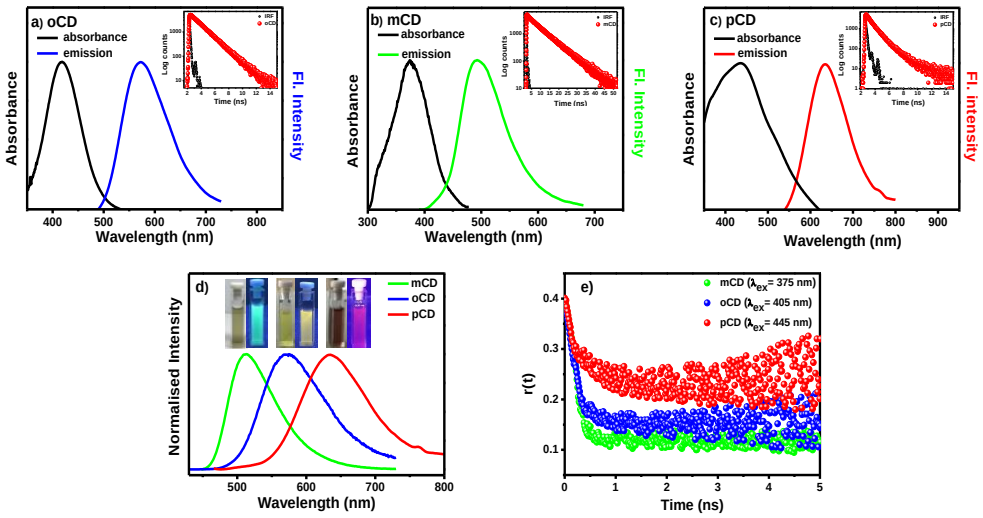

Figure 4.1 *Spectroscopic characterization of the synthesized C-dots. Absorption, emission spectra, and time-resolved decays (inset) of (a) oCD, (b) mCD, (c) pCD and (d) normalized emission spectra indicating widely different emissions and corresponding visible and UV images (λex = 365 nm) of the C-dots, and (e) time-resolved anisotropy of C-dots.*

Table 4.1 *Time-resolved decay parameters of C-dots. Lifetime components, normalized amplitudes of lifetime components and average lifetime of C-dots recorded at T = 25 °C.*

Sample	τ_1 (ns)	τ_2 (ns)	τ_3 (ns)	a_1	a_2	a_3	$<\tau_{avg}>$ (ns)	χ^2
	Laser used: 405 nm , Collected at: 572 nm, T=25°C							
oCD	1.63	-	-	1.00	-	-	1.63	1.13
	Laser used: 375 nm , Collected at: 500 nm, T=25°C							
mCD	1.23	7.56	-	0.36	0.64	-	5.28	1.21
	Laser used: 445 nm , Collected at: 635 nm, T=25°C							
pCD	0.52	1.66	0.03	0.04	0.01	0.95	0.07	1.13

All the C-dots exhibit excitation wavelength dependent emission, which is a typical signature of the C-dots (Figure 4.2).

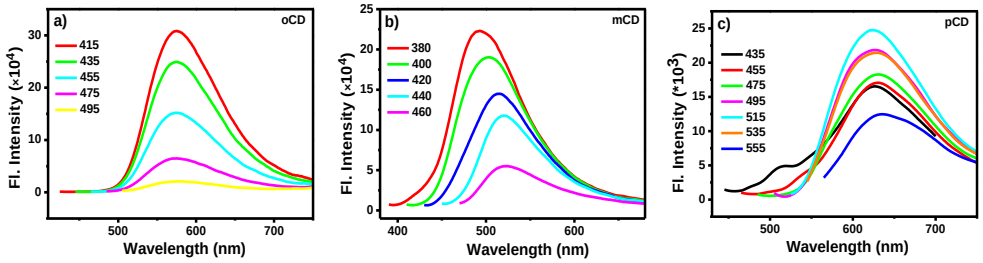

Figure 4.2 *Fluorescence emission spectra of C-dots at different excitation wavelengths as indicated, showing excitation dependent emission of a) oCD, b) mCD and c) pCD.*

The spherical morphology and the mean size of the C-dots as determined by AFM measurements reveal the average size of ~4 nm, ~2 nm, and ~6 nm for oCD, mCD and pCD, respectively (Figure 4.3). The largest size of pCD is consistent with the anisotropy measurements.

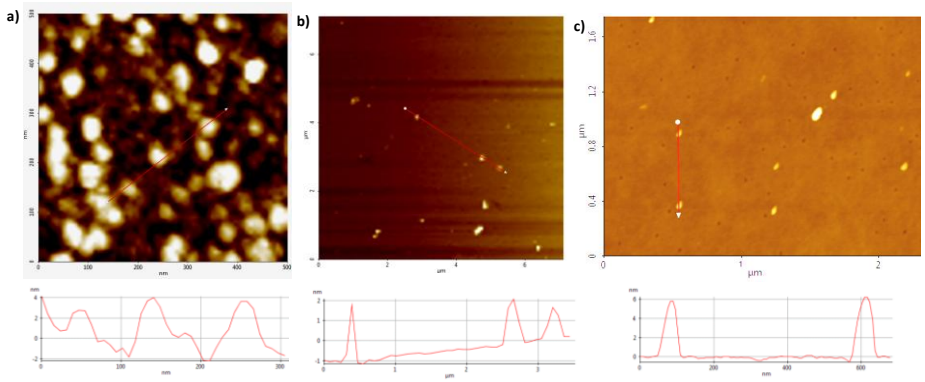

Figure 4.3 *AFM images of synthesized C-dots for a) oCD, b) mCD and c) pCD; and height-profile analysis along the corresponding lines (bottom).*

Further, the FTIR measurements spectra of the three C-dots are similar, which reveals the existence of a similar chemical composition of the C-dots (Figure 4.4). The appearance of some new characteristic peaks corresponding to C−O (1225−1234 cm^{-1}), C−N= (1336−1384 cm^{-1}), and C−H (2848−2920 cm^{-1}) bonds is attributed to the occurrence of several processes involving decomposition, intermolecular cyclization and condensation during the synthesis of C-dots [29].

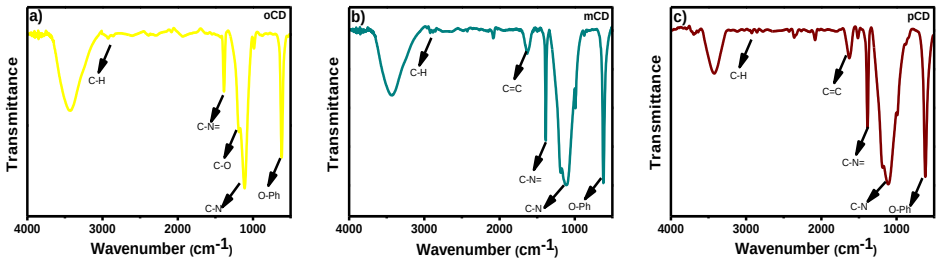

Figure 4.4 *FTIR spectra of the synthesized C-dots for a) oCD, b) mCD and c) pCD.*

4.2.2 <u>Interaction of C-dots with lipid vesicles</u>: The interaction of C-dots with DMPC vesicles is studied by exploiting the emissive features of C-dots. DMPC vesicles were chosen particularly because of the biological relevance of the PC headgroup [38-39]. While oCD exhibits a significant blue shift from 575 to 564 nm upon interaction with DMPC vesicles (Figure 4.5 a), mCD and pCD do not show any interaction (Figure 4.5 b-c). The observation indicates that oCD experiences a distinctly less polar chemical environment upon interaction with the lipid vesicles. The fluorescence lifetime of oCD also increases as a result of the interaction (Figure 4.5 d). The appearance of a long component around 3.0 ns may

be attributed to the C-dots embedded in the lipid vesicles (Table 4.2). A similar trend is also observed in the anisotropy measurement. The rotational relaxation becomes slower for oCD indicating that oCD experiences more confinement in lipid vesicles (Figure 4.5 d inset). However, we observe no change in lifetime and anisotropy of in case of mCD or pCD (Figure 4.5 e-f). The spectroscopic results primarily indicate that lipid vesicles display different affinity toward different C-dots.

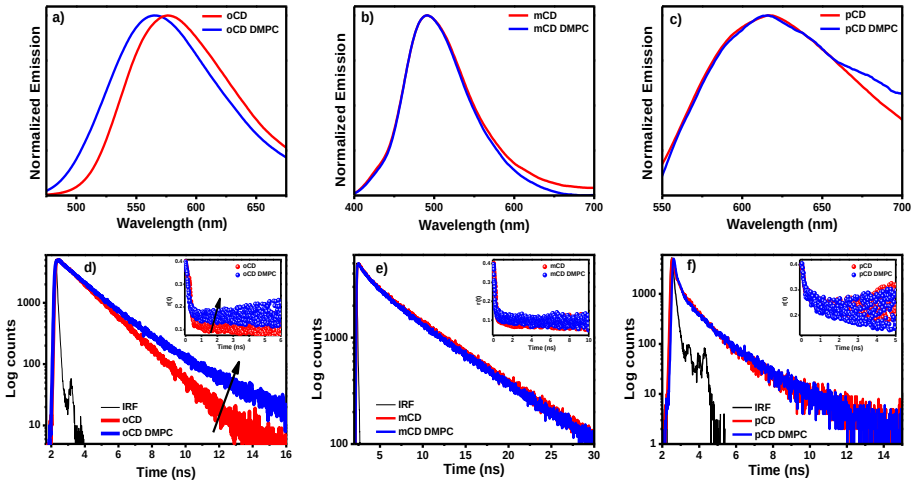

Figure 4.5 *Interaction of C-dots with DMPC lipid vesicles. Steady state fluorescence spectra for (a) oCD (λex = 416 nm), (b) mCD (λex = 372 nm), and (c) pCD (λex = 435 nm); corresponding time-resolved decay curves (d–f) and time-resolved anisotropy (inset d–f) for C-dots dispersed in aqueous medium and DMPC lipid vesicles.*

Table 4.2 *Time-resolved decay parameters of C-dots in presence of DMPC lipid vesicles. Lifetime components, normalized amplitudes of lifetime components and average lifetime of C-dots recorded at T = 25 °C.*

Sample	τ_1 (ns)	τ_2 (ns)	τ_3 (ns)	a_1	a_2	a_3	$<\tau_{avg}>$ (ns)	χ^2
	Laser used: 405 nm, Collected at: 572 nm, T=25°C							
oCD	1.63	-	-	1.00	-	-	1.63	1.13
oCD DMPC	1.50	3.08	-	0.79	0.21	-	1.82	1.16
	Laser used: 375 nm, Collected at: 500 nm, T=25°C							
mCD	1.23	7.56	-	0.36	0.64	-	5.28	1.21
mCD DMPC	1.08	7.53	-	0.32	0.68	-	5.45	1.21

	Laser used: 445 nm, Collected at: 635 nm, T=25°C							
pCD	0.52	1.66	0.03	0.04	0.01	0.95	0.07	1.13
pCD DMPC	0.38	2.00	0.009	0.00	0.00	1.00	0.01	1.10

This observation is supported by confocal fluorescence microscopy images, which depict that unlike mCD and pCD, oCD C-dots are uniformly distributed and embedded inside the DMPC lipid vesicles (Figure 4.6). However, in case of mCD, the fluorescence signal is observed from the interface of the lipid vesicles and there is an increase in the size of the lipid vesicles. This observation primarily indicates that the vesicles possibly undergo aggregation upon interaction with mCD. However, due to the low quantum yield of pCD, we did not observe a strong fluorescence signal. Thus, the above observations signify that oCD is much more efficient in interacting with lipid vesicles as compared to mCD and pCD. The molecular structures of PDA isomers have a significant effect on the fluorescence properties of the obtained C-dots. It is known that the fluorescent properties of C-dots obtained from m- and p-PDA are completely different from the o-isomer [26]. C-dots synthesized from o-PDA can be efficiently uptaken by cancer cells and can be used as fluorescent probes for cellular imaging rather than those obtained from its m- or p-isomers [26].

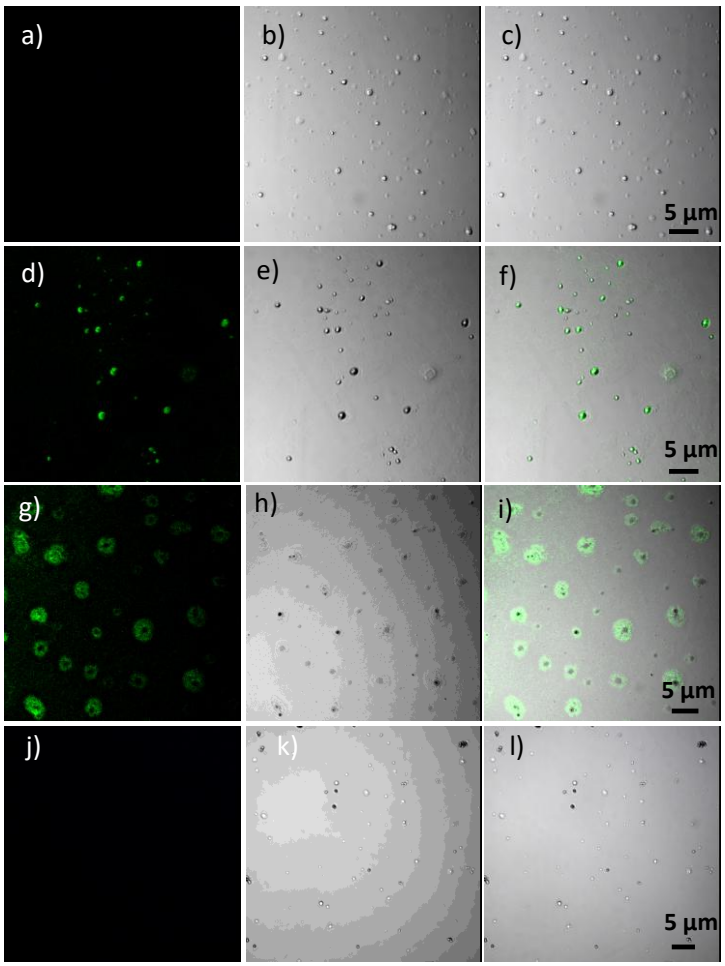

Figure 4.6 *DMPC−C-dot interaction from confocal laser scanning microscopy (CLSM) using fluorescence emission of C-dots. Confocal, bright field and merged images for (a−c) blank DMPC vesicles and in the presence of (d−f) oCD, (g−i) mCD, and (j−l) pCD C-dots.*

One of the possible reasons for the lipid vesicles showing discriminate behavior toward different C-dots could be due to the different location of the C-dots in the vesicles. In order to establish this assumption, we employed FRET which may provide an insight into the possible location of the C-dots. We tagged the lipid vesicles with a membrane probe PRODAN which is located at the membrane interface [30-37]. PRODAN acts as a donor while C-dots act as acceptors for energy transfer purpose. The combination of lipid-embedded PRODAN and C-dots is chosen because of the resultant large spectral overlap, which is a prerequisite for FRET (Figure 4.7).

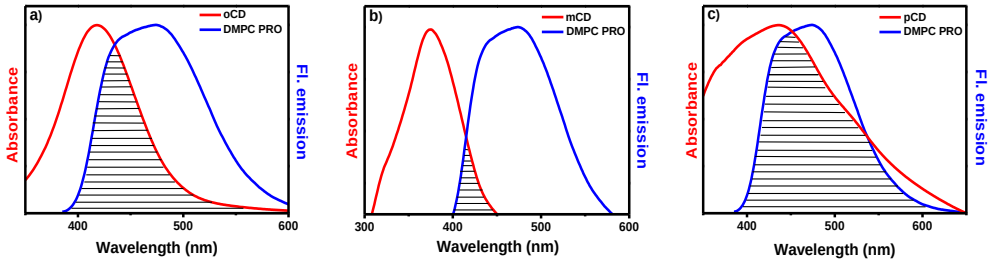

Figure 4.7 *Spectral overlap of the normalized absorbance (red) of the C-dots and normalized fluorescence emission spectra (blue) of the DMPC-embedded PRODAN in a) oCD, b) mCD and c) pCD.*

It is observed that the emission intensity corresponding to DMPC-PRODAN (~440 nm) decreases enormously with a concurrent increase in the emission of C-dots (Figure 4.8 a-c). Notably, a maximum quenching (69%) of the emission intensity of membrane-embedded PRODAN is observed upon interaction with oCD, followed by mCD (56%) and pCD (41%) (Table 4.3). The nonexponential fitting to the time-resolved decays reveal a drop in the fluorescence lifetime of PRODAN from 3.25 to 1.09 ns in the presence of oCD (Figure 4.8 d, Table 4.4). Notably, the quenching percentage in the case of oCD estimated from steady state measurement (69%) is almost similar to its energy transfer efficiency (66%) as estimated from time-resolved data. This observation clearly indicates that the fluorescence quenching in the case of oCD is due to the energy transfer phenomena involved. The observed quenching from the steady state measurement correlates well with the Stern−Volmer quenching constant K_{SV} as estimated from the lifetime decay data (Figure 4.8 d inset, Table 4.3). Here, it is clearly evident that K_{SV} corresponds to the energy transfer process in case of oCD as the acceptor.

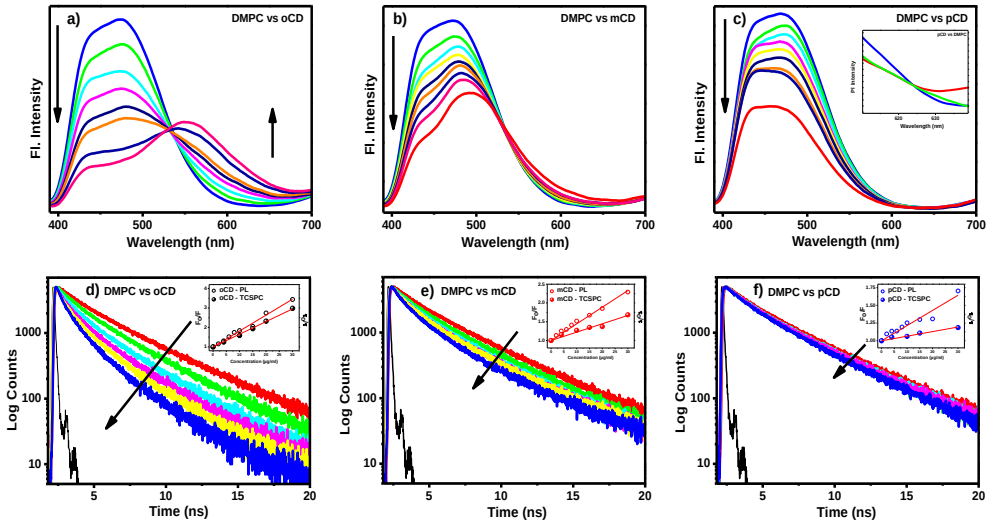

Figure 4.8 *Fluorescence emission spectra of the DMPC-PRODAN upon addition of C-dots for (a) oCD, (b) mCD, and (c) pCD; corresponding time-resolved decay curves (d–f) and Stern–Volmer plots (insets d–f).*

Table 4.3 *Fluorescence emission quenching percentage and energy transfer efficiency as calculated from time-resolved lifetime for the addition of C-dots to DMPC-PRODAN solution. Stern-Volmer constants (K_{sv}) as obtained from the fluorescence emission (F_o/F) vs concentration (C) plot and time-resolved lifetime decay (τ_o/τ) vs concentration plot.*

Acceptor C-dot	Fluorescence quenching % (steady state)	Energy transfer efficiency (from time resolved decay)	F_o/F vs C slope (steady state)	τ_o/τ vs C slope (time-resolved)
oCD	69 %	66 %	0.0817	0.0650
mCD	56 %	40 %	0.0443	0.0222
pCD	41 %	15 %	0.0214	0.0064

Table 4.4 *Time-resolved decay parameters of DMPC-PRODAN in presence of C-dots. Lifetime components, normalized amplitudes of lifetime components and average lifetime recorded at T = 25 °C.*

Sample (µg/mL)	τ_1 (ns)	τ_2 (ns)	τ_3 (ns)	a_1	a_2	a_3	$<\tau_{avg}>$ (ns)	χ^2
DMPC PRODAN	1.70	4.31	-	0.41	0.59	-	3.25	1.15
oCD 4	1.38	3.81	-	0.50	0.50	-	2.60	1.08
oCD 10	1.09	3.41	-	0.59	0.41	-	2.05	1.22

oCD 15	1.64	0.55	3.74	0.44	0.36	0.20	1.68	1.20
oCD 20	1.42	0.43	3.48	0.46	0.37	0.17	1.40	1.15
oCD 30	1.22	0.33	3.25	0.46	0.42	0.12	1.09	1.25
mCD 4	1.52	4.09	-	0.48	0.52	-	2.81	1.19
mCD 10	1.39	3.95	-	0.54	0.46	-	2.56	1.13
mCD 15	1.28	3.89	-	0.57	0.43	-	2.41	1.15
mCD 20	1.25	3.94	-	0.58	0.42	-	2.37	1.11
mCD 30	1.90	4.71	0.59	0.47	0.18	0.35	1.93	1.22
pCD 4	1.64	4.14	-	0.43	0.57	-	3.09	1.15
pCD 10	1.63	4.22	-	0.43	0.57	-	3.05	1.11
pCD 15	1.58	4.05	-	0.45	0.55	-	2.93	1.13
pCD 20	1.64	4.24	-	0.45	0.55	-	3.06	1.06
pCD 30	1.46	3.91	-	0.48	0.52	-	2.74	1.13

Contrary to the results obtained for oCD C-dots, for mCD and pCD the decrement in the lifetime of PRODAN takes place from 3.25 to 1.93 ns and 2.74 ns, respectively (Figure 4.8 e-f). Following these values, the energy transfer efficiency was estimated to be 40% and 15% for mCD and pCD, respectively. Since the quenching efficiency in the case of mCD (56%) and pCD (41%) is much larger than the energy transfer efficiency, we infer that the emission quenching is not solely due to the energy transfer process. For mCD and pCD, the Stern−Volmer plot of steady state measurement reveals a much higher slope as compared to that of the time-resolved experiment (Figure 4.8 e-f inset). The higher quenching mechanism for these two C-dots in steady state measurement is attributed to the formation of a non-fluorescent ground state complex between mCD and pCD C-dots and membrane embedded PRODAN, which results in a static fluorescence quenching. From the above stated observations, two major conclusions are drawn: (i) the oCD C-dots tend to penetrate deeper inside the lipid vesicles as compared to its analogues mCD and pCD; and (ii) mCD and pCD behave differently as they tend to bind to the interfacial region of the lipid vesicles.

As PRODAN is loosely anchored to the interfacial region of lipid vesicles, the ground state complexation of membrane embedded PRODAN with mCD and pCD clearly indicates that these two C-dots are located at the interfacial region of the vesicles. Now the question is why lipid vesicles behave discriminatively toward the C-dots synthesized from different isomeric precursors? One of the possible reasons is the self surface passivation of C-dots due to o-, m- or p-substitution of the isomeric groups at the surface of the C-dots [28]. The differences in the molecular structures of the carbon precursors act as one of the major factors influencing the properties of the derived C-dots. Moreover, oPDA has the largest pKb value (9.53) among the three isomers, followed by mPDA (9.12) and least for pPDA (7.92) [40]. In the case of o-PDA, intramolecular hydrogen bonding between the two amino groups makes nitrogen atoms of amino group less available to form any further bonding with the headgroup of the lipids. The intramolecular hydrogen bonding is further facilitated owing to the less polar environment inside the lipid vesicles. This helps oCD to penetrate deeper and embed inside the lipid vesicles. On the other hand, due to the ease of availability of the electrons in the m- and p-isomers, they may form a complex by interacting at the lipid vesicle interface. This confinement is also responsible for the static quenching as observed in the corresponding Stern−Volmer plot.

Apart from intra- and intermolecular hydrogen bonding, other factors such as electrostatic interaction and particularly hydrophobicity of the carbon source may play a vital role in this aspect. The initial attachment of C-dot to lipid vesicles surface is likely to occur by favorable electrostatic interaction between the positively charged amine group of the C-dot and the negative surface potential of the lipid vesicles via the PC headgroup [39, 41]. The binding of m- and p-isomers to the interfacial region is more facile as compared to that of the o-isomer due to more availability of electrons. Thus, mCD and pCD are preferentially bound to the interfacial region. However, in the case of oCD, where the amino group is less available to bind with the headgroup of the lipids, the hydrophobicity of the precursor plays a crucial role in governing the interaction. The hydrophobic group (i.e., phenyl) is likely to penetrate deeper into the bilayer following the initial

attachment. The hydrophobicity of PDA isomers follow the sequence: oPDA > pPDA > mPDA, with the reported hydrophobic coefficient (hf) largest for oPDA (3.20), followed by pPDA (2.10), and least for mPDA (1.90) [42]. This is in accordance with our observations indicating oCD penetrates deeper into the vesicles whereas mCD and pCD remain on the vesicle interface. The hydrophobic effect may also be responsible for inducing an increase in lipid ordering, due to more efficient packing of the hydrophobic part within the membrane [41]. Moreover, hydrophobic ligands are known to be able to anchor within the membrane [41].

We performed experiments for the interaction of PRODAN with C-dots as the control to rule out the possibility of their interaction in the absence of lipid vesicles (Figure 4.9).

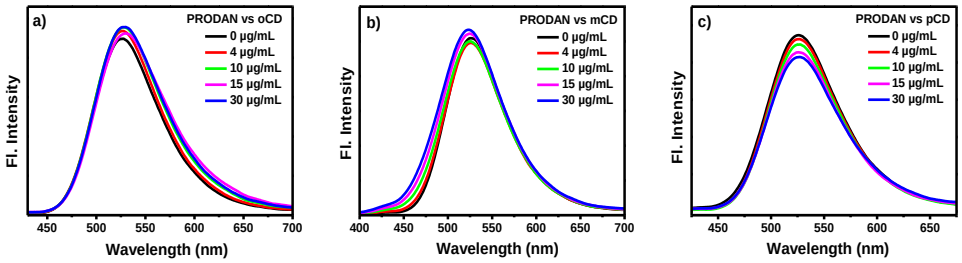

Figure 4.9 *Control experiments for the interaction of PRODAN with C-dots for a) oCD, b) mCD and c) pCD. Here, concentration of PRODAN is fixed at 2 µM while varying the concentration of C-dots from 0 to 30 µg/mL.*

Similarly, we performed the control experiment with different concentrations of C-dots dispersed in Milli-Q water (Figure 4.10) to rule out the possibility of self quenching of the C-dots.

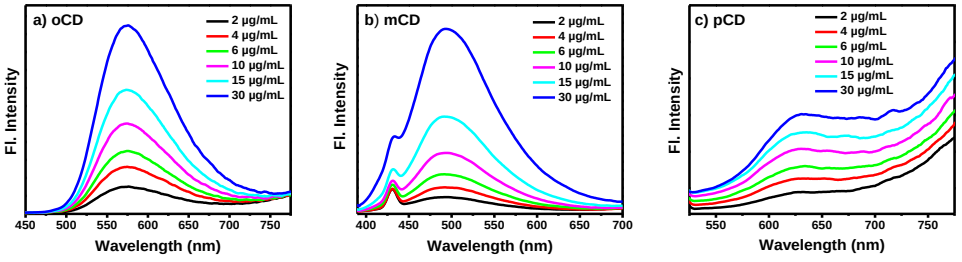

Figure 4.10 *Control experiments for the increasing concentrations of C-dots dispersed in Milli-Q water for a) oCD, b) mCD and c) pCD.*

We also performed similar experiments with DPPC vesicles to account for the effect of fluidity on the binding interaction phenomena. A similar trend of interaction is obtained in case of DPPC lipid vesicles (Figure 4.11). The order of interaction of the lipid bilayer with different C-dots follows a similar trend in both the DMPC and DPPC vesicles. The observation indicates the similar location of the C-dots on both of the vesicles. However, the changes in the lifetime of PRODAN in DPPC vesicles are much smaller as compared to that in DMPC vesicles. This indicates a weaker energy transfer in the former vesicles. This could be due to the the fact that the insertion of C-dots is restricted into the DPPC lipid vesicles because of less fluidity. This may lead to formation of a strong ground state donor-acceptor complex [5]. The modulations of energy transfer efficiency originate from changes in the bilayer fluidity and lipid diffusion processes [5, 43]. Moreover, the membrane distortion for fully saturated gel phase lipids is more limited than that for lipid membranes in the fluid phase. The photostability of the quantum dots is largely dependent on the phase state (organization) of the membrane [44]. Quantum dots may induce changes in the local microenvironment of the lipid membrane, and the interaction may lead to the distortion of membrane organization as well as rearrangement of the surface ligands of the quantum dots [44].

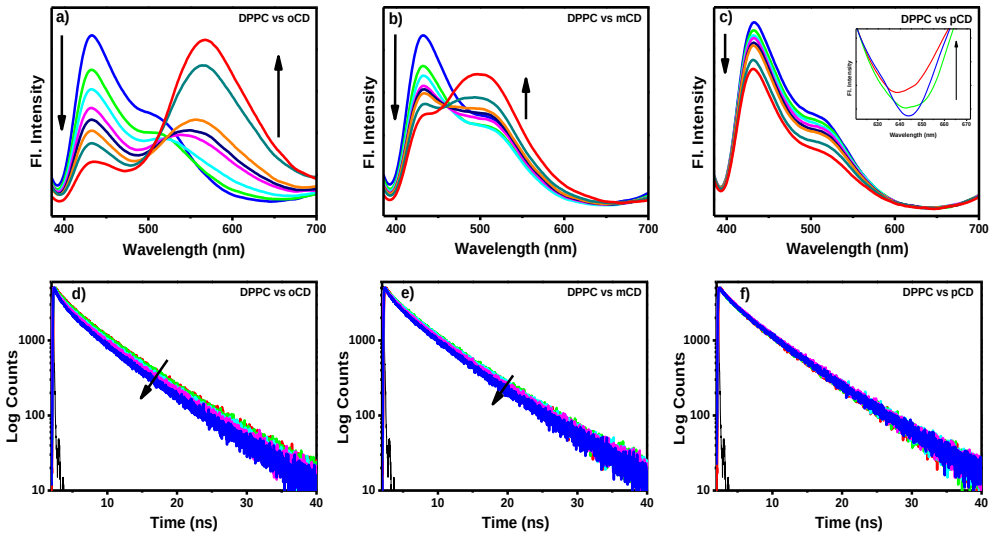

Figure 4.11 *Fluorescence emission spectra of the DPPC-PRODAN upon addition of acceptor C-dots for a) oCD; b) mCD and c) pCD; and corresponding lifetime decay curves (d-f).*

In this context, another important question is whether the impact of C-dots brings any change in the morphology of the lipid vesicles? To investigate the influence of C-dots on the morphology of lipid vesicles, we conducted confocal imaging using the photoluminescence properties of the C-dots (Figure 4.12). The fluorescent signal corresponding to the C-dots (oCD) emission appears from inside the vesicles in the lipid vesicles−C-dot conjugates, thereby indicating the insertion of the C-dots inside the lipid vesicles. Moreover, as a result of this process, the vesicles are not deformed and maintain their morphology intact upon interaction with oCD. The interaction also results in a highly uniform morphology confirming that the embedded oCD do not adversely affect the bilayer organization. This observation is important considering that attaining bilayer integrity and fluorescence distribution in the membranes is considered a major challenge. This property could also be significant from the point of view of its usage as biomarkers for cells and model membranes because of good membrane penetrability and excellent luminescence properties. Interestingly, we observe that upon interaction with mCD, aggregation of the lipid vesicles is observed. We explain this aggregation ability of mCD with different hydration levels of isomeric precursors of the derived C-dots. The hydration features of the m-PDA isomer are widely different from those of the o- and p-isomers of PDA [45]. The coordinated water molecules are mainly localized near the aminic hydrogen atoms and lone-pair sides of the nitrogen atoms for all the PDA isomers. However, in the case of the m-isomer, the solvent localization propagates somewhat to the most hydrophobic region, i.e., the aromatic ring. This feature is not observed in the case of the o- and p-isomers. Thus, we propose that upon interaction of mCD with lipid vesicles, the solvent molecules in an attempt to propagate to the hydrophobic region of the lipid bound C-dots, distort the spherical structure of the lipid vesicles, which results into the formation of overall aggregated structures of the lipid vesicles. It must be noted that even during the formation of aggregated vesicles, the C-dots retain their fluorescence properties intact and do not undergo aggregation themselves as a result of this interaction. Moreover, given that the quantum yield of pCD is low, we did not observe its fluorescent signal. However,

the lipid vesicles did not undergo major aggregation like mCD, as can be seen from the bright field images (Figure 4.12 m-p).

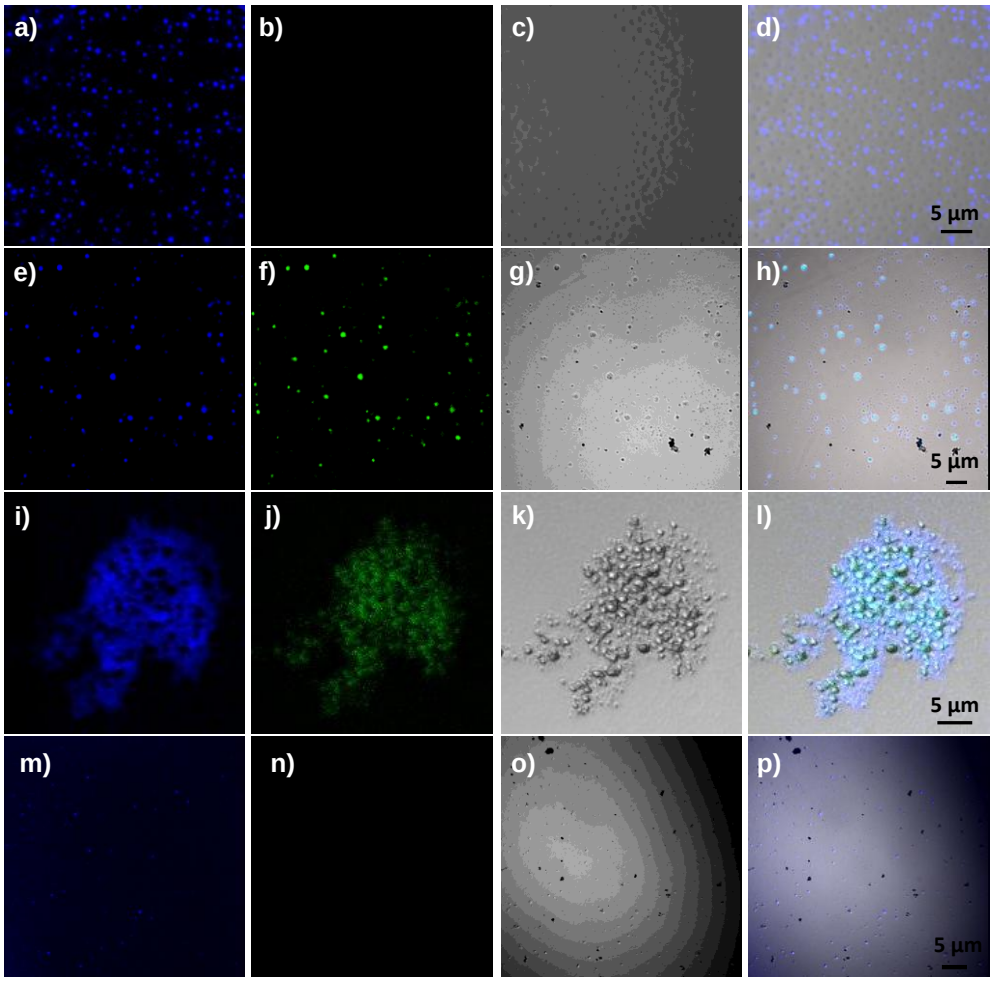

Figure 4.12 *Confocal images of DMPC-PRODAN upon interaction with C-dots using emission of both PRODAN (410−480 nm) and C-dots (510−610 nm). Confocal, bright-field and merged images for (a−d) DMPC-PRODAN and in the presence of (e−h) oCD, (i−l) mCD C-dots and (m-p) pCD.*

The other possibility is that being located at the interfacial region and bearing charges on the surface, mCD and pCD may cross-link with other adjoining lipid vesicles. The cross-linking possibility of C-dots could be facilitated by the intermolecular hydrogen bonding ability. For mCD and pCD, the possibility of intermolecular hydrogen boding of the precursors may bring the adjacent vesicles closer to each other which induce instability in the lipid vesicles resulting into their rearrangement. The aggregation of lipid vesicles is also clearly demonstrated

in the SEM images (Figure 4.13). It is observed that the vesicles maintain their morphology intact upon interaction with oCD. However, mCD induces overall aggregation of the lipid vesicles that corroborates well with the confocal images. The size of the aggregated vesicles increases up to a few microns from their native structure which is 100−200 nm in size. On the other hand, lipid vesicles align closer to each other resulting into a partial aggregation upon interaction with pCD C-dots.

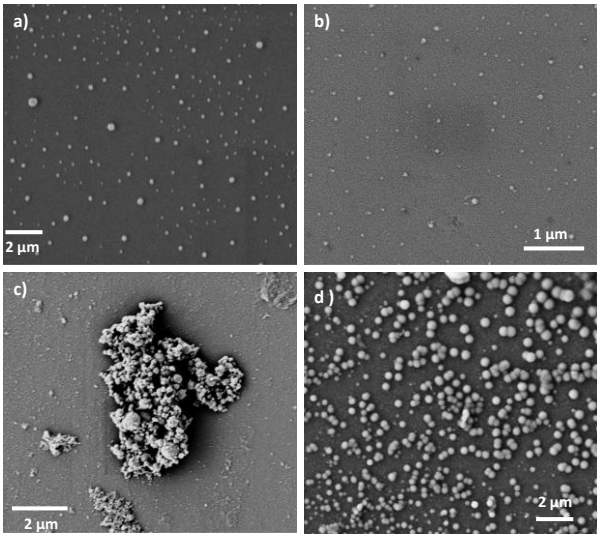

Figure 4.13 *SEM images for the lipid vesicles composed of DMPC (a) and DMPC upon interaction with oCD (b), mCD (c), and pCD (d).*

Further, we performed DLS measurements to understand the effect of C-dots on the size distribution of the lipid vesicles. Figure 4.14 indicates that the DMPC vesicles show an average size of nearly 100 nm. The hydrodynamic size distribution did not change significantly upon interaction with oCD. This is in accordance with the findings of imaging experiments where oCD did not induce aggregation in lipid vesicles and indeed maintained the size of the lipid vesicles intact. We already mentioned that oCD are embedded deeper into the vesicle and thus do not cross-link with neighboring vesicles.

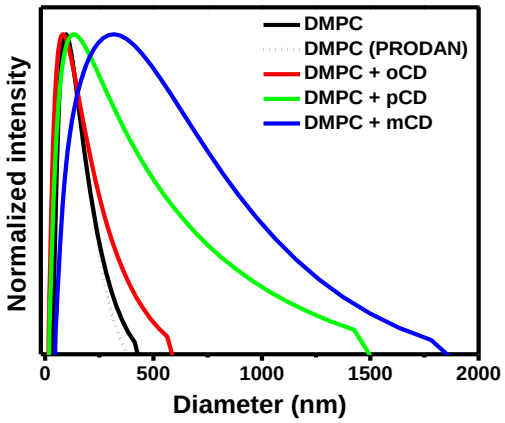

Figure 4.14 *Hydrodynamic size distribution plot for the lipid vesicles composed of DMPC (with and without the presence of PRODAN) and DMPC upon interaction with C-dots (oCD, mCD, and pCD).*

On the other hand, interaction with pCD and mCD results in an increase in the overall hydrodynamic size distribution of the lipid vesicles. The observation indicates the induced fusion of the lipid vesicles. Since mCD and pCD are located on the interfacial region of the lipid vesicles, they induce aggregation in vesicles possibly by cross-linking between the neighboring lipid vesicles and thus giving rise to large and aggregated structures of lipid vesicles. Moreover, it is evident that pCD induces partial aggregation whereas mCD induces total aggregation giving rise to a larger vesicle size. These results corroborate well with the conclusions drawn from imaging experiments. This effect is demonstrated in the form of a pictorial representation as shown in Scheme 4.1.

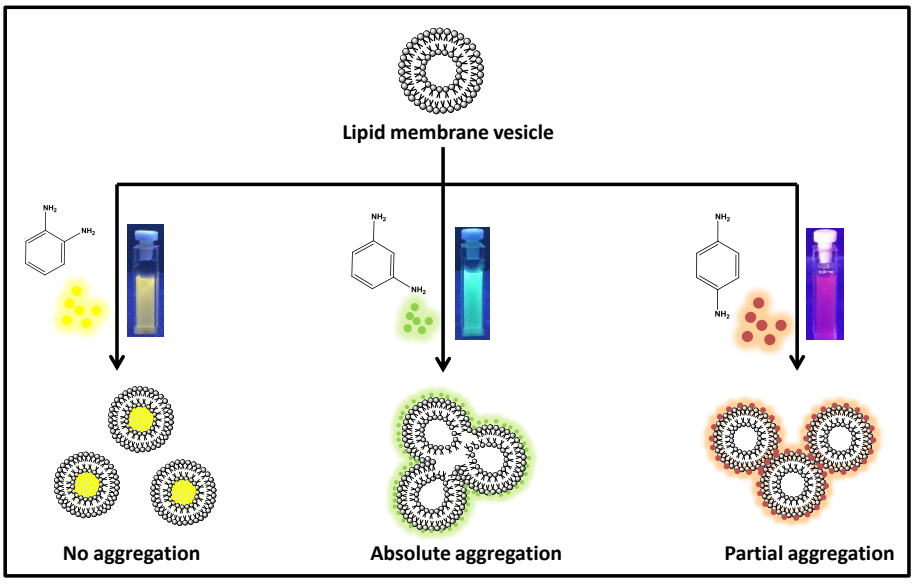

Scheme 4.1 *Representation of the interaction of C-dots derived from different isomeric carbon precursors. While ortho-C-dots (oCD) remain embedded inside the lipid vesicles and do not cause aggregation, meta- and para-C-dots (mCD and pCD) are located on the lipid vesicles interface and cause absolute and partial aggregation, respectively.*

4.3 Conclusion

We studied the interaction of differently emissive C-dots derived from isomeric precursors of phenylenediamine with zwitterionic lipid vesicles composed of DMPC and DPPC lipids. We employed different spectroscopic and imaging techniques as well as dynamic light scattering measurements to unravel this interaction. We observe that C-dots synthesized from different isomers of the same carbon precursor are significantly different from each other in terms of their interaction phenomena with lipid vesicles. The oCD interacts strongly with the lipid vesicles, while the other analogues (mCD and pCD) do not display such interaction. The spectroscopic studies suggest that the oCD C-dots tend to penetrate deeper inside the lipid vesicles while the mCD and pCD remain bound to the interfacial region. The discriminatory behavior of lipid vesicles has been explained in terms of the intra- and intermolecular hydrogen bonding of the corresponding precursors. The ortho phenylenediamine is likely to form

intramolecular hydrogen bonding, which helps corresponding oCD to penetrate deeper inside the lipid vesicles. On the other hand, meta and para isomers of phenylenediamine are capable of intermolecular hydrogen bonding which is responsible for mCD and pCD to be bound to the interfacial region. Moreover, the higher hydrophobicity of o-PDA isomers aids in the insertion of the oCD C-dots inside the vesicles, while m- and p-isomers undergo electrostatic interaction with the PC headgroup of the vesicles at the interfacial region. Interestingly, the interfacial location of mCD and pCD induces instability in the lipid vesicles and results in aggregation. We explain this observation in the light of the structural differences and different hydration levels of the precursors of the C-dots and their cross-linking tendency with nearby lipid vesicles. We conclude that among all C-dots, only oCD is favorable for bioimaging purposes, and this study provides insight regarding the interactions and adsorption processes of C-dots at the interface of biological membranes.

4.4 References

1. Klymchenko, A. S., Kreder, R. (2014), Fluorescent Probes for Lipid Rafts: From Model Membranes to Living Cells. *Chem. Biol.*, 21, 97−113. (DOI: 10.1016/j.chembiol.2013.11.009)

2. Maekawa, M., Fairn, G. D. (2014), Molecular probes to visualize the location, organization and dynamics of lipids. *J. Cell Sci.*, 127, 4801−4812. (DOI: 10.1242/jcs.150524)

3. Faller, R. (2016), Molecular modeling of lipid probes and their influence on the membrane. *Biochim. Biophys. Acta, Biomembr.*, 1858, 2353−2361. (DOI: 10.1016/j.bbamem.2016.02.014)

4. Jan Akhunzada, M., D'Autilia, F., Chandramouli, B., Bhattacharjee, N., Catte, A., Di Rienzo, R., Cardarelli, F., Brancato, G. (2019), Interplay between lipid lateral diffusion, dye concentration and membrane permeability unveiled by a

combined spectroscopic and computational study of a model lipid bilayer. *Sci. Rep.*, 9, 1508. (DOI: 10.1038/s41598-018-37814-x)

5. Nandi, S., Malishev, R., Bhunia, S. K., Kolusheva, S., Jopp, J., Jelinek, R. (2016), Lipid-Bilayer Dynamics Probed by a Carbon Dot-Phospholipid Conjugate. *Biophys. J.*, 110, 2016−2025. (DOI: 10.1016/j.bpj.2016.04.005)

6. Kundu, N., Mukherjee, D., Maiti, T. K., Sarkar, N. (2017), Proteinguided formation of silver nanoclusters and their assembly with graphene oxide as an improved bioimaging agent with reduced toxicity. *J. Phys. Chem. Lett.*, 8, 2291−2297. (DOI: 10.1021/acs.jpclett.7b00600)

7. Kundu, S., Mukherjee, D., Maiti, T. K., Sarkar, N. (2019), Highly Luminescent Thermoresponsive Green Emitting Gold Nanoclusters for Intracellular Nanothermometry and Cellular Imaging: A Dual Function Optical Probe. ACS *Appl. Bio. Mater.*, 2, 2078−2091. (DOI: 10.1021/acsabm.9b00107)

8. Nandi, S., Malishev, R., Parambath Kootery, K., Mirsky, Y., Kolusheva, S., Jelinek, R. (2014), Membrane analysis with amphiphilic carbon dots. *Chem. Commun.*, 50, 10299−10302. (DOI: 10.1039/C4CC03504F)

9. Liang, Z., Kang, M., Payne, G. F., Wang, X., Sun, R. (2016), Probing Energy and Electron Transfer Mechanisms in Fluorescence Quenching of Biomass Carbon Quantum Dots. *ACS Appl. Mater. Interfaces*, 8, 17478−17488. (DOI: 10.1021/acsami.6b04826)

10. Li, J., Zhu, J.-J. (2013), Quantum dots for fluorescent biosensing and bio-imaging applications. *Analyst*, 138, 2506−2515. (DOI: 10.1039/c3an36705c)

11. Liu, M. L., Chen, B. B., Li, C. M., Huang, C. Z. (2019), Carbon dots: synthesis, formation mechanism, fluorescence origin and sensing applications. *Green Chem.*, 21, 449−471. (DOI: 10.1039/C8GC02736F)

12. Semeniuk, M., Yi, Z., Poursorkhabi, V., Tjong, J., Jaffer, S., Lu, Z.-H., Sain, M. (2019), Future Perspectives and Review on Organic Carbon Dots in Electronic Applications. *ACS Nano*, 13, 6224−6255. (DOI: 10.1021/acsnano.9b00688)

13. Li, M., Chen, T., Gooding, J. J., Liu, J. (2019), Review of Carbon and Graphene Quantum Dots for Sensing. *ACS Sens.*, 4, 1732−1748. (DOI: 10.1021/acssensors.9b00514)

14. Wang, X., Feng, Y., Dong, P., Huang, J. (2019), A Mini Review on Carbon Quantum Dots: Preparation, Properties, and Electrocatalytic Application. *Front. Chem.*, 7, 671. (DOI: 10.3389/fchem.2019.00671)

15. Sciortino, A., Cannizzo, A., Messina, F. (2018), Carbon Nanodots: A Review-From the Current Understanding of the Fundamental Photophysics to the Full Control of the Optical Response. *C*, 4, 67. (DOI: 10.3390/c4040067)

16. Ding, H., Yu, S.-B., Wei, J.-S., Xiong, H.-M. (2016), Full-Color Light-Emitting Carbon Dots with a Surface-State-Controlled Luminescence Mechanism. *ACS Nano*, 10, 484−491. (DOI: 10.1021/acsnano.5b05406)

17. Kudr, J., Richtera, L., Xhaxhiu, K., Hynek, D., Heger, Z., Zitka, O., Adam, V. (2017), Carbon dots based FRET for the detection of DNA damage. *Biosens. Bioelectron.*, 92, 133−139. (DOI: 10.1016/j.bios.2017.01.067)

18. Miao, S., Liang, K., Kong, B. (2020), Förster resonance energy transfer (FRET) paired carbon dot-based complex nanoprobes: versatile platforms for sensing and imaging applications. *Mater. Chem. Front.*, 4, 128−139. (DOI: 10.1039/C9QM00538B)

19. Yang, Y., Wu, D., Han, S., Hu, P., Liu, R. (2013), Bottom up fabrication of Photoluminescent carbon dots with uniform morphology via a soft hard template approach. *Chem. Commun.*, 49, 4920−4922. (DOI: 10.1039/c3cc38815h)

20. Sharma, A., Das, J. (2019), Small molecules derived carbon dots: synthesis and applications in sensing, catalysis, imaging, and biomedicine. *J. Nanobiotechnol.*, 17, 92. (DOI: 10.1186/s12951-019-0525-8)

21. Zuo, J., Jiang, T., Zhao, X., Xiong, X., Xiao, S., Zhu, Z. (2015), Preparation and Application of Fluorescent Carbon Dots. *J. Nanomater.*, 2015, 1−13. (DOI: 10.1155/2015/787862)

22. Zhang, J., Wang, H., Xiao, Y., Tang, J., Liang, C., Li, F., Dong, H., Xu, W. (2017), A simple approach for synthesizing of fluorescent carbon quantum dots from tofu wastewater. *Nanoscale Res. Lett.*, 12, 611. (DOI: 10.1186/s11671-017-2369-1)

23. Liu, J.-H., Cao, L., LeCroy, G. E., Wang, P., Meziani, M. J., Dong, Y., Liu, Y., Luo, P. G., Sun, Y.-P. (2015), Carbon "Quantum" Dots for Fluorescence Labeling of Cells. *ACS Appl. Mater. Interfaces*, 7, 19439−19445. (DOI: 10.1021/acsami.5b05665)

24. Molaei, M. J. (2019), Carbon quantum dots and their biomedical and therapeutic applications: a review. *RSC Adv.*, 9, 6460−6481. (DOI: 10.1039/C8RA08088G)

25. Pritzl, S. D., Pschunder, F., Ehrat, F., Bhattacharyya, S., Lohmüller, T., Huergo, M. A., Feldmann, J. (2019), Trans-membrane Fluorescence Enhancement by Carbon Dots: Ionic Interactions and Energy Transfer. *Nano Lett.*, 19, 3886−3891. (DOI: 10.1021/acs.nanolett.9b01071)

26. Song, L., Cui, Y., Zhang, C., Hu, Z., Liu, X. (2016), Microwave-assisted facile synthesis of yellow fluorescent carbon dots from o-phenylenediamine for cell imaging and sensitive detection of Fe^{3+} and H_2O_2. *RSC Adv.*, 6, 17704−17712. (DOI: 10.1039/C6RA02554D)

27. Song, Y., Zhu, S., Yang, B. (2014), Bioimaging based on fluorescent carbon dots. *RSC Adv.*, 4, 27184−27200. (DOI: 10.1039/c3ra47994c)

28. Wang, J., Cheng, C., Huang, Y., Zheng, B., Yuan, H., Bo, L., Zheng, M.-W., Yang, S.-Y., Guo, Y., Xiao, D. (2014), A facile large-scale microwave synthesis of highly fluorescent carbon dots from benzenediol isomers. *J. Mater. Chem. C*, 2, 5028−5035. (DOI: 10.1039/C3TC32131B)

29. Jiang, K., Sun, S., Zhang, L., Lu, Y., Wu, A., Cai, C., Lin, H. (2015), Red, Green, and Blue Luminescence by Carbon Dots: Full-Color Emission Tuning and Multicolor Cellular Imaging. *Angew. Chem. Int. Ed.*, 54, 5360−5363. (DOI: 10.1002/anie.201501193)

30. Parasassi, T., Krasnowska, E. K., Bagatolli, L., Gratton, E. (1998), Laurdan and Prodan as polarity-sensitive fluorescent membrane probes. *J. Fluoresc.*, 8, 365−373. (DOI: 10.1023/A:1020528716621)

31. Krasnowska, E. K., Gratton, E., Parasassi, T. (1998), Prodan as a membrane surface fluorescence probe: partitioning between water and phospholipid phases. *Biophys. J.*, 74, 1984−1993. (DOI: 10.1016/S0006-3495(98)77905-6)

32. Novaira, M., Biasutti, M. A., Silber, J. J., Correa, N. M. (2007), New Insights on the Photophysical Behavior of PRODAN in Anionic and Cationic Reverse Micelles: From which State or States does it Emit? *J. Phys. Chem. B*, 111, 748−759. (DOI: 10.1021/jp065528q)

33. Kanwa, N., De, S. K., Adhikari, C., Chakraborty, A. (2017), Spectroscopic study of the interaction of carboxyl-modified gold nanoparticles with liposomes of different chain lengths and controlled drug release by layer-by-layer technology. *J. Phys. Chem. B*, 121, 11333−11343. (DOI: 10.1021/acs.jpcb.7b08455)

34. Kanti De, S., Kanwa, N., Ahamed, M., Chakraborty, A. (2018), Spectroscopic evidence for hydration and dehydration of lipid bilayers upon interaction with metal ions: a new physical insight. *Phys. Chem. Chem. Phys.*, 20, 14796−14807. (DOI: 10.1039/C8CP01774C)

35. Kanwa, N., Patnaik, A., De, S. K., Ahamed, M., Chakraborty, A. (2019), Effect of surface ligand and temperature on lipid vesicle-gold nanoparticle interaction: a spectroscopic investigation. *Langmuir*, 35, 1008−1020. (DOI: 10.1021/acs.langmuir.8b03673)

36. Kanwa, N., De, S. K., Maity, A., Chakraborty, A. (2020), Interaction of aliphatic amino acids with zwitterionic and charged lipid membranes: hydration and dehydration phenomena. *Phys. Chem. Chem. Phys.*, 22, 3234−3244. (DOI: 10.1039/C9CP06188F)

37. De, S. K., Kanwa, N., Chakraborty, A. (2019), Influence of trivalent metal ions on lipid vesicles: gelation and fusion phenomena. *Langmuir*, 35, 6429−6440. (DOI: 10.1021/acs.langmuir.9b00682)

38. Yeagle, P. L. The Membranes of Cells; Academic Press: Boston, MA, 1993.

39. Troiano, J. M., Olenick, L. L., Kuech, T. R., Melby, E. S., Hu, D., Lohse, S. E., Mensch, A. C., Dogangun, M., Vartanian, A. M., Torelli, M. D., Ehimiaghe, E., Walter, S. R., Fu, L., Anderton, C. R., Zhu, Z., Wang, H., Orr, G., Murphy, C. J., Hamers, R. J., Pedersen, J. A., Geiger, F. M. (2015), Direct probes of 4 nm diameter gold nanoparticles interacting with supported lipid bilayers. *J. Phys. Chem. C*, 119, 534−546. (DOI: 10.1021/jp512107z)

40. Pankratov, A. N., Uchaeva, I. M., Doronin, S. Y., Chernova, R. K. (2001), Gaseous-phase proton affinity of anilines: A quantum chemical evaluation and discussion in view of aqueous basicity. *J. Serb. Chem. Soc.*, 66, 161−172. (DOI: 10.2298/JSC0103161P)

41. Mensch, A. C., Buchman, J. T., Haynes, C. L., Pedersen, J. A., Hamers, R. J. (2018), Quaternary Amine-Terminated Quantum Dots Induce Structural Changes to Supported Lipid Bilayers. *Langmuir*, 34, 12369−12378. (DOI: 10.1021/acs.langmuir.8b02047)

42. Sliwiok, J., Kocjan, B., Korczak, B. (1983), Chromatographic examination of hydrophobic properties of isometric ethylphenols and phenylenediamines. *Chromatographia*, 17, 261−263. (DOI: 10.1007/BF02263036)

43. Ghatak, C., Rao, V. G., Pramanik, R., Sarkar, S., Sarkar, N. (2011), The effect of membrane fluidity on FRET parameters: an energy transfer study inside small

unilamellar vesicle. *Phys. Chem. Chem. Phys.*, 13, 3711−3720. (DOI: 10.1039/C0CP01925A)

44. Zheng, W., Liu, Y., West, A., Schuler, E. E., Yehl, K., Dyer, R. B., Kindt, J. T., Salaita, K. (2014), Quantum Dots Encapsulated within Phospholipid Membranes: Phase-Dependent Structure, Photostability, and Site-Selective Functionalization. *J. Am. Chem. Soc.*, 136, 1992−1999. (DOI: 10.1021/ja411339f)

45. Cottone, G., Noto, R., Fornili, S. L. (1998), Interaction of water with the phenylenediamine isomers Ab initio potential evaluation and molecular dynamics simulation. *J. Chem. Soc. Faraday Trans.*, 94, 2337−2342. (DOI: 10.1039/a802815j)

Chapter 5

Interaction of aliphatic amino acids with zwitterionic and charged lipid membranes: hydration and dehydration phenomena

5.1 Introduction

Lipid bilayer membranes are widely used as model systems to mimic cell membranes [1-2]. They represent the complex cell membranes in simpler forms [3]. These biological membranes are composed of an assembly of lipids and proteins organized into several microdomains. They have diverse structures and vital applications owing to their biocompatible and amphiphilic nature [4-9]. The interaction of these membranes with proteins and peptides plays important roles in a lot of membrane-associated biological functions, such as membrane potential sensing, membrane anchoring and endocytosis [10-13]. The interaction of these membranes may be critical for the living systems. Thus, it is important to study their interaction with various amino acids, proteins and peptides to understand the resultant influences on the surface properties of the membranes [14-16]. In particular, interactions between membranes and amino acids are important to understand as they affect the membrane protein folding, membrane protein channels and transport of metabolites in membranes [17-20].

The literature consists of theoretical studies regarding the interaction of peptides and amino acids with the lipid membranes [21-31]. However, the fundamental understanding of the membrane interaction with amino acids is still a subject of debate. Moreover, experimental investigation on the interaction of lipid membranes of different charges and phase states with amino acids of varying chain lengths and charges is essential to unravel the underlying mechanism behind the interaction. In this context, artificial membranes composed of phospholipids may serve as an important model to understand the role of amino

acids in order to modify the topology and hydration of the membrane surface. The interaction causes local changes in the packing of the polar head group region either by hydration or dehydration [3, 32]. Interestingly, this interaction has been found to be enantioselective according to previous reports [33-34]. Moreover, it peptides composed of different amino acids behave differently in the cell [35]. Thus, it is significant to understand how the charge, polarity and hydrophobicity of the amino acids affect the interaction phenomenon with the lipid bilayer and its properties. The understanding of these interactions relevant to the functions in the human body can be a complex process to study and analyze.

Keeping in view the biological interest of such systems, in the present work, we study the interactions of different aliphatic amino acids with lipid bilayer membranes. The structures of the amino acids and lipids used in the present study are summarized in Table 5.1. The choice of these amino acids is based on the fact that they have divergent nature arising from differences in their hydrophilicity, chirality, polarity and charge. In particular, we used charged amino acids i.e. aspartic acid, glutamic acid, arginine and lysine to gain a better insight into how the terminal charged groups may affect the bilayer membrane. In addition to charge, we used amino acids which are widely different in terms of their hydrophobicity index (particularly serine, leucine and valine). As a result, these amino acids display different interactions with lipid bilayer membranes. Thus, the present work is directed towards the understanding of the influence of these amino acids on the membrane properties, such as fluidity, polarity, hydration and dehydration. We studied the impact of amino acids using zwitterionic and differently charged lipid membranes, as well as membranes in different phase states at experimental temperatures.

Table 5.1 *Molecular structures of the lipids, amino acids and fluorescent membrane probe used in this study.*

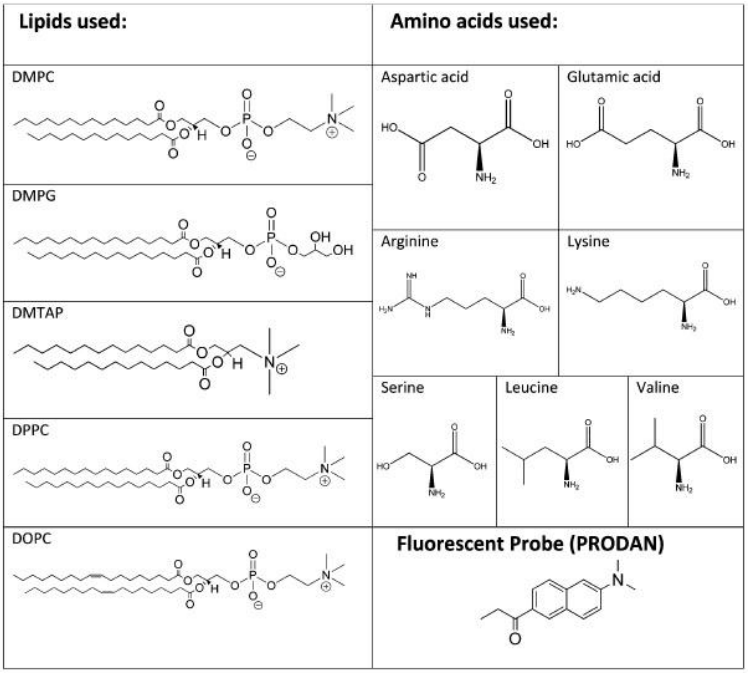

5.2 Results and Discussion

5.2.1 <u>Effect of different lipids on PRODAN</u>: We monitored the emission properties of PRODAN to study the interaction of amino acids with lipid membranes. PRODAN is already known as a membrane polarity sensitive probe and is loosely anchored to the lipid bilayer. In an aqueous medium, PRODAN has an emission band at ~520 nm wavelength. The band is assigned to the twisted intramolecular charge transfer (TICT) state. The partition of PRODAN in a lipid bilayer results in the rise of another band at ~440 nm wavelength. This band is assigned to the locally excited (LE) state of PRODAN [9, 14, 36-40]. The appearance of this band depends on the nature of the lipid bilayer. The band is more prominent in case of the more rigid lipid membrane. As the phase transition temperature of the lipid membrane increases, the emission band at 440 nm becomes more prominent and the lifetime of PRODAN also increases. Thus, we observe that among DPPC, DMPC and DOPC lipid membranes, the LE state is

most prominent in the DPPC bilayer because of its gel state and least prominent in the DOPC lipid bilayer owing to the completely fluid state. The lifetime was also found to be higher in the DPPC bilayer compared to DMPC and DOPC membranes (Figure 5.1, Table 5.2). We already reported that expulsion of water molecules by an external moiety results in the rigidification of the lipid membrane [9, 14, 39-40], which makes the dynamics slower.

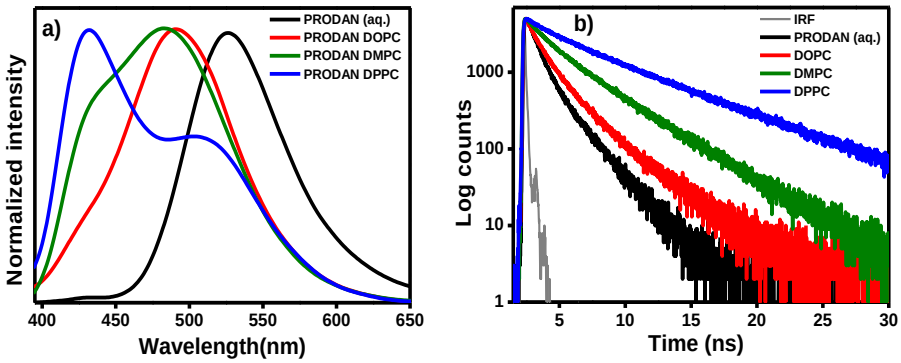

Figure 5.1 *a) Normalized emission spectra of PRODAN in aqueous medium and in different lipid mediums (DPPC, DMPC and DOPC lipid bilayers); (b) representative time-resolved decay of PRODAN in different lipid bilayers collected at 440 nm.*

Table 5.2 *Lifetime components, normalized amplitudes of lifetime components and average lifetime of PRODAN in different lipid mediums collected at 440 nm at 25 °C.*[#]

Sample	τ_1 (ns)	τ_2 (ns)	a_1	a_2	$<\tau_{avg}>$ (ns)	χ^2
PRODAN DOPC	0.76	2.37	0.61	0.39	1.40	1.16
PRODAN DMPC	1.49	4.33	0.38	0.62	3.25	1.11
PRODAN DPPC	1.36	6.39	0.28	0.72	5.00	1.07

[#]*Experimental error is within ±10%.*

5.2.2 Effect of charge and polarity of the amino acids on model membranes:

To investigate the effect of charge and polarity of amino acids on the lipid bilayer, we first chose two negatively charged amino acids, i.e. L-aspartic acid and L-glutamic acid (Table 5.1). Along with varying the charge of the amino acids, we varied the charge of the lipid membrane also in order to unravel the role of surface charge on the interaction properties. We started with a negatively charged lipid membrane composed of DMPC: DMPG followed by a zwitterionic DMPC membrane and a positively charged membrane composed of DMPC:DMTAP. The

steady-state fluorescence emission spectra (Figure 5.2) reveal that the intensity corresponding to the band at ~520 nm decreases and the band at 440 nm becomes more prominent upon interaction with amino acids (aspartic acid and glutamic acid) in the negatively charged DMPC: DMPG lipid membrane. This observation indicates the rigidification of the membrane surface.

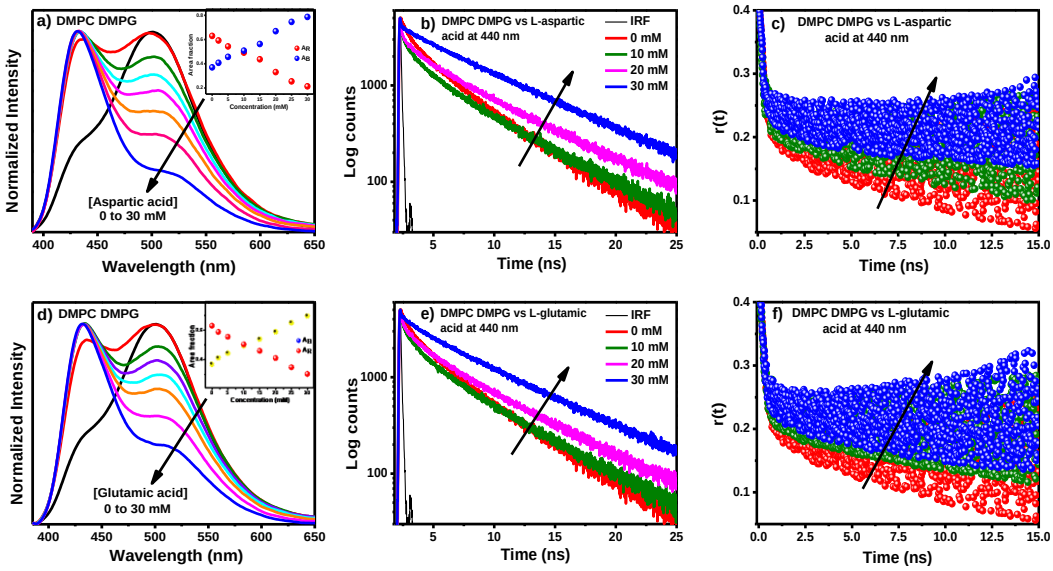

Figure 5.2 *Steady state normalized emission spectra, time-resolved lifetime decay and time-resolved anisotropy plots collected at 440 nm for negatively charged DMPC: DMPG upon interaction with L-aspartic acid (a-c) and glutamic acid (d-f). Corresponding area fraction plots are shown in inset.*

The area fraction plots (Figure 5.2 a, d inset) also indicate the formation of a more stable gel phase of the bilayer. The rigidification or the compactness of the membrane is attributed to the expulsion of water molecules from the membrane surface. This effect is also evident from the time resolved lifetime decay curves (Figure 5.2 b, e). The decays were best fitted using a tri-exponential function (Table 5.3). In particular, the longer lifetime component (τ_2) assigned to the lipid membrane-bound PRODAN increases from 5.23 ns to 7.78 ns and 7.50 ns upon interaction of the DMPC: DMPG lipid membrane with aspartic acid and glutamic acid, respectively.

Table 5.3 *Lifetime components, normalized amplitudes of lifetime components, and average lifetime of PRODAN for DMPC: DMPG vesicles upon interaction with L-aspartic acid and L-glutamic acid collected at 440 nm at 25 °C.*[#]

DMPC: DMPG vs L-aspartic acid @440 nm, 25 °C								
Sample	τ_1 (ns)	τ_2 (ns)	τ_3 (ns)	a_1	a_2	a_3	$<\tau_{avg}>$ (ns)	$\chi 2$
0 mM	1.49	5.23	0.07	0.21	0.21	0.58	1.44	1.17
10 mM	1.32	6.12	0.02	0.04	0.04	0.93	0.29	1.10
20 mM	1.62	7.08	0.02	0.03	0.05	0.93	0.39	1.03
30 mM	2.59	7.78	0.01	0.01	0.04	0.95	0.36	1.06
DMPC: DMPG vs L-glutamic acid @440 nm, 25 °C								
0 mM	1.49	5.23	0.07	0.21	0.21	0.58	1.44	1.17
10 mM	1.30	5.91	0.03	0.07	0.07	0.86	0.52	1.13
20 mM	1.54	6.67	0.03	0.06	0.08	0.86	0.63	1.09
30 mM	2.03	7.50	0.02	0.03	0.11	0.85	0.92	1.02

[#]*Experimental error is within ±10%.*

The strong interaction of aspartic and glutamic acids with the negatively charged membrane is also revealed in the time resolved anisotropy measurements. The rotational relaxation of interfacial PRODAN molecules becomes much slower at 440 nm upon the interaction of aspartic (or glutamic) acid with the negatively charged membrane (Figure 5.2 c and f). At higher concentrations of amino acid, the rotational relaxation decay becomes almost parallel to the X-axis. This observation indicates that the PRODAN molecules experience much hindered rotation due to the dehydration of the lipid membrane surface induced by protonated aspartic (or glutamic) acid [21-22].

Interestingly, the interaction of amino acids is several folds reduced for zwitterionic DMPC membranes (Figure 5.3) and becomes almost nil for positively charged lipid membranes (Figure 5.4). This observation suggests that the primary interaction between the lipid membrane and amino acids takes place between the $-NH_3^+$ group of the amino acid and phosphate group of the lipid membrane which leads to the expulsion of water molecules from the membrane surface. Although amino acids may interact through the $-CO_2^-$ group, the least

interaction in the positively charged lipid membrane proves that the -CO_2^- group does not play any crucial role in the mode of interaction between the amino acids and lipid membrane. Had the CO_2^- group been responsible for the interaction, the maximum interaction would have been observed for the positively charged lipid membrane.

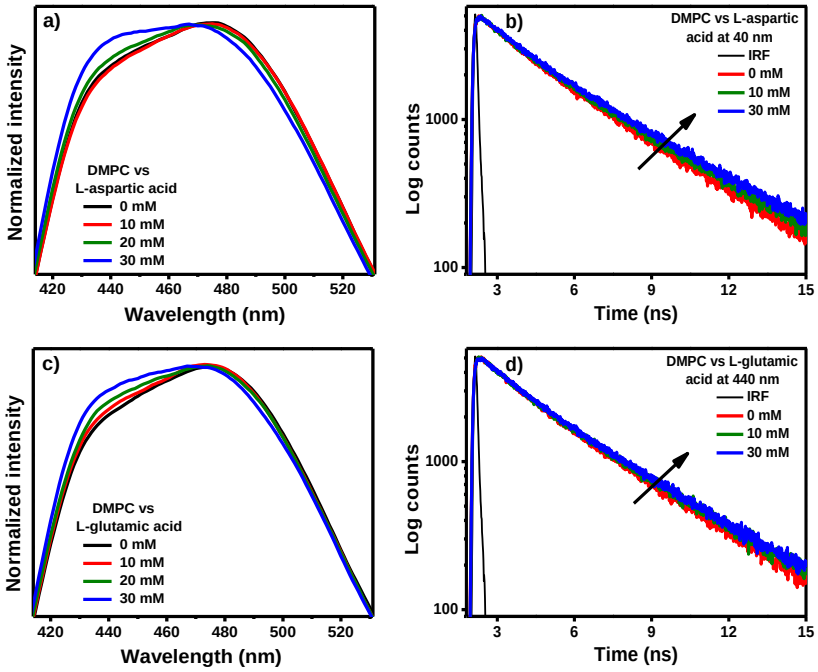

Figure 5.3 *Steady state emission spectra and corresponding time-resolved lifetime decay for DMPC-PRODAN upon interaction with L-aspartic acid (a-b) and L-glutamic acid (c-d).*

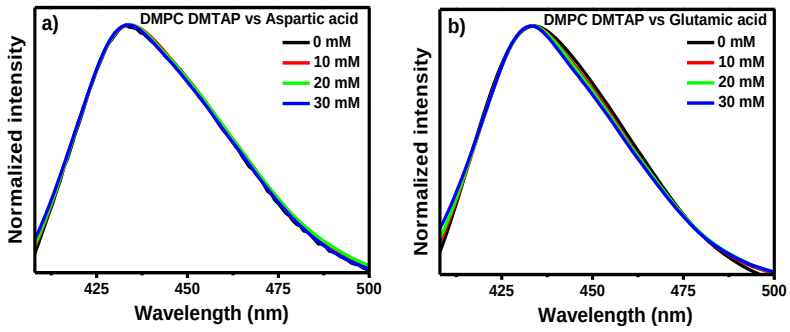

Figure 5.4 *Steady state emission spectra for interaction of negatively charged amino acids with positively charged lipid bilayer DMPC: DMTAP.*

It is known that the pH at the surface of anionic (and not zwitterionic) membranes is lower than the bulk pH [47]. The increase in the anionic lipid content in the

membranes increases the H^+ ions on the surface. Therefore, aspartate or glutamate ions will be protonated at the anionic membrane surface. This eventually results in an increase in the hydrophobicity of the amino acid and eliminates charge repulsion, thereby enhancing membrane affinity [47]. The protonation of interfacial aspartates aids in overcoming the barrier that prevents the insertion of the amino acid inside the hydrophobic region of the bilayer. This also helps to form hydrogen bonding with the phosphate group of the lipid membrane.

The shift in pKa of the amino acids also facilitates the binding affinity of aspartic acid and glutamic acid to the negatively charged membrane. As the pH of the interfacial region of the lipid membrane is lower than the bulk pH, there is an increase in the apparent pKa for binding [47]. The pKa of anionic carboxylic acids shifts from ~1.5 to ~3.0 pH units upon membrane internalization [24]. The large increase in their pKa values leads to the increasing desolvation of the amino acids, resulting in the stabilization of their neutral forms inside the hydrophobic region of the bilayer membrane. Moreover, the ionized carboxylates are destabilized in the phosphate group region of the bilayer headgroup.

From the above discussion, it is concluded that the negatively charged amino acids stabilize the gel phase of the bilayer (particularly negatively charged bilayer) by bringing in rigidification of the membrane. This effect is also evident from the first derivative of the area fraction (A_{435}/A_{500}) vs. the temperature plot, which clearly indicates that the phase transition temperature of the negatively charged lipid bilayer composed of DMPC: DMPG increases from ~23.5 °C to ~25 °C upon interaction with aspartic acid (Figure 5.5).

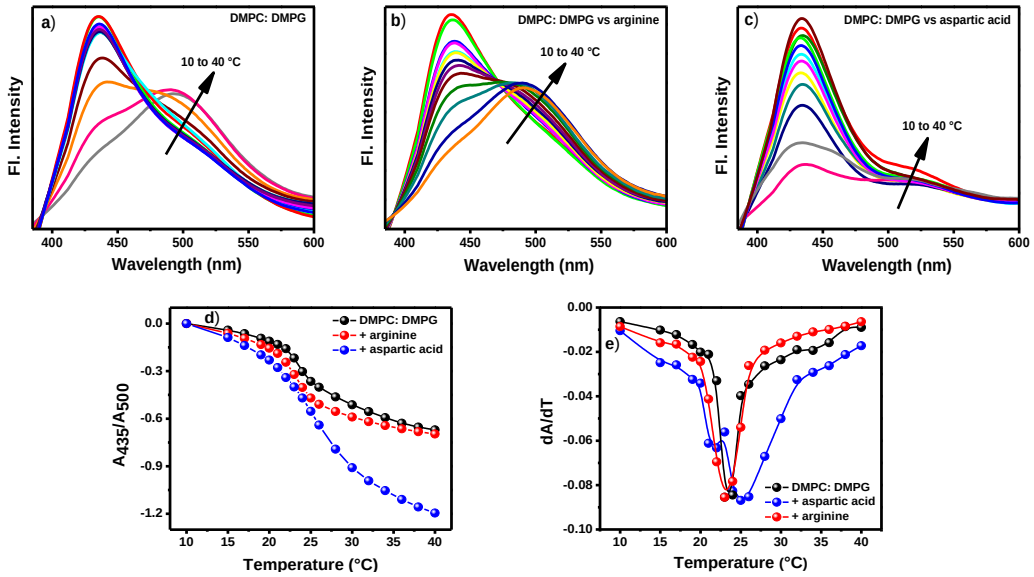

Figure 5.5 *Plots of temperature-induced variation in the steady-state fluorescence spectra of PRODAN in a) negatively charged DMPC: DMPG bilayer, b) upon interaction with arginine and c) aspartic acid, d) area fraction vs temperature plot from 10 °C to 40 °C and e) first derivative of area (dA/dT) vs temperature plot.*

While the negatively charged aspartic acid and glutamic acid display significant interaction by dehydrating the lipid membrane surface, the positively charged arginine and lysine show some different results. We observe that lysine and arginine offer very weak affinity towards zwitterionic DMPC (Figure 5.6) and positively charged DMPC: DMTAP bilayer membranes (Figure 5.7). We already mentioned that the interaction between the lipid bilayer and the amino acids takes place through the $-NH_3^+$ group of the amino acids and phosphate group of the lipid molecules. The electrostatic interaction is primarily the governing force which is minimum in the zwitterionic DMPC lipid and completely eliminated in the cationic lipid membrane.

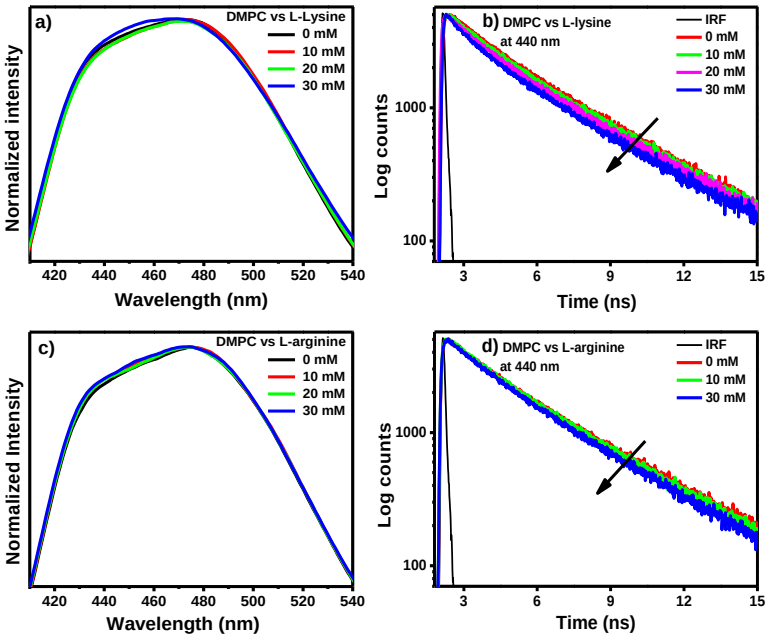

Figure 5.6 *Steady state emission spectra and corresponding time-resolved lifetime decay for DMPC-PRODAN upon interaction with L-lysine (a-b) and L-arginine (c-d).*

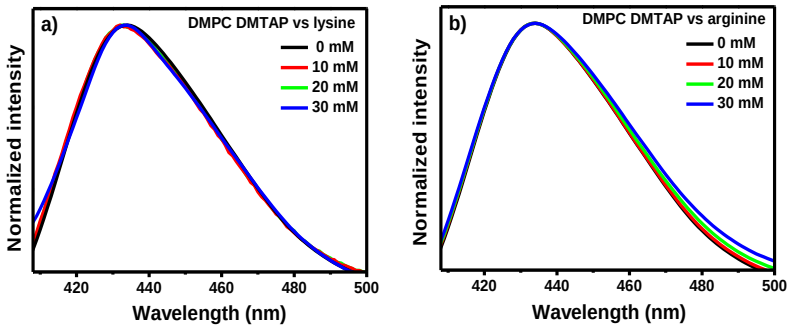

Figure 5.7 *Steady state fluorescence spectra for interaction of positively charged amino acids with positively charged lipid bilayer DMPC: DMTAP.*

The binding of an arginine moiety to a negatively charged bilayer is enthalpically favorable, as opposed to interaction with neutral membranes [27]. Figure 5.8 indicates that at very low concentrations, lysine induces gelation in the lipid bilayer. However, at relatively higher concentrations, lysine increases the fluidity of the membrane as the intensity corresponding to the 440 nm band decreases continuously. We observe similar phenomena for L-arginine. The initial stabilization of the gel phase of the bilayer stems from the fact that the electrostatic interaction takes place very instantaneously. Moreover, hydrogen bonding between arginine (or lysine) and the lipid membrane followed by

subsequent removal of water may be crucial in this regard. Arginine's guanidinium moiety allows a hydrogen-bonding network and the positive charge on the arginine rather supports hydrogen bonding as well as electrostatic interactions with a potential phosphate host [48]. The electrostatic interaction between phosphate and the guanidinium host at the surface of the bilayer membrane is enhanced due to low polarity at the interfacial region of the lipid membrane. The guanidinium functional group of the arginine is mainly responsible for the binding with the phosphate group by providing a hydrogen bonding donor for potential binding with the phosphate host [48]. Arginine also has a stronger tendency to form multiple hydrogen bonds with the headgroup, which results in a strong initial dehydration. The initial gelation at low concentration, therefore, could be attributed to the simple electrostatic interaction in which the cationic terminal group of lysine or arginine is attracted to the phosphate group of the lipid bilayer headgroup.

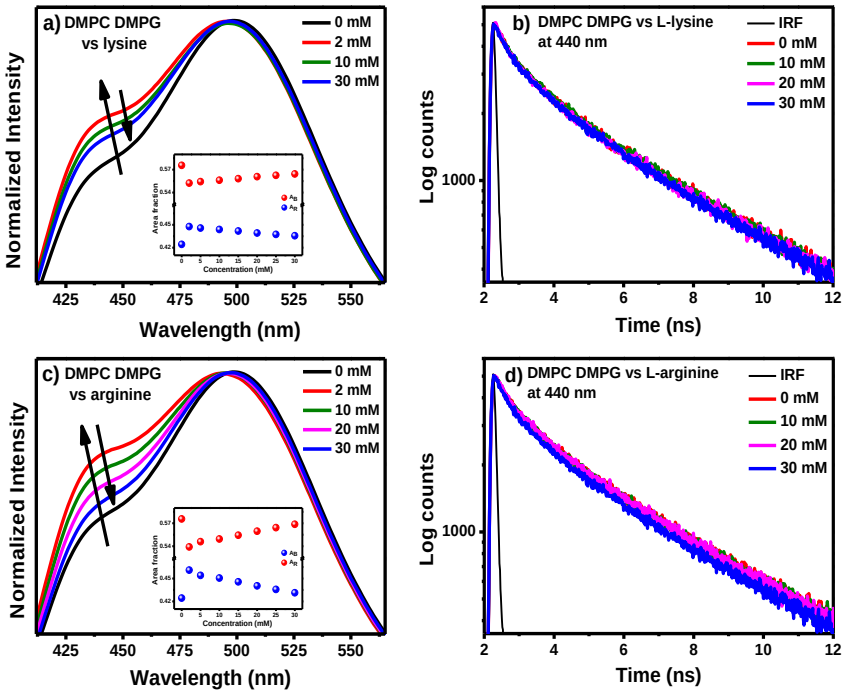

Figure 5.8 *Steady state normalized emission spectra and time-resolved lifetime decay collected at 440 nm for negatively charged DMPC: DMPG upon interaction with L-lysine (a-b) and L-arginine (c-d). Upward arrows in the emission spectra indicate an initial increase in the peak at 440 nm whereas downward arrows indicate a gradual decrease in the peak depicting fluidization of the bilayer. Corresponding area fraction plots are depicted in inset.*

The most striking observation is that lysine and arginine bring in fluidization in the lipid bilayer at a higher concentration (Figure 5.8). This observation is opposite to that obtained for negatively charged amino acids (aspartic acid and glutamic acid). As the positively charged amino acids (arginine or lysine) enter the DMPC: DMPG membrane, it deforms the lipid bilayer by carrying a significant amount of water as well as lipid headgroups into the hydrocarbon core of the membrane [22, 35]. Our experimental result is in agreement with the earlier theoretical prediction and implies that both lysine and arginine are able to wet the surface and the hydrocarbon core of the lipid membrane.

Interestingly, a major finding in our results suggests that arginine is more capable of hydrating the membrane at higher concentrations as compared to lysine (Figure 5.8). The significant difference in fluidizing the surface upon interaction with lysine and arginine is because of the fact that arginine carries a larger number of water molecules (~23) than lysine and also tends to pull more lipid headgroups inside the hydrocarbon core while penetrating inside the membrane core [35]. As a result, arginine induces pores in the lipid bilayer and causes greater membrane deformations [35]. Arginine has a strong tendency to interact with the negatively charged membrane by penetrating deep inside the bilayer, which results in the rearrangement of the acyl chains and distortion of the symmetrical shape of the bilayer [13]. In this context, the large difference in the pKa shift for arginine and lysine needs to be noted. The theoretical studies suggest that the change in pKa of lysine takes place from 10.5 to 1 on going from aqueous solution to the centre of the membrane. On the other hand, the change in the pKa value for arginine remains above 7 throughout the membrane [35]. Thus, even in the hydrocarbon core of the bilayer, lysine may deprotonate whereas arginine efficiently carries its charge even after suffering a little pKa shift. The guanidinium group in arginine seeks hydration so strongly that it would rather prefer to exit the lipid bilayer than to deprotonate [49]. This makes arginine a unique amino acid to maintain its charge even in the hostile environment of the core of the lipid membrane [25, 35]. This property further aids arginine in carrying excess water molecules as well as

lipid headgroups to the centre of the hydrocarbon core. This causes destabilization of the lipid membrane.

5.2.3 Effect of hydrophobicity of the amino acids on model membranes: In this section, we used amino acids of different hydrophobicity (serine, leucine and valine) to study the interaction with lipid membranes of different charge states. These amino acids are different in terms of their varying hydrophobicity index. The hydrophobicity indices indicate that serine is a hydrophilic amino acid owing to the presence of an –OH group on the terminal carbon atom of the side chain, unlike leucine and valine, which are hydrophobic in nature. Our primary objective in choosing these amino acids is to investigate if hydrogen bonding plays any crucial role in governing the interaction between the lipid bilayer and amino acids. It has been reported that the interaction of the lipid membrane with amino acids or peptides is governed by both electrostatic and hydrophobic forces [13, 50].

We observe a blue shift in the steady state emission spectra of PRODAN (Figure 5.9 a–c) upon interaction of amino acids with the zwitterionic DMPC bilayer. This observation implies the stabilization of the gel phase of the bilayer. This effect is also clearly evident from the corresponding area fraction plots (Figure 5.9 d–f). The gelation is attributed to the expulsion of water molecules from the interfacial region of the bilayer, which makes it more hydrophobic owing to the adsorption of amino acids on the membrane surface. The interaction between the phospholipid membrane and amino acid side chains could be facilitated by the replacement of water molecules, with a consequent weakening of the vibrational force constants [51].

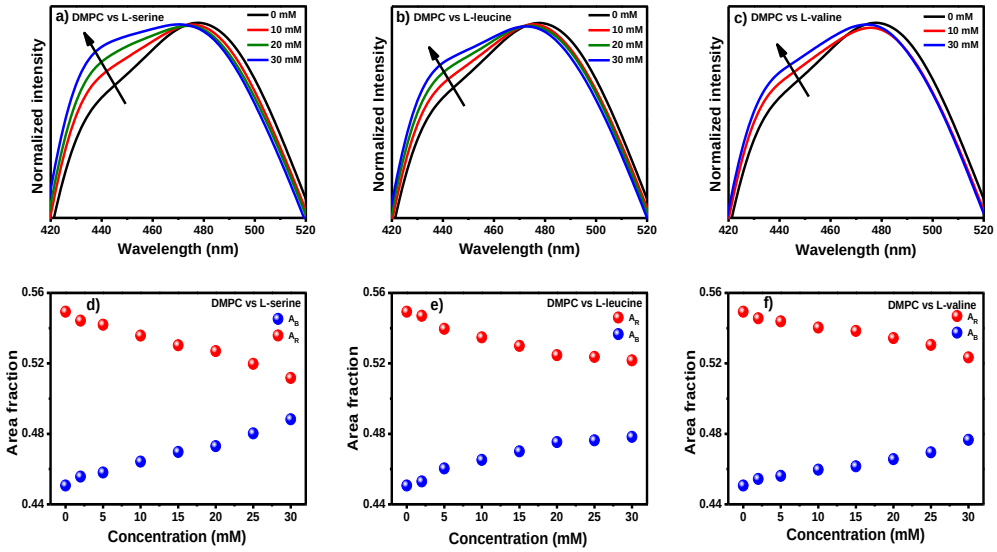

Figure 5.9 *Steady state normalized emission spectra (a–c) and corresponding area fraction plots (d–f) for DMPC–PRODAN upon interaction with amino acids.*

Interestingly, the observed changes (as revealed from the normalized curves) indicate that the maximum interaction takes place for serine (Figure 5.10). We attributed this observation to the hydrogen bonding ability of L-serine with the phosphate group of the lipid membrane owing to the presence of a hydroxyl group at the terminal carbon. It is thus validated that hydrogen bonding is a key driving force for the binding of amino acids to lipid membranes.

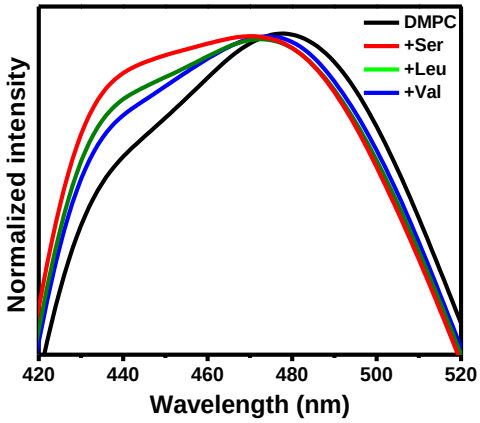

Figure 5.10 *Comparison of steady state emission spectra for L-amino acids upon interaction with zwitterionic DMPC membrane.*

This effect is also evident from Confocal imaging (Figure 5.11), which indicates the formation of more compact structures upon the addition of L-serine. The CLSM imaging also indicates the encapsulation of dye without any evident leakage and formation of uniformly sized spherical vesicles.

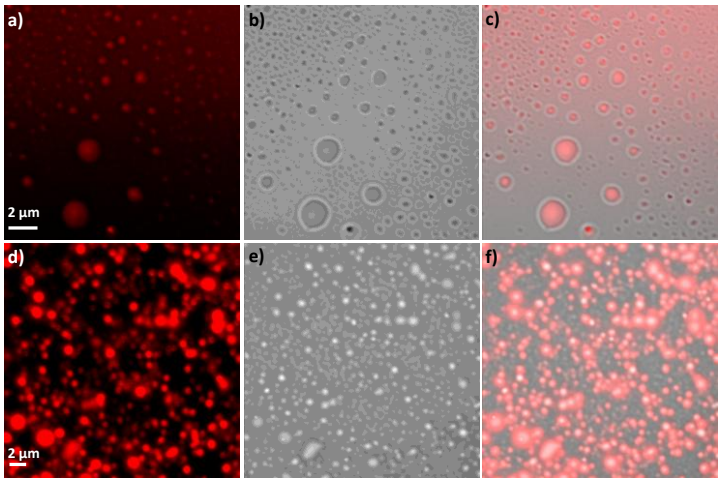

Figure 5.11 *Binding of amino acids using confocal scanning laser microscopy (CLSM). Confocal, bright field and merged images for DMPC vesicles (a-c), DMPC + L-serine (d-f).*

We also find that the interaction is highly specific to the L-amino acids due to the formation of stereospecific hydrogen bonds at the side chains of the L-amino acids. As a consequence, D-amino acids do not show any interaction with the bilayer membrane (Figure 5.12).

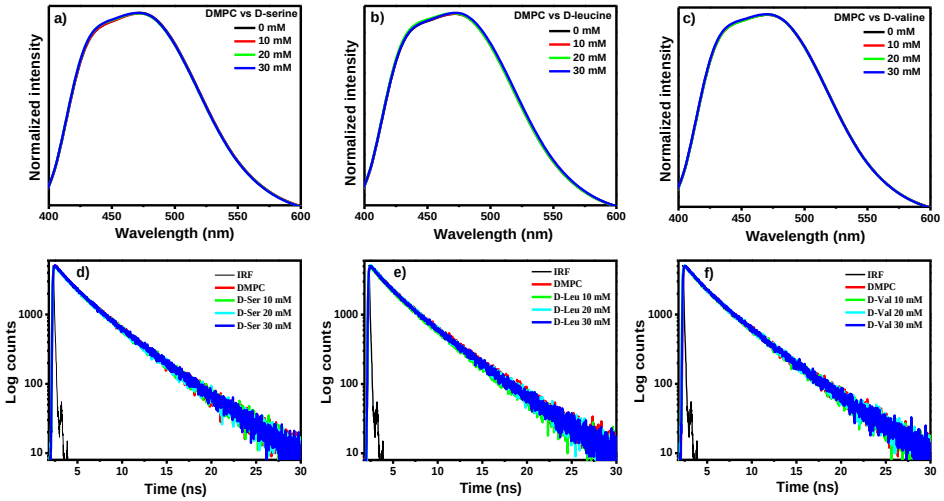

Figure 5.12 *Steady state emission spectra (a-c) and time-resolved lifetime decay curves (d-f) for DMPC-PRODAN upon interaction with D-amino acids.*

In this context, surface charge on the bilayer membrane could play a significant role in governing the binding of amino acids to the membrane surface because the initial interaction between the amino acid and lipid membrane is governed by the electrostatic interaction. We find that the binding affinity of all the L-amino acids towards the negatively charged DMPC: DMPG bilayer is almost the same for all amino acids (Figure 5.13 a–c). Moreover, amino acids show absolutely no interaction with DMPC: DMTAP (Figure 5.13 d–f). This observation is important and leads to the conclusion that the electrostatic interaction takes place between the $–NH_3^+$ group of the amino acid and the phosphate group of the lipid bilayer. As discussed earlier, had the CO_2^- group been responsible for electrostatic interaction, we would have obtained maximum interaction for the positively charged membrane. As the electrostatic interaction takes place through the $–NH_3^+$ group of the amino acid, this renders DMPC: DMTAP less interacting with the phospholipid bilayer.

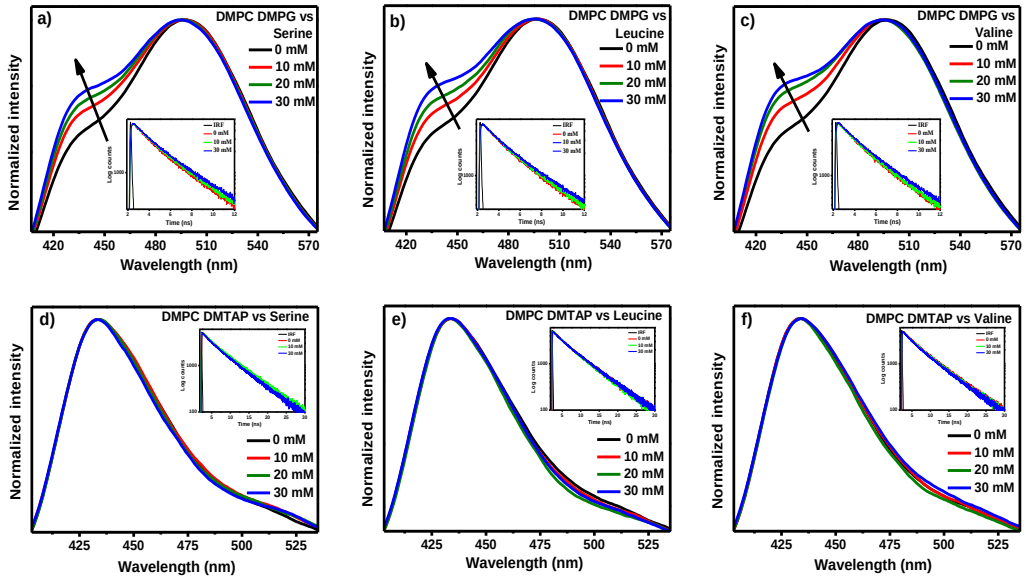

Figure 5.13 *Steady state normalized emission spectra and time resolved lifetime decay curves (inset) of L-amino acids with negatively charged lipid bilayer DMPC: DMPG (a–c) and positively charged lipid DMPC:DMTAP (d–f). The upward arrows at 440 nm indicate the gel phase dominance.*

We next studied the effect of amino acids on the lipid bilayers having phase transition temperatures well above and below the experimental temperature (25

°C) and compared the result with that obtained from DMPC. In the first case, we studied the DPPC (T_m = 41 °C) lipid bilayer membrane which remains in the gel phase under the experimental conditions. It is observed that the interaction of L-amino acids with the DPPC bilayer also results in shifting of the emission peak towards the blue end indicating the stabilization of the gel phase of the bilayer (Figure 5.14). However, the interaction with the membrane in the gel phase is much weaker as compared to that in DMPC. The lifetime decay also increases minimally upon interaction of L-amino acids. It seems that DPPC being in rigid gel phase at the experimental temperature does not allow amino acids to penetrate deeper inside the bilayer.

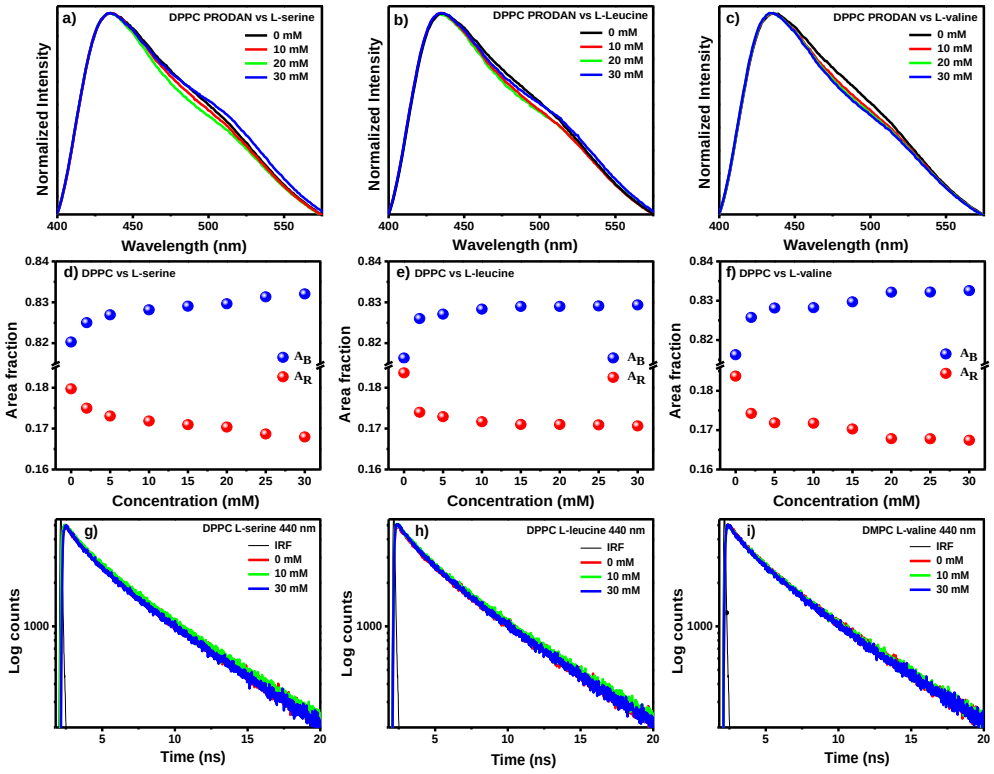

Figure 5.14 *Steady state emission spectra (a-c), area fraction plots (d-f) and time resolved lifetime decay curves (g-i) for DPPC-PRODAN upon interaction with L-amino acids.*

We further evaluated the changes in the fluorescence spectra and lifetime decay parameters for DOPC upon interaction with L-amino acids (Figure 5.15). It is observed that DOPC (T_m = 17 °C) upon addition of L-amino acids does not reveal significant changes in the emission spectra and lifetime decay. This could be

explained by the fact that since DOPC remains predominantly in the fluid phase at the experimental temperature (25 °C), the phase state remains almost intact upon addition of amino acids. Therefore, we conclude that the maximum effect in terms of stabilization of the gel phase is observed for a lipid bilayer membrane near its phase transition temperature (Tm) rather than being far above the Tm of the lipid [52].

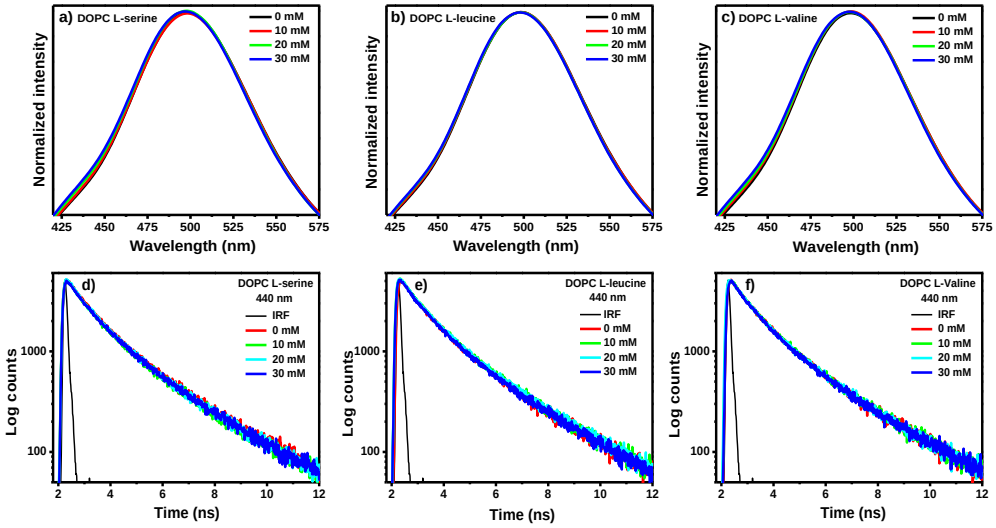

Figure 5.15 *Steady state normalized emission spectra (a-c) and time resolved lifetime decay curves (d-f) of L-amino acids with DOPC.*

5.2.4 <u>Effect of amino acids on hydrodynamic size of the lipid vesicles</u>: To study the effect of amino acids on the size of the lipid vesicles, we conducted DLS measurements. In the context of the effect of charge, the lipid vesicles composed of negatively charged DMPC: DMPG show an average hydrodynamic size of nearly 210 nm. The hydrodynamic size distribution decreases as a result of interaction of the negatively charged aspartic acid and glutamic acid with the lipid vesicles (Figure 5.16 a). This observation is attributed to the stabilization of the gel phase of the vesicles leading to an overall shrinkage of the lipid vesicles. On the other hand, interaction with positively charged amino acids, lysine and arginine results in the increase in overall hydrodynamic size distribution. This may be due to fluidization of lipid vesicles which results in the hydration of the

lipid bilayer and it may induce fusion in the vesicles. These results corroborate well with the conclusions drawn from steady state and time-resolved experiments.

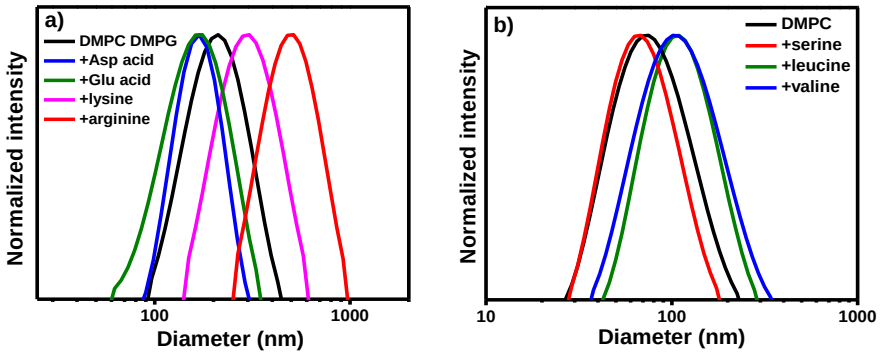

Figure 5.16 *Hydrodynamic size distribution curves obtained by DLS measurements for (a) negatively charged DMPC: DMPG upon addition of charged amino acids and (b) zwitterionic DMPC upon addition of L-amino acids.*

Furthermore, upon considering the effect of hydrophobicity of amino acids, the interaction with serine reduces the size of DMPC vesicles by nearly 10 nm (Figure 5.16 b). On the other hand, the size distribution increases upon interaction with hydrophobic leucine and valine. The possible reason for the decrease in size upon addition of serine may be due to the stabilization of the gel phase of the lipid vesicles. The dehydration makes the vesicles more compact, which leads to an overall shrinkage of the vesicles as discussed above. However, interaction with their hydrophobic analogues does not stabilize the gel phase very effectively and results in an overall increase in hydrodynamic radius. The effect of different amino acids is summarized in Scheme 5.1.

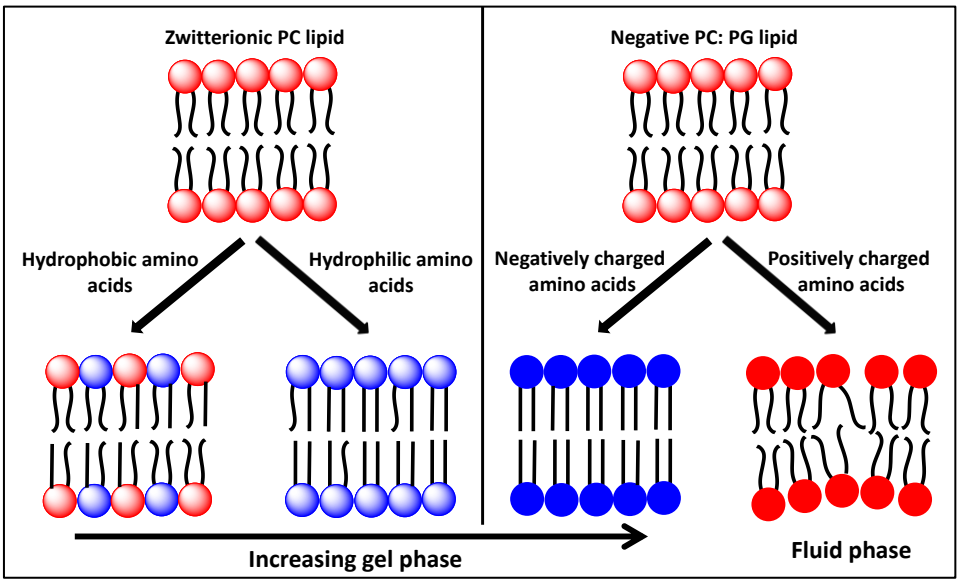

Scheme 5.1 *Illustration of the interaction of various amino acids on the lipid bilayer membrane for the zwitterionic phosphatidylcholine and negatively charged lipid membrane. The shaded red colored lipid membrane represents nearly fluid phase at room temperature, shaded blue represents nearly gel phase, the deep blue colored lipid membrane represents highly gel and ordered phase (stiffened acyl chains) and deep red represents completely fluid or disordered phase (loosely packed acyl chains).*

5.3 Conclusion

The interaction of lipid bilayer membranes with amino acids depends on the properties of both the amino acids and the membrane itself. The major observations of the present study are summarized as follows:

(a) Charge of the amino acid plays a major role in the interaction strength with the lipid bilayer membrane. Interaction with negatively charged amino acids results in very large dehydration. On the other hand, cationic amino acids arginine and lysine significantly fluidize the membrane. We explain these observations by the shift in pKa of amino acids in the vicinity of the lipid membranes as well as the solvation and desolvation processes in the light of recent computer simulations.

(b) We observe that the aliphatic amino acids bring about gelation in the lipid membrane. Among all the amino acids, serine is found to offer stronger

interaction compared to other amino acids owing to the hydrogen bonding capacity with the lipid headgroup. The maximum change in the lipid membrane takes place near the phase transition temperature of the lipid. Thus, among all the lipid membranes, DMPC displays maximum changes as the experimental temperature is very close to the phase transition temperature.

(c) In the case of anionic lipid membrane, the interaction strength is similar for all aliphatic amino acids irrespective of their hydrophobicity. The cationic lipid membrane, on the other hand, does not induce any substantial changes in the bilayer membrane.

In general, it is reasonable to say that L-amino acids can efficiently stabilize the lipid vesicles, and thus they can be used for various biological applications.

5.4 References

1. Sarangi, N. K., Patnaik, A. (2012), L-Tryptophan-induced electron transport across supported lipid bilayers: an alkyl-chain tilt-angle, and bilayer- symmetry dependence. *ChemPhysChem*, 13, 4258–4270. (DOI: 10.1002/cphc.201200655)

2. Vereb, G., Szöllősi, J., Matkó, J., Nagy, P., Farkas, T., Vígh, L., Mátyus, L., Waldmann, T. A., Damjanovich, S. (2003) Dynamic, yet structured: The cell membrane three decades after the Singer–Nicolson model. *Proc. Natl. Acad. Sci. U. S. A.*, 100, 8053–8058. (DOI: 10.1073/pnas.1332550100)

3. Arias, J. M., Tuttolomondo, M. E., Díaz S. B., Altabef, A. B. (2018), Molecular view of the structural reorganization of water in DPPC multilamellar membranes induced by L-cysteine methyl ester. *J. Mol. Struct.*, 1156, 360–368. (DOI: 10.1016/ j.molstruc.2017.11.124)

4. Maiti, B., Dey, N. Bhattacharya, S. (2019), Engaging Dynamic Surfactant Assemblies in Improving Metal Ion Sensitivity of 1,4,7-Triazacyclononane Based Receptor: Differential Optical Response for Cysteine and Histidine. *ACS Appl. Bio Mater.*, 2, 2365–2373. (DOI: 10.1021/acsabm.9b00083)

5. Parassasi, T., Satasio, G. D., Ubaldo, A., Gratton, E. (1990), Phase fluctuation in phospholipid membranes revealed by Laurdan fluorescence. *Biophys. J.*, 57, 1179–1186. (DOI: 10.1016/S0006-3495(90)82637-0)

6. Sahoo, S. K., Labhasetwar, V. (2003), Nanotech approaches to drug delivery and imaging. *Drug Discovery Today*, 8, 1112–1120. (DOI: 10.1016/S1359-6446(03)02903-9)

7. Li, J., Wang, X., Zhang, T., Wang, C., Huang, Z., Luo, X., and Deng, Y. (2015), A review on phospholipids and their main applications in drug delivery systems. *Asian J. Pharm. Sci.*, 10, 81–98. (DOI: 10.1016/j.ajps.2014.09.004)

8. Allen, T. M., Cullis, P. R. (2013), Liposomal drug delivery systems: From concept to clinical applications. *Adv. Drug Delivery Rev.*, 65, 36–48.

9. Kanwa, N., De, S. K., Adhikari C., Chakraborty, A. (2017), Spectroscopic study of the interaction of carboxyl-modified gold nanoparticles with liposomes of different chain lengths and controlled drug release by layer-by-layer technology. *J. Phys. Chem. B*, 121, 11333–11343. (DOI: 10.1021/acs.jpcb.7b08455)

10. Liu, A., Wenzel, N., Qi, X. (2005), Role of lysine residues in membrane anchoring of saposin C. *Arch. Biochem. Biophys.*, 443, 101–112. (DOI: 10.1016/j.abb.2005.09.007)

11. Jiang, Y., Ruta, V., Chen, J., Lee, A., MacKinnon, R. (2003), The principle of gating charge movement in a voltage-dependent K^+ channel. *Nature*, 423, 42–48. (DOI: 10.1038/nature01581)

12. Duchardt, F., Fotin-Mleczek, M., Schwarz, H., Fischer R., Brock, R. (2007), A comprehensive model for the cellular uptake of cationic cell-penetrating peptides. *Traffic*, 8, 848–866. (DOI: 10.1111/j.1600-0854.2007.00572.x)

13. Zhang, J., Yang, W., Tan, J., Ye, S. (2018), In situ examination of a charged amino acid induced structural change in lipid bilayers by sum frequency

generation vibrational spectroscopy. *Phys. Chem. Chem. Phys.*, 20, 5657. (DOI: 10.1039/C7CP07389E)

14. Thakur, R., Das, A., Chakraborty, A. (2014), Interaction of human serum albumin with liposomes of saturated and unsaturated lipids with different phase transition temperatures: a spectroscopic investigation by membrane probe PRODAN. *RSC Adv.*, 4, 14335–14347. (DOI: 10.1039/C4RA01214C)

15. Banerjee, P., Pal, S., Kundu, N., Mondal, D., Sarkar, N. (2019), Spectroscopic and Microscopic Approach to Monitor the Changes in Bilayer Rigidity during Cell Penetrating Peptide Induced Self-Reproduction of Phospholipid Vesicles. *Biophys. J.*, 116, 216a. (DOI: 10.1016/j.bpj.2018.11.1194)

16. Perkins, R., Vaida, V. (2017), Phenylalanine Increases Membrane Permeability. *J. Am. Chem. Soc.*, 139, 14388–14391. (DOI: 10.1021/jacs.7b09219)

17. Hong, H., Park, S., Jiménez, R. H. F., Rinehart D., Tamm, L. K. (2007), Role of aromatic side chains in the folding and thermodynamic stability of integral membrane proteins. *J. Am. Chem. Soc.*, 129, 8320–8327. (DOI: 10.1021/ja068849o)

18. Domene, C., Vemparala, S., Klein, M. L., Vénien-Bryan C., Doyle, D. A. (2006), Role of aromatic localization in the gating process of a potassium channel. *Biophys. J.*, 90, L01–L03. (DOI: 10.1529/biophysj.105.072116)

19. Stroobant P., Kaback, H. R. (1979), Reconstitution of ubiquinone- linked functions in membrane vesicles from a double quinone mutant of Escherichia coli. *Biochemistry*, 18, 226–231. (DOI: 10.1021/bi00568a035)

20. Perkins, R. J., Kukharchuk, A., Delcroix, P., Shoemaker, R. K., Roeselova, M., Cwiklik, L., Vaida, V. (2016), The partitioning of small aromatic molecules to air−water and phospholipid interfaces mediated by non-hydrophobic interactions. *J. Phys. Chem. B*, 120, 7408–7422. (DOI: 10.1021/acs.jpcb.6b05084)

21. MacCallum, J. L., Bennett, W. F. D., Tieleman, D. P. (2008), Distribution of amino acids in a lipid bilayer from computer simulations. *Biophys. J.*, 94, 3393–3404. (DOI: 10.1529/biophysj.107.112805)

22. Pogorelov, T. V., Vermaas, J. V., Arcario, M. J., Tajkhorshid, E. (2014), Partitioning of amino acids into a model membrane: capturing the interface. *J. Phys. Chem. B*, 118, 1481–1492. (DOI: 10.1021/jp4089113)

23. Dunne, S. J., Cornell, R. B., Johnson, J. E., Glover, N. R., Tracey, A. S. (1996), Structure of the membrane binding domain of CTP: phosphocholine cytidylyltransferase. *Biochemistry*, 35, 11975–11984. (DOI: 10.1021/bi960821+)

24. Teixeira, V. H., Vila-Viçosa, D., Reis, P. B. P. S., Machuqueiro, M. (2016), pK_a Values of Titrable Amino Acids at the Water/Membrane Interface. *J. Chem. Theory Comput.*, 12, 930–934. (DOI: 10.1021/acs.jctc.5b01114)

25. MacCallum, J. L., Bennett, W. F. D., Tieleman, D. P. (2007), Partitioning of amino acid side chains into lipid bilayers: results from computer simulations and comparison to experiment. *J. Gen. Physiol.*, 129, 371–377. (DOI: 10.1085/jgp.200709745)

26. Hu, Y., Liu, X., Sinha, S. K., Patel, S. (2014), Translocation thermodynamics of linear and cyclic nonaarginine into model DPPC bilayer via coarse-grained molecular dynamics simulation: implications of pore formation and nonadditivity. *J. Phys. Chem. B*, 118, 2670–2682. (DOI: 10.1021/jp412600e)

27. Takechi, Y., Yoshii, H., Tanaka, M., Kawakami, T., Aimoto, S., Saito, H. (2011), Physicochemical mechanism for the enhanced ability of lipid membrane penetration of polyarginine. *Langmuir*, 27, 7099–7107. (DOI: 10.1021/la200917y)

28. Maioloa, J. R., Ferrerb, M., Ottingera, E. A. (2005), Effects of cargo molecules on the cellular uptake of arginine-rich cell-penetrating peptides. *Biochim. Biophys. Acta*, 1712, 161–172. (DOI: 10.1016/j.bbamem.2005.04.010)

29. Hitz, T., Iten, R., Gardiner, J., Namoto, K., Walde, P., Seebach, D. (2006), Interaction of α-and β-Oligoarginine-Acids and Amides with Anionic Lipid Vesicles: A Mechanistic and Thermodynamic Study. *Biochemistry*, 45, 5817–5829. (DOI: 10.1021/bi060285d)

30. Nandi, S., Mondal, P., Chowdhury, R., Saha, A., Ghosh, S., Bhattacharyya, K. (2016), Amyloid beta peptides inside a reconstituted cell-like liposomal system: aggregation, FRET, fluorescence oscillations and solvation dynamics. *Phys. Chem. Chem. Phys.*, 18, 30444–30451. (DOI: 10.1039/C6CP06143E)

31. Mahata, T., Mondal, P., Bhunia, D., Nandi, S., Kurkute, P., Bhattacharyya K., Ghosh, S. (2019), Self-Assembly of Antimitotic Peptide at Membranes: Computational and Experimental Investigation. *ACS Omega*, 4, 745–754. (DOI: 10.1021/acsomega.8b01568)

32. Banerjee, P., Pal, S., Kundu, N., Mondal, D., Sarkar, N. (2018), A cell-penetrating peptide induces the self-reproduction of phospholipid vesicles: understanding the role of the bilayer rigidity. *Chem. Commun.*, 54, 11451–11454. (DOI: 10.1039/c8cc07176d)

33. Bombelli, C., Borocci, S., Lupi, F., Mancini, G., Mannina, L., Segre, A. L., Viel, S. (2004), Chiral recognition of dipeptides in a biomembrane model. *J. Am. Chem. Soc.*, 126, 13354–13362. (DOI: 10.1021/ja0470057)

34. Ishigami, T., Suga, K., Umakoshi, H. (2015), Chiral Recognition of l-Amino Acids on Liposomes Prepared with l-Phospholipid. *ACS Appl. Mater. Interfaces*, 7, 21065–21072. (DOI: 10.1021/acsami.5b07198)

35. Li, L., Vorobyov, I., Allen, T. W. (2013), The different interactions of lysine and arginine side chains with lipid membranes. *J. Phys. Chem. B*, 117, 11906–11920. (DOI: 10.1021/jp405418y)

36. Parasassi, T., Krasnowska, E. K., Bagatolli, L., Gratton, E. (1998), Laurdan and Prodan as Polarity-Sensitive Fluorescent Membrane Probes. *J. Fluoresc.*, 8, 365–373. (DOI: 10.1023/A:1020528716621)

37. Krasnowska, E. K., Gratton, E., Parasassi, T. (1998), Prodan as a membrane surface fluorescence probe: partitioning between water and phospholipid phases. *Biophys. J.*, 74, 1984–1993. (DOI: 10.1016/S0006-3495(98)77905-6)

38. Novaira, M., Biasutti, M. A., Silber, J. J., Correa, N. M. (2007), New Insights on the Photophysical Behavior of PRODAN in Anionic and Cationic Reverse Micelles: From Which State or States Does It Emit?. *J. Phys. Chem. B*, 111, 748–759. (DOI: 10.1021/jp065528q)

39. De, S. K., Kanwa, N., Ahamed, M., Chakraborty, A. (2018), Spectroscopic evidence for hydration and dehydration of lipid bilayers upon interaction with metal ions: a new physical insight. *Phys. Chem. Chem. Phys.*, 20, 14796–14807. (DOI: 10.1039/C8CP01774C)

40. De, S. K., Kanwa, N., Chakraborty, A. (2019), Influence of Trivalent Metal Ions on Lipid Vesicles: Gelation and Fusion Phenomena. *Langmuir*, 35, 6429–6440. (DOI: 10.1021/acs.langmuir.9b00682)

41. Justo, O. R., Moraes, A. M. (2005), Kanamycin incorporation in lipid vesicles prepared by ethanol injection designed for tuberculosis treatment. *J. Pharm. Pharmacol.*, 57, 23–30. (DOI: 10.1211/0022357055092)

42. Pons, M. Foradada, M., Estelrich, J. (1993), Liposomes obtained by the ethanol injection method. *Int. J. Pharm.*, 95, 51–56. (DOI: 10.1016/0378-5173(93)90389-W)

43. Batzri, S., Korn, E. D. (1973), Single bilayer liposomes prepared without sonication. *Biochim. Biophys. Acta*, 298, 1015–1019. (DOI: 10.1016/0005-2736(73)90408-2)

44. Wei, F., Li, H., Ye, S. (2013), Specific Ion Interaction Dominates over Hydrophobic Matching Effects in Peptide–Lipid Bilayer Interactions: The Case of Short Peptide. *J. Phys. Chem. C*, 117, 26190–26196. (DOI: 10.1021/jp411413u)

45. Wei, F., Ye, S., Li, H., Luo, Y. (2013), Phosphate Ions Promoting Association between Peptide and Modeling Cell Membrane Revealed by Sum Frequency

Generation Vibrational Spectroscopy. *J. Phys. Chem. C*, 117, 11095–11103. (DOI: 10.1021/jp400378d)

46. Yang, W., Tian, K., Ye, S. (2015), Interaction between Potassium Phosphate Buffer Solution and Modeling Cell Membrane Investigated by Sum Frequency Generation Vibrational Spectroscopy. *Chin. J. Chem. Phys.*, 28, 518–524. (DOI: 10.1063/1674-0068/28/cjcp1504070)

47. Johnson, J. E., Xie, M., Singh, L. M. R., Edge, R., Cornell, R. B. (2003), Both acidic and basic amino acids in an amphitropic enzyme, CTP: phosphocholine cytidylyltransferase, dictate its selectivity for anionic membranes. *J. Biol. Chem.*, 278, 514–522. (DOI: 10.1074/jbc.M206072200)

48. Neal, J. F., Zhao, W., Grooms, A. J., Flood, A. H., Allen, H. C. (2018), Arginine–Phosphate Recognition Enhanced in Phospholipid Monolayers at Aqueous Interfaces. *J. Phys. Chem. C*, 122, 26362–26371. (DOI: 10.1021/acs.jpcc.8b03531)

49. Martfeld, A. N., Greathouse, D. V., Koeppe II, R. E. (2016), Ionization properties of histidine residues in the lipid-bilayer membrane environment. *J. Biol. Chem.*, 291, 19146–19156. (DOI: 10.1074/jbc.M116.738583)

50. Zhang, X., Ge, N., Keiderling, T. A. (2007), Electrostatic and hydrophobic interactions governing the interaction and binding of beta-lactoglobulin to membranes. *Biochemistry*, 46, 5252–5260. (DOI: 10.1021/bi602483p)

51. Arias, J. M., Tuttolomondo, M. E., Díaz, S. B., Altabef, A. B. (2015), FTIR and Raman analysis of l-cysteine ethyl ester HCl interaction with dipalmitoylphosphatidylcholine in anhydrous and hydrated states. *J. Raman Spectrosc.*, 46, 369–376. (DOI: 10.1002/jrs.4659)

52. Kanwa, N., Patnaik, A., De, S. K., Ahamed, M., Chakraborty, A. (2019), Effect of Surface Ligand and Temperature on Lipid Vesicle-Gold Nanoparticle Interaction: A Spectroscopic Investigation. *Langmuir*, 35, 1008–1020. (DOI: 10.1021/acs.langmuir.8b03673)

Chapter 6

Materials, methods and Instrumentation

6.1 Materials

Phospholipids (DPPC, DMPC, DLPC, DOPC, DMPG, DMTAP) and inverse phospholipid (DOCP) were purchased from Avanti Polar lipids. Phosphate buffer salts were purchased from Merck. $HAuCl_4$, PRODAN, 3-mercaptopropionic acid, trisodium citrate, cysteamine, DOX, gold nanoparticles (5 nm) and polymer (Polydiallyldimethylammonium chloride) were purchased from Sigma- Aldrich. Glutathione and sodium borohydride were purchased from Sisco Research Laboratories. The phenylenediamine (PDA) isomer, oPDA, was purchased from SDFCL, mPDA was purchased from Alfa Aesar and pPDA from Loba Chemie Pvt. Ltd. The amino acids, L-aspartic acid and L-glutamic acid, were purchased from Merck; L-arginine was purchased from HiMedia; L-serine, L-valine, and L-leucine were purchased from SRL chemicals and D-serine, D-valine, D-leucine, and L-lysine were purchased from Sigma-Aldrich. All amino acids used were of ≥98% purity. All materials were used as received. In all cases, we used Milli-Q water to prepare the solutions.

6.2 Methods

Chapter 2

6.2.1 Preparation of lipid vesicles: Lipid vesicles were prepared in phosphate-buffered saline (pH = 7.4, I = 0.025 M) by dissolving the lipid in ethanol (0.01% of the hydrating solution) and injecting in a preheated PRODAN solution above the phase transition of the specific lipid. The solution was stirred at this temperature for nearly an hour and cooled down to room temperature before performing any further studies. The total concentration of the lipid and PRODAN was fixed at 0.6 mM and 2 μM respectively for all of the experiments. For confocal imaging, the vesicles were prepared by thin-film hydration method to

yield vesicles of size ca. ~1.5 μm and stained with ~20 nM rhodamine-B dye for at least 2 h.

6.2.2 Synthesis of citrate-capped gold nanoparticles: Citrate capped AuNPs were synthesized following the classical citrate reduction of $HAuCl_4$, using a previously described protocol with slight modification [1]. All glassware used for the synthesis were cleaned in freshly prepared aqua regia solution, rinsed with Milli-Q water, and dried in an oven. Further, trisodium citrate solution (38.8 mM, 10 mL) was rapidly injected to a boiling HAuCI4 solution (1.0 mM, 100 mL) under vigorous stirring. The resulting wine red colloidal solution was boiled for 30 min, cooled down to room temperature, and stored at 4 °C for further use. The obtained citrate capped AuNPs had a concentration of 13.4 nM.

6.2.3 Functionalization of gold nanoparticles: Citrate-capped AuNPs were functionalized with MPA and GSH following a previously described protocol with slight modification [2]. Briefly, MPA (25 mM, 10 μL) or GSH (25 mM, 10 μL) was added to citratecapped AuNPs (13.4 nM, 746 μL), incubated overnight, and stored at 4 °C for further use. The final concentration of the obtained MPA or GSH-functionalized AuNPs is ~13.27 nM. Freshly prepared AuNP solutions were used for each experiment.

6.2.4 Synthesis of cationic gold nanoparticles: Cysteamine functionalized gold nanoparticles (cys-AuNPs) were synthesized following a previously described protocol with slight modification [3]. Briefly, 1.2 mL of 213 mM cysteamine and 1.42 mM $HAuCl_4$ were mixed and then the mixture was blended under ambient temperature for 20 min. Subsequently, 30 mL of 10 mM $NaBH_4$ was added to the above solution and the mixture was stirred for another 25 min at room temperature in the dark and stored at 4 °C for further use.

Chapter 3

6.2.5 Liposome preparation: Liposomes were prepared in phosphate buffer saline (PBS, pH = 7.4, I = 0.01 M). The lipids were dissolved in a mixture of chloroform and ethanol, and the solvents were removed completely in a rotary

evaporator under gentle conditions (P = 180 mBar, T = 30 °C). The flask containing a dry lipid film was placed under ultrahigh vacuum overnight to remove any residual solvent. The film was hydrated with PBS 7.4, which was already kept above the phase transition temperature of the lipids. The obtained liposomes were extruded through 200 nm polycarbonate membranes to yield small monodispersed unilamellar liposomes. For preparation of DOX loaded liposomes, the DOX solution already prepared in ethanol was added before placing the sample in the rotary evaporator. The total lipid concentration was fixed at 0.6 mM for all of the PRODAN-related experiments and 1 mM for all DOX-related experiments.

6.2.6 Functionalization of gold nanoparticles: AuC were prepared by functionalization of gold nanoparticles [size: 5 nm, CAS number: 752568, stored in PBS solution] by 3-mercaptopropionic acid by a previously described method [4-5]. Briefly, an appropriate amount of gold nanoparticles was taken in a round-bottom flask; then, the required amount of 3-mercaptopropionic acid was added to it, and the mixture was shaken by hand for 5 min followed by incubation for 24 h at room temperature. The mixture was dialyzed for 2 days to remove unreacted acids. After that, we kept the prepared AuC solution at 4 °C for further use.

6.2.7 Capsule preparation: The capsules were formed by coating of liposome−AuC assemblies with polymer and lipid following an LBL fashion [6-7]. The liposome−AuC assembly was prepared by adding excess AuC to freshly prepared liposome solution followed by incubation for nearly 12 hours. For the polyelectrolyte layer, a stock solution of polymer was prepared in PBS (pH = 7.4). Then, the polyelectrolyte layer was formed by adding polymer solution (1 mg/mL) to the liposome−AuC solutions followed by stirring for 15−20 min at room temperature. For the lipid-coated layer, the polymer coated system (i.e., liposome−AuC−P) solution was incubated with the negatively charged liposomes (DMPC:DMPG, prepared in a ratio of 8:2) for 30 min above the phase transition temperature of the negatively charged liposome [7]. The coating conditions for each formulation were optimized beforehand. The optimal AuC, polymer, or lipid

to capsule ratio was obtained experimentally by zeta potential values as obtained by titration of the respective capsules upon gradual addition of the polymer or lipid, respectively. The drug release experiments were conducted using a Pur-ALyzer Maxi Dialysis tube (polycarbonate membrane, MWCO 12−14 kDa) purchased from Sigma-Aldrich. A certain amount of sample was added to the dialysis tubes, kept in the release medium, from which a specific amount of sample was collected atregular intervals to monitor the amount of released drug. Throughout the drug release experiment, we maintained an ionic strength of I = 0.01 M and temperature of T = 25 °C. The pH of the systems was maintained at the pH at which release was monitored (pH = 7.4 and 5.0).

Chapter 4

6.2.8 Synthesis of C-dots: Differently emissive C-dots were synthesized from phenylenediamine (PDA) isomers as reported earlier with slight modification [8]. In brief, C-dots were synthesized by a bottom up approach following a hydrothermal method by heating oPDA, mPDA, and pPDA in an ethanol solution (0.1 g/mL) at 180 °C for 12 h in an autoclave and purified by dialysis of the obtained product. The resulting C-dots were lyophilized followed by putting under ultra high vacuum to remove any remaining solvent. The resultant C-dots were dispersed in Milli-Q water for further experiments. The products were named oCD, mCD, and pCD obtained from the precursors oPDA, mPDA and pPDA, respectively. The concentration of the synthesized C-dots was estimated after lyophilizing the solutions and was estimated to be 0.57 mg/mL for oCD, 0.70 mg/mL for mCD, and 4.41 mg/mL for pCD. The fluorescence quantum yield of C-dots was estimated relative to quinine sulfate ($\phi f = 0.55$) in 0.1 M H_2SO_4 at λex = 365 nm and a quantum yield 0.10, 0.09, and 0.028 for oCD, mCD, and pCD, respectively, was estimated. The obtained C-dots show an absorption peak at 416 nm, 372 nm, and 435 nm for oCD, mCD, and pCD, respectively. The emission maxima of the C-dots were observed at 570 nm, 490 nm, and 635 nm for oCD, mCD, and pCD, respectively.

6.2.9 Preparation of lipid vesicles: The lipid vesicles were prepared in Milli-Q

water by dissolving the lipid in ethanol (0.01% of the hydrating solution) and rapidly injecting in a preheated PRODAN solution above the phase transition of the specific lipid (T_m = 24 °C for DMPC and 41 °C for DPPC). The solution was stirred above this temperature for nearly an hour and cooled down to room temperature before performing any further studies. The total concentration of the lipid was fixed at 0.6 mM, while that of PRODAN was fixed at 2 μM for all of the experiments. This technique yields vesicles with an average size of ∼100−200 nm which were employed for all the spectroscopic and DLS measurements. C-dot solutions were added to the prepared lipid solutions in desired concentrations (maximum concentration being 30 μg/mL) for the spectroscopic analysis. All the solutions were prepared in Milli-Q.

However, for confocal imaging, the lipid vesicles were prepared by the thin film hydration method to yield vesicles of ∼500−700 nm size and stained with ∼20 μM PRODAN for at least 2 h. The unbound PRODAN was removed by dialysis. The final concentration of PRODAN was ∼5−7 μM in the vesicles. Briefly, the required lipid was dissolved in an organic stock solution (chloroform), followed by preparation of a lipid thin film by evaporating the organic solvent using a rotary evaporator. The thin film obtained was stored under ultrahigh vacuum for at least 4 h to ensure the complete removal of the organic solvent. This was followed by hydration of the lipid thin film in an aqueous medium above the phase transition of the lipid to obtain multilamellar vesicles. These lipid vesicles were extruded using an Avanti mini extruder to obtain uniformly sized vesicles for Confocal imaging.

Chapter 5

6.2.10 Preparation of lipid bilayer: Lipid bilayer membranes were prepared in Milli-Q water by dissolving the lipid in ethanol (0.01% of the hydrating solution) and rapidly injecting into a preheated PRODAN solution above the phase transition temperature of the specific lipid [9-13]. The solution was stirred at this temperature for nearly an hour and cooled down to room temperature before performing any further studies. The total concentration of the lipid was fixed at 0.6 mM, while that of PRODAN was fixed at 2 mM for all of the experiments.

Amino acid solutions were added to the prepared lipid solutions in desired concentrations for spectroscopic analysis. All the solutions were prepared in Milli-Q water in order to avoid any effect arising as a result of salts used in the buffer as previously reported by Ye and co-workers [14-16]. For confocal imaging, the vesicles were prepared by the thin film hydration method to yield vesicles of ~500–700 nm size and stained with ~5 mM Rhodamine-B dye for at least 2 hours. Briefly, the required lipid was dissolved in an organic stock solution (chloroform), followed by preparation of a lipid thin film by evaporating the organic solvent using a rotary evaporator. The thin film obtained was stored under ultra-high vacuum for at least four hours to ensure the complete removal of the organic solvent. This was followed by hydration of the lipid thin film in an aqueous medium above the phase transition temperature of the lipid to obtain multilamellar vesicles. These vesicles were extruded to obtain uniformly sized lipid vesicles for confocal imaging.

6.3 Instrumentation and techniques

Spectroscopic techniques:

Absorption spectra were recorded using a Varian UV−vis spectrophotometer (Cary 100 Bio) in a quartz cuvette (10 × 10 mm^2). Steady-state fluorescence spectra were recorded using a FluoroMax- 4p spectrofluorometer from Horiba Jobin Yvon (model: FM- 100). All fluorescence emission spectra were analyzed using OriginPro 8.1 software. The area fraction curve was plotted by deconvolution of the spectra into two peaks at 435 and 500 nm and by plotting the fraction (A435nm/A490nm) versus experimental temperature using Origin 8.1. The lipid vesicle−nanoparticle interaction was studied by varying the concentration of gold nanoparticles in a fixed concentration of lipid and PRODAN. Briefly, we prepared a set of solutions in different volumetric flasks that contained 2 μM PRODAN, 0.6 mM lipid and different concentrations of AuNPs. The lipid vesicles−C-dot interaction was studied by varying the concentration of C-dots (from 0 to 30 μg/mL) at a fixed concentration of lipid (0.6

mM) and PRODAN (2 μM). The samples were excited at 375 nm. The fluorescence spectra were corrected for the spectral sensitivity of the instrument. The excitation and emission slits were 2 nm each for all of the PRODAN emission measurements. Throughout all of the titration experiments, we maintained pH 7.4, I = 0.025 M, and the desired experimental temperature.

For time-correlated single-photon counting (TCSPC), we used a picosecond TCSPC machine from Horiba (FluoroCube- 01-NL). The samples were excited at 375 nm using a picosecond diode laser (model: Pico Brite-375L), and the decays were collected at 440 and 500 nm. We used a filter on the emission side to eliminate the scattered light. The signals were collected at magic angle (54.75°) polarization using a photomultiplier tube (TBX-07C) as the detector. The full width at half-maximum of the instrument response function of our setup was ~140 ps. The data analysis was performed using IBH DAS version 6 decay analysis software. Throughout all of the titration experiments, we maintained pH 7.4, I = 0.025 M, and the desired experimental temperature. The decays were fitted with a multiexponential function

$$D(t) = \sum_{i=1}^{n} a_i \exp\left(\frac{-t}{\tau_i}\right) \qquad (1)$$

Where, *D(t)* denotes normalized fluorescence decay and a_i are the normalized amplitude of decay components τ_i respectively. The average lifetime was obtained from the equation:

$$\langle \tau \rangle = \sum_{i=1}^{n} a_i \tau_i \qquad (2)$$

The quality of the fit was judged by reduced χ-square (χ^2) values and corresponding residual distribution. The acceptable fit has a χ^2 near to unity.

The same setup was used for anisotropy measurements. For the anisotropy decays, we used a motorized polarizer in the emission side. The emission intensities at parallel and perpendicular polarizations were collected alternatively

until a certain peak difference between parallel and perpendicular decay was achieved. The same software was also used to analyze the anisotropy data. The time-resolved anisotropy decay was described with the following equation:

$$r(t) = \frac{I_{\parallel}(t) - GI_{\perp}(t)}{I_{\parallel}(t) + 2GI_{\perp}(t)} \qquad (3)$$

where *r(t)* is the rotational relaxation correlations function, $I_{\parallel}(t)$ and $I_{\perp}(t)$ are the parallel and perpendicular components of the fluorescence and G is the correction factor.

DLS and ζ potential measurements of the AuNPs were performed on a NanoPlus ζ/particle size analyzer (NanoPlus-3 model). Fourier transform infrared (FTIR) spectra were recorded using KBr pellets on a Bruker Tensor 27 FTIR spectrophotometer.

Imaging techniques:

The FE-SEM study to reveal the morphology of the samples was conducted using a ZEISS Supra55 field-emission scanning electron microscope. AFM images were recorded in tapping mode using the NX-10 PARK system. The samples were dropcasted on a freshly cleaved mica surface and dried under vacuum. The high-resolution transmission electron microscopy (TEM) study was conducted using a Tecnai T20 transmission electron microscope with an operating voltage of 200 keV. For the confocal imaging of samples, we used a Confocal microscope from OLYMPUS, model no. IX-83. A Multiline Ar laser (gas laser) with an excitation wavelength of 488 nm was used. The observation mode was laser scanning microscopy (LSM), the scan mode was XY, and the scan direction was one way. The liquid samples were dropped on glass slides, spin-coated, and fixed with coverslips before imaging. For imaging purposes, we used a concentration of 1 mg/mL of lipid and 90 μg/mL of C-dots in order to get a strong signal and clearer visuals of images.

6.4 References

1. Zhao, J., Wu, Y., Tao, H., Chen, H., Yang, W., Qiu, S. (2017), Colorimetric Detection of Streptomycin in Milk Based on Peroxidase-Mimicking Catalytic Activity of Gold Nanoparticles. *RSC Adv.*, 7, 38471−38478. (DOI: 10.1039/C7RA06434A)

2. Wang, F., Liu, J. (2015), Self-Healable and Reversible Liposome Leakage by Citrate-Capped Gold Nanoparticles: Probing the Initial Adsorption/Desorption Induced Lipid Phase Transition. *Nanoscale*, 7, 15599−15604. (DOI: 10.1039/C5NR04805B)

3. Zhao, J., Wu, Y., Tao, H., Chen, H., Yang, W., Qiu, S. (2017), Colorimetric Detection of Streptomycin in Milk Based on Peroxidase-Mimicking Catalytic Activity of Gold Nanoparticles. *RSC Adv.*, 7, 38471−38478. (DOI: 10.1039/C7RA06434A)

4. Pornpattananangkul, D., Olson, S., Aryal, S., Sartor, M., Huang, C.–M., Vecchio, K., Zhang, L. (2010), Stimuli-responsive liposome fusion mediated by gold nanoparticles. *ACS Nano*, 4, 1935–1942. (DOI: 10.1021/nn9018587)

5. Adhikari, C., Das, A., Chakraborty, A. (2015), Controlled release of a sparingly water-soluble anticancer drug through pH-responsive functionalized gold-nanoparticle-decorated liposomes. *ChemPhysChem*, 16, 866–871. (DOI: 10.1002/cphc.201402748)

6. Shin, S. H. R., Lee, H.-Y., Bishop, K. J. M. (2015), Amphiphilic nanoparticles control the growth and stability of lipid bilayers with open edges. *Angew. Chem., Int. Ed.*, 54, 10816–10820. (DOI: 10.1002/anie.201504362)

7. De Temmerman, M.-L., Rejman, J., Lucas, B., Vandenbroucke, R. E., Libert, C.; Demeester, J., De Smedt, S. C. (2012), Modulation of dendritic cells by lipid grafted polyelectrolyte microcapsules. *Adv. Funct. Mater.*, 22, 4236–4243. (DOI: 10.1002/adfm.201103151)

8. Jiang, K., Sun, S., Zhang, L., Lu, Y., Wu, A., Cai, C., Lin, H. (2015), Red, Green, and Blue Luminescence by Carbon Dots: Full-Color Emission Tuning

and Multicolor Cellular Imaging. *Angew. Chem. Int. Ed.*, 54, 5360−5363. (DOI: 10.1002/anie.201501193)

9. De, S. K., Kanwa, N., Ahamed, M., Chakraborty, A. (2018), Spectroscopic evidence for hydration and dehydration of lipid bilayers upon interaction with metal ions: a new physical insight. *Phys. Chem. Chem. Phys.*, 20, 14796–14807. (DOI: 10.1039/C8CP01774C)
10. De, S. K., Kanwa, N., Chakraborty, A. (2019), Influence of Trivalent Metal Ions on Lipid Vesicles: Gelation and Fusion Phenomena. *Langmuir*, 35, 6429–6440. (DOI: 10.1021/acs.langmuir.9b00682)
11. Justo, O. R., Moraes, A. M. (2005), Kanamycin incorporation in lipid vesicles prepared by ethanol injection designed for tuberculosis treatment. *J. Pharm. Pharmacol.*, 57, 23–30. (DOI: 10.1211/0022357055092)
12. Pons, M. Foradada, M., Estelrich, J. (1993), Liposomes obtained by the ethanol injection method. *Int. J. Pharm.*, 95, 51–56. (DOI: 10.1016/0378-5173(93)90389-W)
13. Batzri, S., Korn, E. D. (1973), Single bilayer liposomes prepared without sonication. *Biochim. Biophys. Acta*, 298, 1015–1019. (DOI: 10.1016/0005-2736(73)90408-2)
14. Wei, F., Li, H., Ye, S. (2013), Specific Ion Interaction Dominates over Hydrophobic Matching Effects in Peptide–Lipid Bilayer Interactions: The Case of Short Peptide. *J. Phys. Chem. C*, 117, 26190–26196. (DOI: 10.1021/jp411413u)
15. Wei, F., Ye, S., Li, H., Luo, Y. (2013), Phosphate Ions Promoting Association between Peptide and Modeling Cell Membrane Revealed by Sum Frequency Generation Vibrational Spectroscopy. *J. Phys. Chem. C*, 117, 11095–11103. (DOI: 10.1021/jp400378d)
16. Yang, W., Tian, K., Ye, S. (2015), Interaction between Potassium Phosphate Buffer Solution and Modeling Cell Membrane Investigated by Sum Frequency Generation Vibrational Spectroscopy. *Chin. J. Chem. Phys.*, 28, 518–524. (DOI: 10.1063/1674-0068/28/cjcp1504070)

Chapter 7

Conclusion and Future Aspects

7.1 Conclusion:

Research work reported in this thesis discusses the binding of various nanoparticles and biomolecules to model lipid membranes and the huge impact they cast on the overall membrane properties. In particular, the binding behaviour of these entities based on different factors, such as their size, surface ligands, isomeric precursors and hydrophobicity have been explored. For the interaction studies, lipid bilayers of varying chain lengths, surface charges and phase transition temperatures were explored. The properties of a fluorescent membrane probe PRODAN were employed to study the systems with the help of different spectroscopic, imaging and other techniques.

The modification of membrane surfaces by interfacial interactions have been used for the development of efficient drug carriers and bio-imaging models. In particular, the lipid-based system was employed for the controlled release of an anticancer drug, Doxorubicin (DOX). Moreover, the suitability of C-dots for the cellular imaging purpose was explored.

Since the lipid vesicles act as biomimetic systems, the membrane interaction studies using model membranes account for the underlying mechanisms and the resultant influence at the nano-bio interface in biological membranes. Thus, they help in providing a better understanding of the interactions which can help to bridge the gap between the lipid systems *in vivo* and *in vitro* at the membrane interface.

7.2 Future aspects:

The biocompatible materials obtained by the interaction of lipid membranes with nanoparticles, carbon dots and biomolecules will provide several opportunities to use them as efficient systems for applications in biomedical sciences. The employment of lipid-based systems as drug carriers provides an insight into the behaviour of drug in the presence of cell membrane-like atmosphere. Overall the work presented in this thesis will give valuable information regarding the development of various lipid-based systems and expected to encourage design of biosystems in the future.

Thus as a future prospect, these developments are expected to add new dimensions toward the potential usage of lipid membrane based assemblies for better experimental models for drug delivery, bioimaging and other bio-inspired applications.